Charles University
Faculty of Science

Study program: Molecular and Cellular Biology, Genetics and Virology

Mgr. Irina Soldatova

Mouse polyomavirus: The way of virus translocation to the cell nucleus and sensing of viral genomes by sensors of innate immunity

Myší polyomavirus: Způsob translokace do buněčného jádra a rozpoznání virových genomů sensory vrozené imunity

Doctoral thesis

Supervisor: doc. RNDr. Jitka Forstová, CSc.

Prague, 2021

Prohlášení:

Prohlašuji, že jsem závěrečnou práci zpracovala samostatně a že jsem uvedla všechny použité informační zdroje a literaturu. Tato práce ani její část nebyla předložena k získání jiného nebo stejného akademického titulu.

Statement:

I declare that I prepared the PhD thesis independently and I stated all used sources of information and literature. This thesis or its substantial part has not been submitted to obtain another or equivalent academic degree.

In Prague 29.6.2021 .....

Signature

Acknowledgements

I would like to thank to my supervisor doc. RNDr. Jitka Forstová, CSc. for the invaluable help, advices, support and comments that she have provided me during my study and the elaboration of this doctoral thesis. Additionally, I would like to thank to Sandra Huerfano, PhD for precious advices and support. I very thank to all my colleagues from the Laboratory of Molecular Virology for very friendly and kind attitude to me. Finally, I would like to thank to my family for their unlimited love, patience, support and trust.

This work was supported by the STARS program, Faculty of Sciences, Charles University, by the Grant Agency of the Czech Republic (GAUK No. 359615), by the Grant agency of the Czech Republic (GAČR 16-07977S), by the Charles University in Prague (Project UNCE 204013), by the project BIOCEV—Biotechnology and Biomedicine Centre of the Academy of Sciences and Charles University (CZ.1.05/1.1.00/02.0109) and by the Grant agency of the Czech Republic (GAČR 19-14445S).

Abstract

To understand molecular mechanisms of individual steps of virus infection is a prerequisite for successful design of specific and effective antiviral drugs. Polyomaviruses, replicating in the cell nucleus, travel from plasma membrane to the endoplasmic reticulum (ER) in endosomes. However, it is not clear how they deliver their DNA genomes from ER to the nucleus. In this thesis, we found that partially disassembled virions of the Murine polyomavirus (MPyV) interact with importin β1 at around 6 hours post infection. Mutational disruption of the nuclear localization signal (NLS) of the major capsid protein, VP1, and/or common NLS sequence of the minor capsid proteins VP2 and VP3 did not affect the structure and composition of virions, but it resulted in decreased viral infectivity (up to 80%). Virions are thus released from ER to cytosol and translocate to the nucleus via nucleopores. Mutation analyses of NLSs of individual capsid proteins showed that MPyV virions can utilize VP1 and VP2/VP3 NLSs in concert. However, one functional NLS, either that of VP1 or VP2/3 seems to be sufficient for the delivery of VP1-VP2/3 complexes into the nucleus, although none of these proteins is delivered into the nucleus separately. Thus, the conformation of NLS regions given by the presence of all three capsid proteins seems to be important for importin binding.

Knowing that partially disassembled virions appear free in cytoplasm prior to their translocation into the nucleus, we were interested whether viral genomes are sensed by DNA sensors to induce interferon type I response. Surprisingly, we did not detect IFN-β production before active viral genome replication started. We found IFN response to MPyV to be dependent on stimulator of interferon genes (STING) and interferon regulatory factors 3 (IRF3). DNA sensors, cyclic guanosine-adenosine synthetase (cGAS) and p204 (mouse analogue of IFI16) were found to participate in viral genome sensing and IFN induction. Our results indicate that MPyV infection activates IFN-β production by p204 sensing of viral minichromosomes in the cell nucleus and by cGAS recognition of leaked viral DNA and micronuclei in cytoplasm.

Key words: Mouse polyomavirus, capsid proteins, nuclear localization signal, delivery to the nucleus, viral genome sensing, cGAS sensor, p204 sensor, IFN-β induction

Abstrakt

Pochopení molekulárních mechanismů jednotlivých kroků virové infekce je předpokladem pro úspěšný návrh specifických a účinných antivirotik. Polyomaviry replikující se v buněčném jádře putují od cytoplazmatické membrány v endosomech do endoplazmatického retikula (ER). Není však jasné, jak jsou jejich DNA genomy dopravovány z ER do jádra. V této práci jsme zjistili, že částečně rozložené viriony myšího polyomaviru (MPyV) interagují s importinem β1 přibližně 6 hodin po infekci. Mutace vedoucí k oslabení nebo zrušení jaderného lokalizačního signálu (NLS) kapsidových proteinů VP1 a/nebo společné signální sekvence proteinů VP2 a VP3 neovlivnilo strukturu a složení virionů, ale mělo za následek sníženou infektivitu viru (až o 80%). Viriony se tak dostávají z ER do cytosolu a do jádra jsou dopravovány přes jaderné póry. Mutační analýzy NLS jednotlivých kapsidových proteinů ukázaly, že MPyV viriony mohou využívat NLS hlavního i minoritních kapsidových proteinů v koordinaci, nebo zástupně. Jeden funkční NLS, ať už VP1 nebo VP2/VP3, se však jeví jako dostatečný pro dopravu komplexů VP1-VP2/VP3 do jádra, ačkoli žádný z těchto proteinů se do jádra nedostává samostatně. Konformace NLS daná přítomností všech tří kapsidových proteinů se zdá být důležitá pro vazbu importinů.

Poznání, že částečně rozložené viriony se ocitnou volné v cytoplazmě před jejich translokací do jádra nás vedlo ke zkoumání, zda jsou polyomavirové genomy rozpoznávány DNA senzory pro indukci interferonu typu I. Překvapivě jsme nedetekovali produkci IFN-β před zahájením aktivní replikace virového genomu v buněčném jádře. Zjistili jsme, že indukce IFN myším polyomavirem závisí na stimulátoru interferonových genů (STING) a interferonového regulačního faktoru 3 (IRF3). Bylo zjištěno, že rozpoznání virového genomu senzory DNA a indukce IFN se účastní cyklická guanosin-adenosin syntetáza (cGAS) a protein p204 (myší ortolog IFI16). Naše výsledky naznačují, že infekce MPyV aktivuje produkci IFN-β pomocí sensoru p204 rozpoznáním virových minichromozomů v buněčném jádře a rozpoznáním virové DNA uniklé z jádra a mikrojader obsahujících hostitelskou DNA sensorem cGAS v cytoplazmě.

Klíčová slova: Myší polyomavirus, kapsidové proteiny, jaderný lokalizační signál, doprava virových genomů do jádra, rozpoznání virových genomů, cGAS, p204, indukce interferonu β

Table of Content

Abbreviations

aa	Amino acids
A	Alanine
AIM2	Absence in melanoma 2
ALRs	Absent in melanoma 2 (AIM2)-like receptors
BKPyV	BK polyomavirus
BSA	Bovine serum albumin
CARDs	Caspase activation and recruitment domains
cGAMP	Cyclic guanosine monophosphate (GMP)-adenosine monophosphate (AMP)
cGAS	Cyclic guanosine-adenosine synthetase
cGAS wt	MEF cGAS wild type cell line
cGAS KO	MEF cGAS knockout cell line
CTD	C-terminal domain
CpG	2′-deoxyribo cytidine-phosphate-guanosine
DAI	DNA dependent activator of IFN regulatory factors
DDX41	DExD/H-box helicase 4
DDX60	DExD/H-box helicase 60
DHX9	DEAH box polypeptide 9
DHX36	DEAH box polypeptide 36
ds	Double-stranded
DSS	Disuccinimidyl suberate
EEA1	Early endosome antigen 1
ER	Endoplasmic reticulum
ERGIC	Endoplasmic-reticulum–Golgi intermediate compartment
ERp57	Endoplasmic reticulum protein 57
FISH	Fluorescence in situ hybridization
G	Glycine
HAU	Hemagglutination units
γH2AX	Phosphorilated H2A histone family member X

hpi	Hours post-infection
hpt	Hours post-transfection
HSV-1	Herpes simplex virus 1
IFIT3	IFN-inducible protein with tetratricopeptide repeats
IFI16	Interferon gamma inducible protein 16
IFIX	Interferon-inducible protein X
IFNs	Interferons
IFN-β	Interferon beta
IgG	Immunoglobulin G
IRF3	Interferon regulatory factors 3
JCPyV	JC polyomavirus
K	Lysine
Kbp	Kilobase pair
LC-MS	Liquid chromatography–mass spectrometry
LGP2	Laboratory of genetics and physiology 2
LRRFIP1	Leucine-rich repeat flightless-interacting protein 1
LT	Large T antigen
MAVS	Mitochondrial antiviral signaling
MCPyV	Merkel cell carcinoma polyomavirus
MDA-5	Melanoma differentiation associated gene-5
MEF	Mouse embryo fibroblasts
MHC-I	Major histocompatibility class I
MI	Mock infected cells
MOI	Multiplicity of infection
MPyV	Murine polyomavirus
mT	Middle T antigen
MX-1	Mouse myxovirus resistance protein 1
NF-kB	Nuclear factor kappa-light-chain-enhancer of activated B cells
NLS	Nuclear localization signal
NPC	Nuclear pore complex
Ori	Origin of replication
PAMPs	Pathogen-associated molecular patterns
PBS	Phosphate-buffered saline

PCR	Polymerase chain reaction
pDNA	Plasmid DNA
PDI	Protein disulphide isomerase (PDI)
PFA	Paraformaldehyde
PLA	Proximity ligation assay
PML	Progressive multifocal leukoencephalopathy
Poly I:C	Polyinosinic:polycytidylic acid
PRRs	Pattern recognition receptors
p53	Tumor protein 53
p-p53	Phospho-p53
p53BP1	Tumor suppressor p53-binding protein 1
p53 wt	MEF p53 wild type cells
p53 KO	MEF p53 knockout cells
p-IRF3	Phosphor-IRF3
p-STING	phospho-STING
qPCR	Quantitative real-time RT-PCR
Q	Glutamine
R	Arginine
RIG-I	Retinoic acid-inducible gene I
RLRs	Retinoic acid-inducible gene I (RIG-I)-like receptors
S	Serine
SD	Standart deviation
SDS	Sodium deoxycholate
siRNA	Small interfering RNA
ssRNA	Single-stranded RNA
sT	Small T antigen
STING	Stimulator of interferon genes
STING wt	MEF STING wild type cell line
STING KO	MEF STING knockout cell line
SV40	Simian virus 40
TBK1	Tank binding kinase-1

IR	Toll IL-1 receptor domain
TLRs	Toll-like receptors
TRAF	TNF receptor-associated factor
TRIM25	Tripartite motif protein 25
VLPs	Virus-like particles
VP1	Viral protein 1; the major capsid protein 1
VP2	Viral protein 2; the minor capsid protein 2
VP3	Viral protein 3; the minor capsid protein 3
Wt	Wild type

1. Introduction

For over half a century of polyomavirus studies, data were generated about many aspects of polyomavirus genome replication, transcription, RNA splicing, gene product functions, their tumorigenicity or pathogenicity. Nevertheless, there are important aspects of polyomavirus life cycle which are not fully elucidated.

Polyomaviridae is a family of small DNA viruses representing around 76 species. Their natural hosts are mammals, birds, and fish. Fifteen species of polyomaviruses are spread in human population and according to serological studies, from 35% to 90% of healthy individuals are asymptomatically infected with them [Calvignac-Spencer et al., 2016; Moens et al., 2017; Dalianis, Hirsch 2013]. After reactivation, human polyomaviruses can cause serious diseases in immunocompromised individuals such as skin cancer, transplantation allograft rejection, fatal neurodegenerative disease and etc. Thus, JC polyomavirus (JCPyV) is associated with a progressive multifocal leukoencephalopathy (PML) which is a fatal demyelinating disease [Padgett et al., 1971]. BK polyomavirus (BKPyV) infection is responsible for diseases of urinary tract - hemorrhagic cystitis and ureteral stenosis [Arthur, Shah, 1989]. Merkel cell carcinoma polyomavirus (MCPyV) is the main causal agent of Merkel cell carcinoma, an aggressive cutaneous malignancy [Feng et al., 2008].

Studies of model polyomaviruses, MPyV and Simian virus 40 (SV40), showed that infection of non-permissive cells with these viruses induced malignant transformation in absence of viral replication and production of capsid proteins [Asselin et al., 1983]. Later, different researchers found that polyomaviruses have been associated with specific tumor types such as mesotheliomas, lymphomas, bone tumors, neuroblastomas and medulloblastomas [Fluck, Haslam, 1996; Zu Rhein, 1983; Butel et al., 2003; Abend et al., 2009]. Investigations of Merkel cell carcinoma demonstrated that in about 80% of cases there is clonally integrated genome of relatively newly discovered Merkel cell polyomavirus (MCPyV), thus confirming the tumorigenic character of polyomaviruses [Feng et al., 2008].

Persistence of polyomaviruses in the human population, their ability to cause severe disease in immunosuppressed individuals and renal transplantation failure, their tumorigenic potential - all this is a reason to thoroughly study the mechanisms of replication cycle of polyomaviruses, their interaction with the host immune system and the mechanisms used by these cytolytic viruses to establish persistence in their hosts.

2. Literature Overview

2.1. Polyomaviruses

2.1.1. From history to nowadays

One of the first polyomaviruses, MPyV, was discovered in 1953 by Ludwik Gross. He was studying leukemia in mice and found that some cell-free extracts caused carcinomas and sarcomas of the salivary glands. He showed that the leukemia agent could be (upon certain conditions) pelleted by centrifugation, whereas salivary tumor causing agent stayed in a supernatant, thus indicating the presence of a different virus [Gross, 1953]. Later, Stewart and Eddy, called this virus polyomavirus (from Greek roots), reflecting the fact that it may induce "many tumors". MPyV infects newborn mice and can be transmitted by respiratory rote. It can be found in urine, feces, and saliva of infected animals. In colonies of mice naturally infected with MPyV, no tumorigenesis was observed, whereas naive animals or animals with immunodeficiency have high probability of cancer development [Rowe et al., 1958]. In the 1990s, several investigators developed cell cultures for analysis of MPyV properties in vitro [Sachs, Winocour, 1959; Vogt, Dulbecco, 1960]. The discovery of MPyV provided the impetus for the detection of other tumor viruses.

The second polyomavirus, SV40, was discovered between 1959 and 1960. Bernice Eddy from the National Institute of Health, and Benjamin Sweet and Maurice Hilleman from the Merck and Co Company found the virus, which induced cancer in animal models, in rhesus monkey kidney cells used for the production of the oral vaccine against poliovirus. They called this virus SV40 because it was the 40^{th} simian virus found in monkey kidney cells [Horwin et al., 2003]. At that time, millions of individuals were vaccinated with polio vaccine contaminated with SV40. However, cases of tumor development, possibly induced by SV40 were not detected [Shah, 2004]. SV40 infection is asymptomatic in healthy monkeys and can be persistent. In immunocompromised animals, the virus induces acute infection and can be found in many organs. Additionally, it was found that SV40 can induce brain cancers, malignant mesotheliomas, bone tumors, and systemic lymphomas in animal models. Nowadays, it is suggested, that SV40 can lead to human cancer in natural conditions and should be included in a list of 2A carcinogens, which are indicative but not definitive for carcinogenesis in humans [Vilchez, Butel, 2004].

Then, in 1970, BKPyV and JCPyV were discovered. Sylvia Gardner, a scientist from the Virus Research Laboratory in London, found that urine from kidney transplant recipients induced cytopathic effect in rhesus monkey kidney cells and human embryonic kidney cells. Thus, she discovered BKPyV named by initials of the patient, from which it was isolated

[Gardner et al., 1971]. In the same year, JC polyomavirus was discovered in Madison, Wisconsin. The electron microscopy of the brain material sections from the J.C. patient with progressive multifocal leukoencephalopathy showed the presence of viral particles with icosahedral symmetry. They named the virus JC polyomavirus [Padgett et al., 1971]. Both viruses can induce primary asymptomatic infection in childhood. BKPyV can be found in the kidney and urinary tract, and after activation, it can induce nephropathy and hemorrhagic cystitis. JCPyV persists in a kidney and causes progressive multifocal leukoencephalopathy. According to serological studies, 80% of the world population is seropositive for JCPyV and BKPyV [Kwak et al., 2002]. Thirty seven years later, two more human polyomaviruses have been discovered. Allander et al. reported the detection of human KI polyomavirus in the respiratory tract and feces of patients [Allander et al., 2007]. WU polyomavirus was discovered in the respiratory tract of a child with pneumonia [Gaynor et al., 2007]. One year later, MCPyV sequences were found by the group of Yuan Chang and Patrick Moore (University of Pittsburgh, USA), through direct genome search of samples of Merkel cell carcinoma - the rare skin cancer [Spurgeon and Lambert, 2013]. Other discoveries followed soon. Two human polyomaviruses 6 and 7, were discovered in 2010 [Schowalter et al., 2010]. In the same year, Trichodysplasia spinulosa-associated polyomavirus was found in immunocompromised patients [van der Meijden et al., 2010].

Nowadays, fifteen human polyomaviruses are known. Human polyomavirus 9 was identified in a kidney transplant patient under immunosuppressive treatment [Scuda et al., 2011]. Another two isolates were detected in stool of a healthy child from Malawi [Siebrasse et al., 2012; Lim et al., 2013]. The most newly discovered human polyomavirus 12 [Mishra et al., 2014], New Jersey polyomavirus [Korup et al., 2013], and Lyon IARC polyomavirus [Gheit et al., 2017] are almost not detectable in the human population [Kamminga et al., 2018]. In 2019, Quebec polyomavirus was detected in fecal samples from a single study of hospital patients in Canada [Ondov et al., 2019]. Recently, polyomavirus subtypes which can infect not only mammals and birds, but also fish and invertebrates were found [Buck et al., 2016]. At present, according to the current classification, 73 of 76 known polyomaviruses are grouped into four genera: 1) *Alphapolyomavirus* includes 36 species, which infect primates (humans, apes, and monkeys), rodents, bats and other mammals (MPyV, MCPyV). 2) *Betapolyomavirus* includes 26 species, infecting primates (humans and monkeys), bats, rodents, etc. (SV40, BKPyV, JCPyV). 3) *Deltapolyomavirus* includes 4 human polyomaviruses and, 4) *Avipolyomavirus* includes 11 species of avian polyomaviruses. Another three polyomaviruses are not classified yet, due to some ambiguity [Calvignac-Spencer et al., 2016].

The first discovered MPyV and SV40 have played an important role in studies of processes of viral replication, oncosupression, oncogenesis, endocytosis, nuclear localization signals discovery, etc. [Hilleman, 1998; Kelly, 1988; Fluck and Haslam 1996].

2.1.2. Structure of polyomavirus virions

Polyomaviruses are small, non-enveloped viruses with a diameter around 45 nm. The capsid of the most known polyomaviruses is formed by 72 capsomers composed of pentamers of the major capsid protein 1 (VP1) and two minor capsid proteins VP2 and VP3 (Figure 1) [Rayment et al., 1982]. Interestingly, the capsid of the MCPyV is composed of VP1 and VP2 proteins only. VP3 protein was detected neither in virions nor in MCPyV infected cells [Schowalter and Buck, 2013].

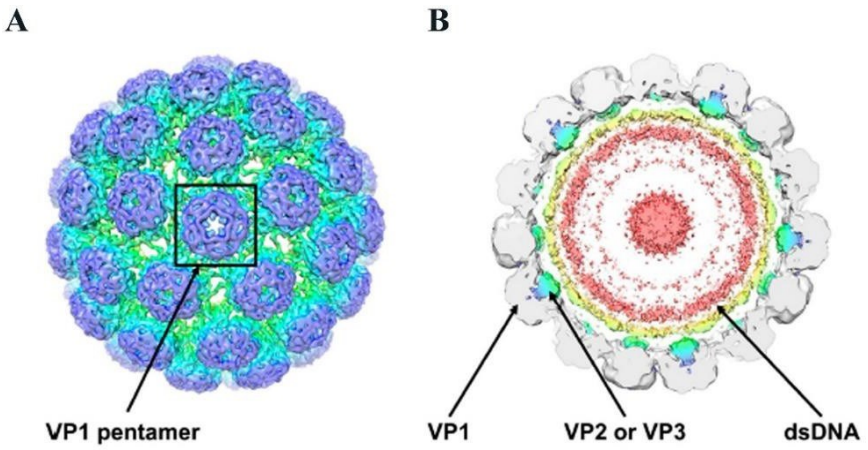

Figure 1. Cryo-electron microscopy structure of BKPyV particle. **(A)** Outside view of the polyomavirus virion with highlighted VP1 pentamer. **(B)** A 40-Å thick slab of a virion map shown at a contour level of 0.0034. Pyramidal density below each VP1 penton and two shells of electron density adjacent to the inner capsid layer can be seen. The density within 6 Å of the coordinates for SV40 VP1 is colored grey. The density for VP2 and VP3 is colored blue/green and for encapsidated double-stranded (ds) DNA with histones yellow-pink. The figure is taken from Helle et al., 2017.

The capsid shell consists of VP1 pentamers, which interact with each other through C-termini of VP1 chains, tying the shell together [Garcea et al., 1987]. These interactions are stabilized by calcium ions [Brady et al., 1977; Stehle et al., 1996]. The minor proteins VP2 and VP3 are longer and shorter version of the same sequence. Longer VP2 has a unique N-terminus (Figure 2A). They are not exposed on the capsid surface; each VP1 pentamer interacts with the common C-terminus of VP2 or VP3 molecule. They localize in an unusual, hairpin-like manner in the interior of axial cavities of VP1 pentamers (Figure 2B) [Chen et al., 1998]. The upper part of VP2 does not form any specific interactions with the top of the cavity, whereas there are specific hydrogen bonds between lover parts of VP2 and VP1 [Chen et al., 1998]. Furthermore,

the cavity of VP1 and VP2/VP3 binding domain are both hydrophobic. This hydrophobicity is important for stabilization VP1-VP2 or VP1-VP3 complexes [Rayment et al., 1982; Barouch and Harrison, 1994]. N-termini of both minor proteins are free and flexible [Chen et al., 1998].

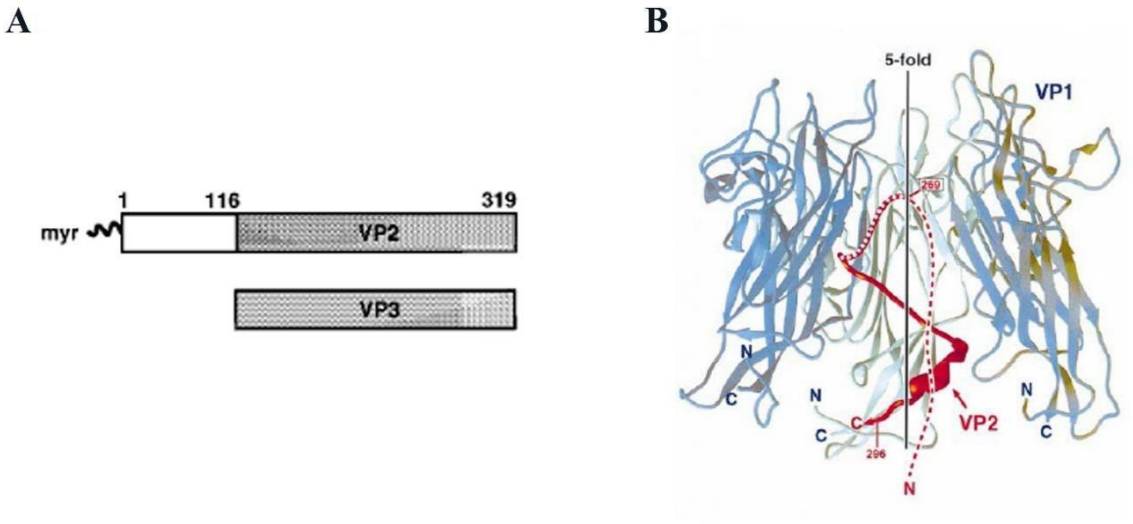

Figure 2. Comparison of polyomavirus VP2, VP3 minor capsid proteins sequences and schema of VP1-VP2 interaction. (A) Linear alignment of VP2 and VP3 proteins showing the extent of a common C-terminal segment and the N-terminal VP2-unique region. **(B)** VP2 protein (red) and three of five monomers of VP1 in light green (middle) and blue (left and right) make a contact with VP2. The two remaining VP1 monomers that lie above the plane of the paper are not show. Not visible N-termini of VP2 is shown as dashed line. The figure is adapted according to Chen et al., 1998.

The capsid of polyomaviruses encloses circular, double-stranded (ds) DNA genome, approximately 5 kilobase pair (kbp) long organized into supercoiled minichromosome. Polyomavirus DNA associates with cellular histones (H2A, H2B, H3, H4). H1 histone is absent in viral minichromosome condensed inside the capsid [Rayment et al., 1982; Moreland et al., 1991]. MPyV VP1 protein can bind all regions of the viral DNA but the strongest interaction occurs in a regulatory region of the genome [Carbone et al., 2004]. VP1 pentamers of polyomaviruses bind DNA non-specifically [Soussi 1986]. The MPyV minor capsid proteins VP2 and VP3 do not have DNA binding activity [Carbone et al., 2004], while the C-termini of VP2 and VP3 of SV40, BKPyV and JCPyV interact with DNA [Clever et al., 1993; Hurdiss et al., 2016; Huang et al., 2003].

2.1.3. Polyomavirus genome organization and gene products

MPyV genome can be divided into the early and late regions, separated with regulatory sequence containing promoters, transcription enhancer and origin of replication (Ori). Transcription of early and late regions occurs in bidirectional manner from sequences near the Ori. During the early phase of infection, efficient transcription of the early genes by host RNA

polymerase II takes place, while only weak basal transcription of the late region occurs. Primary early transcript is then spliced into mRNAs, for production of large tumor (LT), and small tumor (sT) antigens. In addition, middle tumor (mT) antigen is encoded by genomes of MPyV and other rodent polyomaviruses. Also, shorter forms of LT sequence are produced by some polyomaviruses [Garren et al., 2015; Farmerie and Folk, 1984]. First expression of early genes can be detected at 6-8 hours post infection (hpi) [Chen and Fluck, 2001; Hyde-Deruyscher and Carmichael, 1988].

The products of the early region induce host cells entry to S phase, important for viral DNA replication, which is realized by the host cell enzymes and factors [Benjamin, 2001]. Replication of the viral genome starts by LT antigen binding into the viral Ori. LT unwinds DNA in Ori by its helicase activity [Wang and Prives, 1991]. After association with replication protein A and DNA polymerase α-primase, LT recruits host cell replication machinery to the viral genome. The replication can be detected at 12-20 hpi [Piper, 1979]. Regulation of LT activity occurs via its phosphorylation [Howes et al., 1996].

VP1, VP2 and VP3 are encoded in the late region of the polyomavirus genome. Their abundant production occurs in the late phase after the start of viral DNA replication. Genomes of primate polyomaviruses, for example SV40, BKPyV and JCPyV encode also another late regulatory protein called agnoprotein, involved in different processes such as viral transcription, replication or virion morphogenesis [Jay et al.,1981; White et al., 2009].

Interestingly, the promoter of the late region of viral DNA is switched on even in early phase of infection and regulation of expression is rather connected with a change in the processing of late-strand transcripts (termination/polyadenylation and splicing) [Hyde-Deruyscher and Carmichael, 1988; Garren et al., 2015]. Organization of MPyV genome is shown in Figure 3.

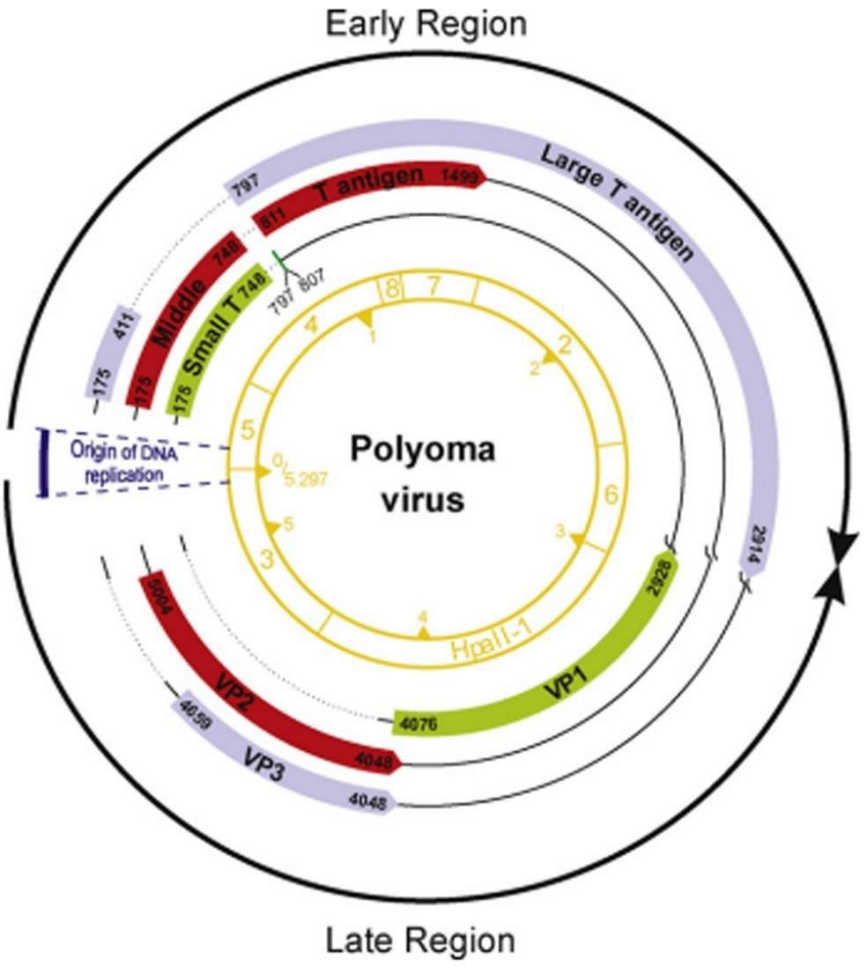

Figure 3. Organization of the mouse polyomavirus genome. The viral dsDNA is shown with the original HpaII restriction map divisions. Numbering of nucleotide pairs starts from bi-directional Ori. The mRNA products and the direction of transcription are shown by black lines outside. Alternative introns are shown by broken lines, non-coding regions are shown by solid lines and proteins are presented by colored lines. Figure is taken from Atkin et al., 2009.

2.1.4. Intracellular trafficking

Initiation of polyomavirus infection starts from interaction of the major capsid VP1 with cellular receptors. All polyomaviruses use sialic acid containing receptors [Ströh and Stehle, 2014; O'Hara et al., 2014]. MPyV interacts with ganglioside receptors GD1a, GT1b and α4β1 integrin heterodimer (as post attachment receptor) [Tsai et al., 2003; You et al., 2015; Caruso et al., 2003]. Human polyomaviruses BKPyV and MCPyV both bind sialic acids on GD1b and/or GT1b gangliosides [Erickson et al., 2009; Low et al., 2006], whereas SV40 utilizes GM1 receptor. [Tsai et al., 2003; You et al., 2015; Caruso et al., 2003]. Furthermore, additional cell-surface interactions of polyomaviruses have been described — BKPyV with N-linked glycoprotein containing α(2,3)-linked sialic acid [Dugan et al., 2005], or SV40 with class I major histocompatibility proteins (MHC-I) [Atwood et al., 1989]. Interestingly, virions of

SV40 and MCPyV interact with both branches of GM1 and GT1b receptors, respectively, while MPyV and BKPyV interact only with the one branch. While VP1 of SV40 and MPyV have contacts with one molecule of sialic acid, VP1 of MCPyV and BKPyV requires (according to *in vitro* studies) presence of two sialic acid molecules (Figure 4) [Erickson et al., 2009].

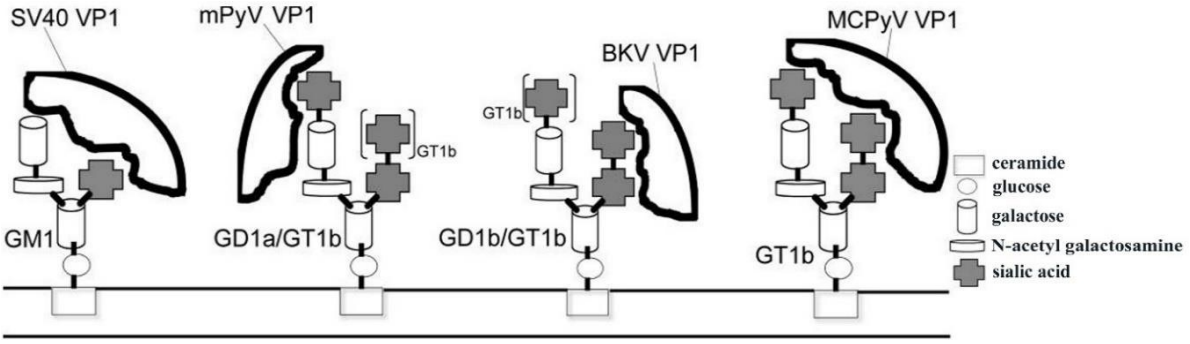

Figure 4. Model of interaction between polyomaviruses and different ganglioside receptors on the cell surface. Figure is taken from Erickson et al., 2009.

After adsorption of the virus, small invaginations are formed around virus particles [Ewers et al., 2010; Mackay and Consigli, 1976]. These invaginations grow into smooth monopinocytotic vesicles. Vesicles utilized by SV40 and MPyV are caveolin-enriched, but the presence of caveolin on smooth monopinocytic vesicles is not required [Norkin, 1999; Anderson et al., 1996; Richterova et al., 2001; Damm et al., 2005; Gilbert, Benjamin, 2000; Liebl et al., 2006]. BKPyV and MCPyV enter to cells also via vesicles, derived from caveolin rich domains, while JCPyV is internalized into clathrin-coated pits [Moriyama et al., 2007; Schowalter et al., 2011; Pho at al., 2000]. In addition, recently was shown that BK and JC polyomaviruses can be transmitted into cells by exosomes, independently of cellular receptors [Handala et al., 2020, Morris-Love et al., 2019].

On the productive pathway, vesicles containing viral particles fuse with early endosome antigen 1 (EEA1) positive vesicles. The colocalization of EEA1 with MPyV VP1 protein can be detected already at 30 minutes post infection. Acidic pH of these endosomes is required for productive infection of MPyV, SV40 and BKPyV [Liebl et al., 2006; Engel et al., 2011; Jiang et al., 2009]. Jiang et al. found that acidic pH induces rearrangements in a capsid of BK polyomavirus and is required during all stages of virus trafficking from the early endosomes to ER [Jiang et al., 2009]. Treatment of 3T6 and normal mouse mammary gland cells with bafilomycin A1, which prevents endosomal acidification completely abolished MPyV infection [Liebl et al., 2006].

After appearance of MPyV or SV40 in early, Rab5 GTPase positive endosomes, the

virus can be detected in Rab7-positive late endosomes [Zila et al., 2014].

The virus is further sorted to the endoplasmic reticulum prior to its entry into the cell nucleus. Qian et al. demonstrated that only particles, trafficking in complex with ganglioside receptors, but not glycoproteins, can translocate to ER, while the rest of virions is transported to lysosomes for degradation [Qian et al., 2009; Qian, Tsai, 2010].

Upon polyomavirus arrival to the ER, covalent bonds participating in stabilization of viral capsid are reduced and isomerized by chaperons present in ER. Schelhaas et al. found that SV40 disassembly within ER occurs through a multifunctional redox chaperones - protein disulphide isomerase (PDI) and endoplasmic reticulum protein 57 (ERp57). They show that ERp57 isomerizes interchain disulfides in VP1 pentamers. It results in uncoupling 12 of 72 VP1 pentamers from the virus capsid [Schelhaas et al., 2007]. MPyV utilizes ERp29-PDI-ERp57 network, which is required for the exposing of the C-terminus arms of VP1 molecules leading to formation of hydrophobic virion particles with affinity to a lipid bilayer. Additionally, ERp72 can individually act on MPyV virion structure in ER [Magnuson et al., 2005; Walczak, Tsai, 2010]. Similar to other polyomaviruses, productive infection of JCPyV requires interaction with ER chaperones PDI, ERp57, ERp72 and ERp29. Knockdown of any of these proteins results in significant reduction of viral infection [Nelson et al., 2012]. Later, another member of the protein disulfide isomerase family of proteins localized to the endoplasmic reticulum, ERdj5, was found to interact with BKPyV and SV40 capsids [Inoue et al., 2015]. Conformational changes, occurring in the capsid of polyomaviruses lead to exposure of hydrophobic domains of the VP2 and VP3 proteins [Magnuson et al., 2005; Inoue, Tsai, 2013]. These minor capsid proteins have viroporin activity and can disrupt ER membrane during translocation of polyomaviruses to the cell nucleus (Figure 5) [Giorda et al., 2013, Huerfano et al., 2017].

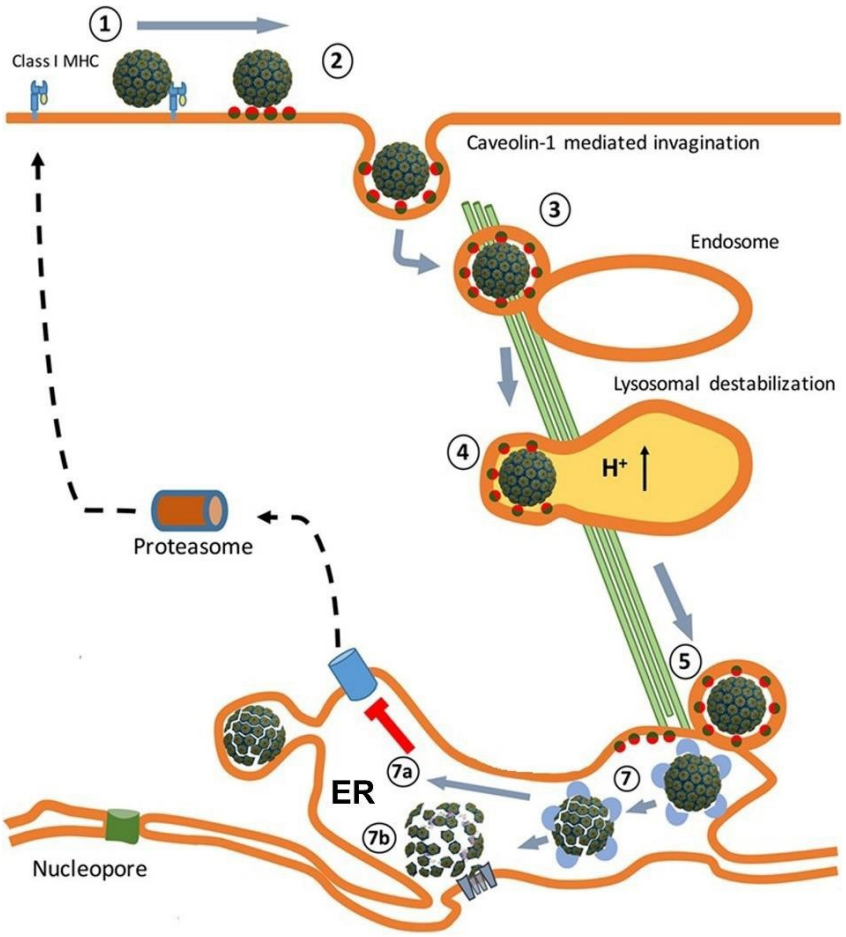

Figure 5. Model of SV40 trafficking from the cell receptor to the ER. (1) Virus interaction with MHC-I molecule on the cell surface. **(2)** Release from MHC-I molecules, interaction with GM1 receptors and formation of caveolae vesicles. **(3)** Endosome internalization. **(4)** Endosome maturation and particle destabilization. **(5)** Release from endolysozomal compartment and trafficking to the ER. **(7)** ER mediated particle destabilization. **(7a)** Transport for the degradation. **(7b)** Viroporin mediated perforation of ER membrane. The figure is adapted from Toscano and de Haan, 2018.

1.5 Nuclear entry of polyomaviruses

MPyV, as other polyomaviruses, replicates its genome in the cell nucleus. Thus, nuclear import of MPyV DNA is essential for productive infection.

Over the years, three different ways of entering the virus to the nucleus have been proposed: i) direct fusion of the virus carrying vesicles with the nuclear envelope or the alteration of nuclear envelope integrity during the virions translocation from cytosol to the nucleus ii) virus penetration through inner nuclear membrane directly from ER to the cell nucleus, and iii) release of virions from ER to the cytosol and following translocation from cytosol to the nucleus mediated by cellular importins and occurring via nuclear pores.

i) Early electron microscopy analysis studies suggested that SV40 and MPyV enter the nucleus by fusion of vesicles carrying virions directly with the nuclear envelope, bypassing

nuclear pores (Figure 6) [Hummeler et al., 1970; Mackay and Consigli, 1976]. Hummeler et al. found SV40 particles in the nucleus as soon as 1 hpi. They also observed disturbance of nuclear membrane near to the particle appearing in the nucleus. However, the particles observed in the nucleus were unenveloped, that pointed to the fusion of membranes of the virus carrying vesicles with a nuclear envelope during virion entry to the nucleus [Hummeler K. et al., 1970]. Similar observation has been described by other authors [Maul et al., 1978; Griffith et al., 1988; Nishimura et al., 1991]. Drachenberg and co-authors also showed the fusion of vesicles containing BKPyV virions with nuclear membranes. Location of BK virus in close vicinity to nuclear pores was rarely observed [Drachenberg et al., 2003].

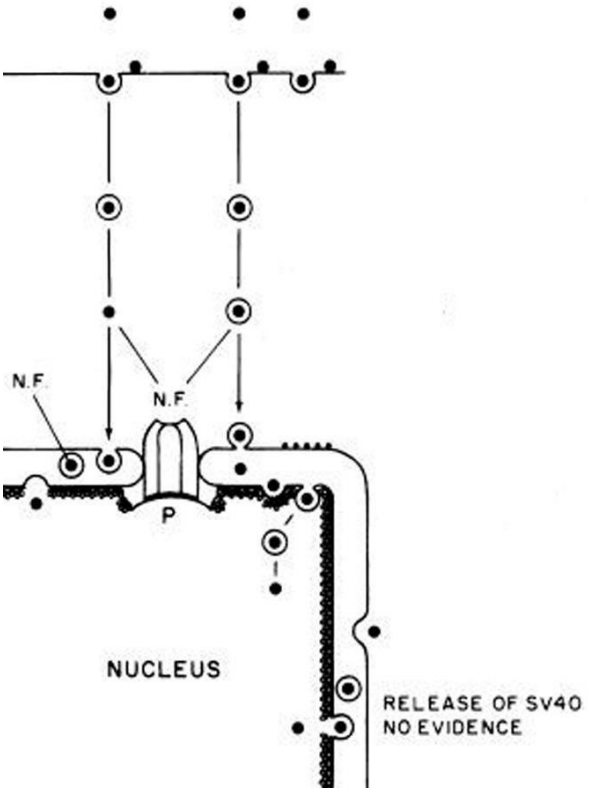

Figure 6. Schematic representation of the first possible mechanism of SV40 entry into the cell nucleus. NF - not found, P - nuclear pore. Adapted from Maul et al., 1978.

Two other ways of virus entry to the nucleus assume that virions must pass through the endoplasmic reticulum before they can be translocated to the nucleus.

ii) Direct translocation of SV40 from ER to the cell nucleus was proposed by Butin-Israeli et al. They found that SV40 induced nuclear envelope deformation and dephosphorylation of lamin A/C epitopes before and during viral entry to the nucleus of non-dividing cells. Interestingly, the VP1 pentamer was sufficient for induction of the signals leading to fluctuations in lamin A/C during viral trafficking from ER to the nucleus (Figure 7) [Butin-Israeli et al., 2011]. According to their hypothesis, the appearance of the capsid proteins

in the cytosol does not represent a productive pathway of the virus but, it is a part of a degradation pathway and is in an agreement with the fact that the majority of viral particles are unable to inter the cell nucleus.

iii) Regarding the third pathway, Norkin et al. demonstrated that SV40 virions, delivered to the rough endoplasmic reticulum by retrograde endocytic pathway, undergo conformational changes, which lead to exposing of VP2 and VP3 minor capsid proteins to ER membrane. Hydrophobic domains of the minor capsid proteins help virions to escape from ER to the cytosol. On the next stage, viral DNA in complex with capsid proteins translocates from cytosol to the nucleus [Norkin et al., 2002].

Bennett suggested that polyomaviruses use the canonical route of trafficking through the nuclear pore complex with involvement of importins (Figure 7) [Bennet, 2014]. Importins mediate the nuclear entry of proteins that contain a classical NLS [Adam, Gerace, 1991]. All capsid proteins (VP1, VP2 and VP3) of SV40, MPyV and BKPyV polyomaviruses, as well as cellular histones, presenting in virus nucleocore, contain NLS [Liddington et al., 1991; Chang et al. 1993; Ishii et al. 1994; Chen et al., 1998; Bennet et al. 2015; Baake et al., 2001]. Nakanishi et al. demonstrated that the nuclear entry of SV40 occurs through NLS of VP3 protein which interacts with α2β importins. VP3 null mutants can normally assemble in virion-like particles in transfected cells, but they are impaired for delivery of viral genome to the nucleus in newly infected cells. VP1 protein also has NLS signal, but its sequence overlaps with DNA binding domain and is masked from importin recognition [Nakanishi et al., 2002]. In agreement, it was demonstrated that infectivity of BKPyV also depends on NLSs of the minor capsid proteins VP2 and VP3. Site-direct mutagenesis in NLS of minor proteins reduced viral infectivity to half [Bennet et al., 2015]. However, Qu et al. showed that the nuclear translocation of JC virus like particles (VLPs) composed of VP1 and viral DNA, occurs through the interaction of VP1 NLS with cellular importins. [Qu et al., 2004].

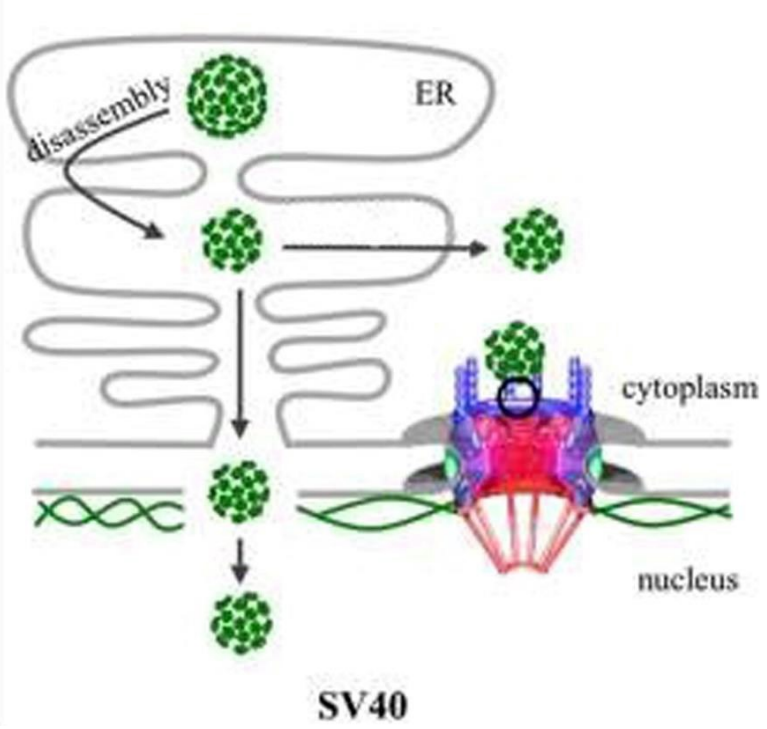

Figure 7. Second and third possible mechanisms used by SV40 for the nuclear entry. SV40 partially disassembles inside the ER, and subviral particles could pass through two different pathways to deliver their genomes into the cell nucleus. The first one suggests direct translocation from ER to the nucleus with disruption of the inner nuclear membrane. The second way involves exit of viral particles from ER to cytosol and transport through nuclear pore with participation of importins. Figure is adapted from Fay and Pante, 2015.

2.1.6. Mechanism of importin mediated trafficking through the nuclear pore

Transport of molecules from the cytoplasm to the nucleus and back is controlled by nuclear pore complex (NPC). The number of NPCs depends on the cell size and intensity of transcription [Freitas and Cunha, 2009].

The NPC provides two types of transport: passive diffusion of small molecules (up to ~40 kDa) and active transport of larger molecules and complexes [Timney et al., 2016]. The classical active transport is mediated by soluble receptors karyopherins α and β. The karyopherin β-family (importin β) represents the major class of receptors which can associate with imported cargoes directly or via karyopherins α (importins α) [Pumroy and Cingolani, 2015]. More than 10 isoforms of importin β and 6 isoforms of importin α were identified in mouse cells (KPNA1, KPNA2, KPNA3, KPNA4, KPNA6, and KPNA7) [Okada et al., 2008; Mason et al., 2009; Tsuji et al., 1997; Hu et al., 2010]. It was shown, that during cell differentiation, production of individual subfamilies of alpha importins in mouse cells can change. In some mouse organs (e.g. kidney) all types of alpha importins are present, whereas in others (brain) there are only some subtypes [Yasuhara et al., 2013; Kamei et al., 1999].

Nuclear localization sequences are the best characterized signals for recognition with alpha importins. The firstly described NLS belongs to SV40 LT antigen [Kalderon et al., 1984]. NLSs contain one or more clusters of basic amino acids and can be monopartite or bipartite [Dingwall and Laskey, 1991].

Importin alpha has two large NLS binding domains (major and minor) built form armadillo repeats. Fontes et al. showed that monopartite NLS of SV40 LT antigen binds the major domain of alpha importins, while bipartite NLS of nucleoplasmin binds both domains simultaneously [Fontes et al., 2000]. Chang et al. identified classical monopartite NLSs in MPyV VP1 and VP2 capsid proteins required for their transport to the nucleus for virus assembly [Chang et al., 1992].

During the classical nuclear transport, importin α interacts with a protein carrying nuclear localization signal. Then, through its N-terminus domain, importin α binds importin β1. The trimeric complex importin α - protein with NLS - importin β1 translocates to the cell nucleus, where GTP-binding nuclear protein Ran (RanGTP) recognizes the N-terminus of importin β1, destabilizes the complex and cargo protein releases from the import complex. Importins α and β1 - RanGTP exit to the cytosol where importin β1 is released upon RanGTP hydrolysis. After that, importins again can participate in the next round of trafficking (Figure 8) [Wubben et al., 2020].

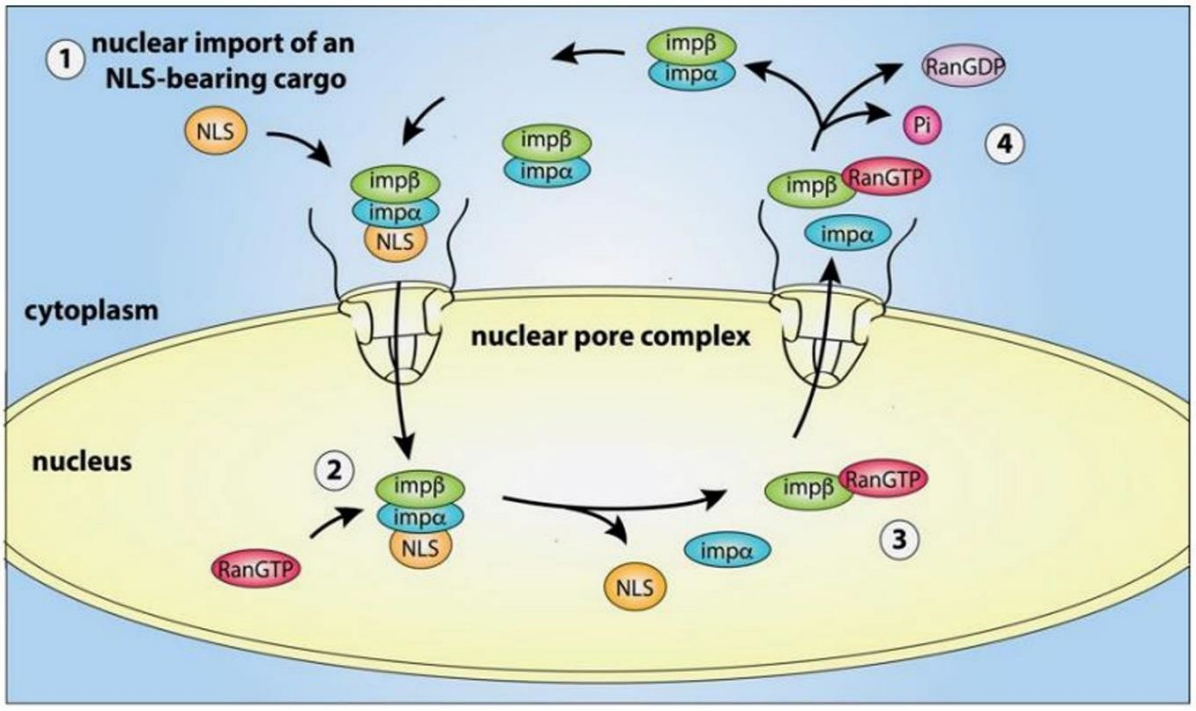

Figure 8. The schema of classical active import through nucleopore. (1) NLS-bearing cargo interacts with importin α/β complex in cytosol and translocates through nuclear pore complex into the nucleus. **(2)** Following import, RanGTP binds importin β. **(3)** This induces the release of cargo and **(4)** recycling of importins α, β and RanGTP. Figure is taken from Wubben et al., 2020.

2.2. Immune system

The immune system is a large network of organs, cells and chemicals which protect organisms from different pathogens. Many species have two subtypes of immune system: innate immunity and adaptive immunity.

The innate immunity serves as the first line of defense against different germs and viruses and enclose almost all tissues in mammals. The virus invasion can initiate innate defense through pattern recognition receptors (PRRs) which recognize pathogen-associated molecular patterns (PAMPs), small molecular motifs conserved within microbes. They include e.g. lipopolysaccharides, lipoproteins or proteins of bacteria. For viruses, primarily nucleic acids, such as DNA, ds- and single-stranded RNA (ssRNA), RNA with 5'-triphosphate ends and also viral proteins can be recognized by PRRs [Sparrer and Gack, 2015]. Currently, several types of PRRs have been shown to be involved in the identification of viral components, namely some toll-like receptors (TLRs), intracellular receptors - retinoic acid-inducible gene I (RIG-I)-like receptors (RLRs), absent in melanoma 2 (AIM2)-like receptors (ALRs) and, other DNA sensors [Brubaker et al., 2015; Aoshi et al., 2011]. Detection of viral components by these receptors activates production of IFNs and various cytokines (interleukins). There are three groups of IFN: IFN I, IFN II and IFN III. Type I IFNs are known as antiviral IFNs and include IFN-α (produced in leukocytes), IFN-β (produced in fibroblasts), IFN-ε, IFN-ω, IFN-κ, IFN-δ, IFN- τ and IFN- ζ [Imanishi, 1994; Li et al., 2018]. Additionally, type I IFNs have immunomodulatory functions [González-Navajas et al., 2012]. IFN II is presented by only IFN-γ and produced mainly in natural killer cells and activated lymphocytes and has antiviral, immunomodulatory and antitumor properties [Stetson et al., 2003; Kasahara et al., 1983; Gresser, 1990]. IFN-III includes four IFN-λ molecules: IFN-λ1, IFN-λ2, IFN-λ3, and IFN-λ4 and protects mucosal epithelial cells from viral infection [Wack et al., 2015].

Signaling from different sensors also induces production of restriction factors, which prevent viral transcription and/or replication and establish antiviral immunity. For instance, structural maintenance of chromosome proteins 5 and 6 (SMC5/6) complex, participating in a genome maintenance represses the transcription of hepatitis B virus [Niu et al., 2017]. Apolipoprotein B mRNA editing enzyme, catalytic polypeptide-like 3G (APOBEC3G) induces mutagenesis in human immunodeficiency virus (HIV) DNA and prevents its reverse transcription and chromosomal integration. Human MxA protein blocks secondary transcription and replication of influenza A virus, while mouse myxovirus resistance protein 1 (MX-1) blocks primary transcription of viral RNAs [Yan, Chen, 2012]. Pathogens that

overcome innate defense mechanisms encounter adaptive immunity. This type of immune system is made up of T and B lymphocytes and antibodies [Bonilla, Oettgen, 2010]. T cells recognize antigens presented on the cell surface and either kill infected cells or stimulate B cells for production of specific antibodies. Antibodies bind viral particles in the blood and mucosal surfaces and prevent spreading of infection [Nicholson, 2016]. Subpopulation of B cells does not produce antibodies and converts into long-living memory cells. Upon infection with the same pathogen, they are reactivated and synthesize specific antibodies [Kurtz, 2004]. Addittionaly, T cells also differentiate into memory cells [Pennock et al., 2013].

Innate and adaptive immune systems are able to communicate during viral infection that allows to shape the specific response. This cross-talk occurs through cytokines and cell-to-cell contacts and can be bidirectional between two systems [Getz, 2005].

2.2.1. RNA sensors

RNA sensors can be classified as endosomal or cytoplasmic PRRs. Cytoplasmic RNA sensors are the kye pathogen sensors which activate expression of antiviral genes and production of IFN I and other cytokines in infected cells and surrounding tissues. They belong to the family of RLRs, which includes retinoic acid-inducible gene I (RIG-I), melanoma differentiation associated gene-5 (MDA-5) and laboratory of genetics and physiology 2 (LGP2) [Takeuchi, Akira, 2010]. RIG-I and MDA-5 have two N-terminal tandem caspase activation and recruitment domains (CARDs) which function in signaling, DExD/H-box helicase domain and C-terminal domain (CTD), known as the repressor domain [Sun, 1997; Zhang et al., 2000; Onomoto et al., 2007]. CARDS mediate downstream signal transduction, while helicase and CTD domains work together to detect immunostimulatory RNAs [Rehwinkel, Gack, 2020]. LGP2 has only the helicase and CTD domains and lacks the CARD domain (Figure 9) [Saito et al., 2007].

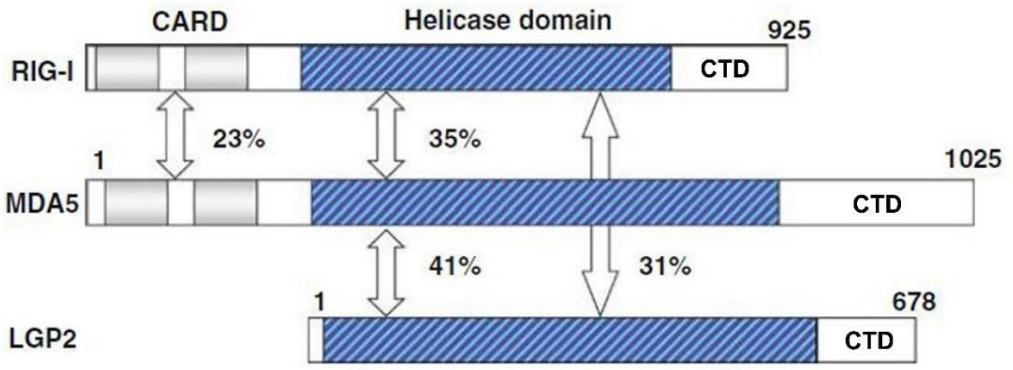

Figure 9. Schema of the structure of RIG-I-like receptors. RIG-I and MDA-5 receptors contain CARD, helicase and CTD domains. LGP2 protein has only helicase and CTD domains**.** Percentage indicates amino acid identity between corresponding domains. Figure is taken from Onomoto et al., 2007.

RIG-I is the first recognized and studied RLR sensor, which is highly conserved among mammals. Moreover, RIG-like molecules are found in nematodes, sea anemones and sponges [Kolakofsky et al., 2012]. RIG-I predominantly recognizes short dsRNA molecules, which have 5′-triphosphate or diphosphate groups [Hornung et al., 2006; Pichlmair et al., 2006]. Such groups are very often presented at the ends of positive ssRNA viruses (for example, Sendai virus, flavivirus) but can be also formed by negative-strand RNA viruses (vesicular stomatitis virus, influenza virus, Rift Valley fever virus, measles) [Kato et al., 2005; Chang et al., 2006; Loo, Gale, 2011]. Saito et al. found that A/U-rich motif in the 3′-untranslated region of the hepatitis C virus genome can be detected with RIG-I [Saito et al., 2008]. Moreover, RIG-I can associate with microRNAs, snRNAs, which participate in important cellular processes, such as expansion of cancer cells, therapy resistance and activation of B cells independentlyof T cells [Karlsen, Brinchmann, 2013; Boelens et al., 2014; Ranoa et al., 2016]. Also, exosomes from breast cancer cells transfer non-coding repetitive viral elements, which can be recognized by RIG-I and activate IFN I pathway resulting in therapy resistance [Boelens et al., 2014]. Qiang et al. and Hou et al. showed that RIG-I also suppresses tumorigenesis in acute myeloid leukemia and hepatocellular carcinoma cells [Qiang et al., 2011; Hou et al., 2014]. Previously, it was shown, that 13 base pairs of dsRNA are the minimal length needed for activation RIG-I [Anchisi et al., 2015]. Then, Kohlway et al. demonstrated that 10 base pairs dsRNA loops can also activate type I IFN production in cells and mice [Kohlway et al., 2013].

MDA-5 is found in different vertebrates – mammals, birds, fish, amphibians [Zou et al., 2009]. This protein interacts with long molecules of cytosolic RNA without end specificity [Kato H. et al., 2008]. Such molecules are formed in the genomes of dsRNA or single-stranded

positive RNA viruses, such as encephalomyocarditis virus [Kato et al. 2011; Triantafilou et al., 2012]. Moreover, it was found that MDA5 can activate IFN production during malaria infection [Ye et al., 2018]. Interestingly, unlike RIG-I, which interacts with RNA ends, MDA5 binds dsRNA stems [Wu et al., 2013].

The autoinhibition of RIG-I was found in resting cells. This occurs, when CTD domain of RIG-I interacts with RNA binding domain and helicase domain [Saito et al., 2007]. CARDs of RIG-I can also fold one over other in non-infected cells [Kowalinski et al., 2011]. After interaction with viral RNA, RIG-I hydrolyzes ATP. That results in conformational changes and release of CARD domains [Qiang et al., 2011; Kowalinski et al., 2011]. It is suggested that MDA-5 can also exist in closed and open forms [Brisse, Ly, 2019]. In inactivated form, MDA-5 and RIG-I are phosphorylated with protein kinase C α/β (PKC-α/β), choline kinase β (CKβ) (RIG-I), and RIO 3 kinase (MDA-5) [Maharaj et al., 2012; Sun et al., 2011; Takashima et al., 2015]. Also, RIG-I has acetylated C-terminal domain in the absence of RNA and requires deacetylation with histone deacetylase 6 for the sensing [Choi et al., 2016].

Due to the fact, that LGP2 lacks CARD domains, it does not have the independent signaling activity. Several researchers demonstrated that LGP2 plays a role of the negative and positive regulator of RIG-I and MDA-5 activity [Rodriguez et al., 2014].

TLR3, TLR7, and TLR8 represent endosomal RNA sensors [Kawai, Akira, 2010]. TLR3 recognizes viral dsRNA, Polyinosinic:polycytidylic acid (Poly I:C), small interfering RNAs (siRNA), and self-RNAs derived from damaged cells [Alexopoulou et al., 2001; Kariko et al., 2004; Bernard et al., 2012]. TLR3 is expressed at high levels in myeloid dendritic cells (DCs) [Matsumoto et al., 2003]. Also, it can be find in macrophages, fibroblasts and epithelial cells [Matsumoto et al., 2002; Erdinest et al., 2014]. TLR7 recognizes single-stranded viral RNA (for example, RNA of vesicular stomatitis virus, influenza A virus and human immunodeficiency virus) and is expressed predominantly in plasmacytoid DCs (pDCs) [Lund et al., 2004; Beignon et al., 2005; Mancuso et al., 2009]. Human TLR8 also recognizes ssRNA of different viruses such as influenza virus, Sendai virus, and coxsackie B virus [Finberg et al., 2007]. This receptor is mainly expressed in monocytes/macrophages and myeloid dendritic cells [Alexopoulou et al., 2012; Hornung et al., 2002]. TLRs are composed of an ectodomain containing leucine-rich repeats involved in PAMP recognition, a transmembrane domain and the intracellular Toll IL-1 receptor (TIR) domain, subdivided into three boxes and enabling downstream signal transduction (Figure 10) [Tesar, 2007].

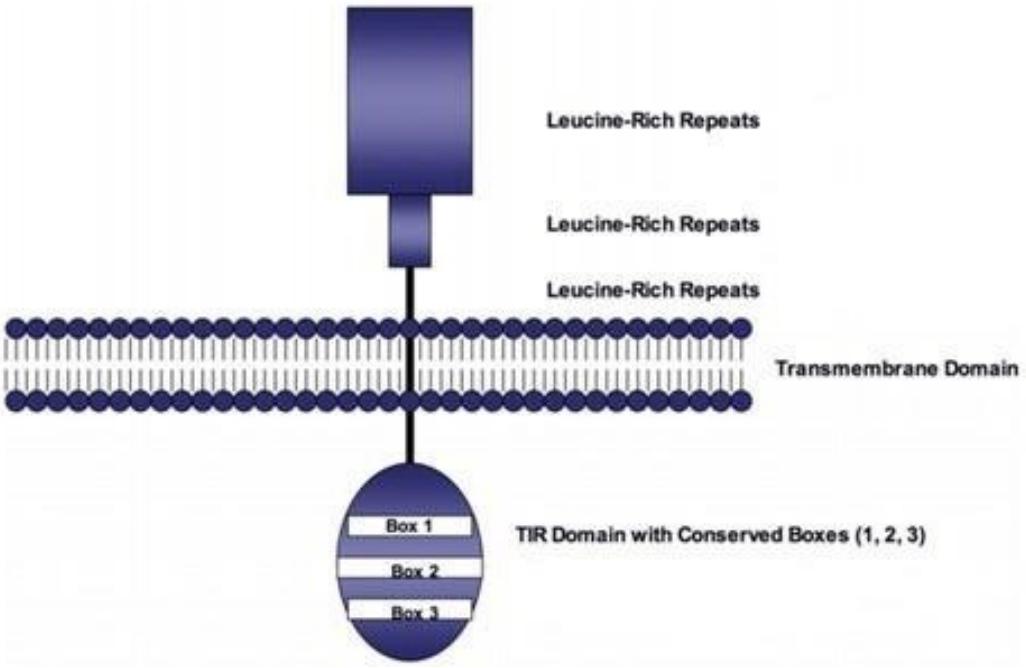

Figure 10. Scheme of of TLR structure. Leucine-rich repeats are involved in recognition of PAMPs and subsequent signal transduction. The cytoplasmic TIR domain has 3 conserved boxes that vary in size and are used for interaction with downstream signal adaptor molecules. Adapted from Tesar, 2007.

TLRs are produced in ER and transported to Golgi, where they are sorted to endosomes [Lee et al., 2013]. After delivery to the endosome, TLRs undergo proteolytic cleavage by cathepsins to have an active form recuired for RNA recognition and signaling [Garcia-Cattaneo et al., 2012; Ishii et al., 2014]. Activation of TLRs leads to production of different cytokines and and type I IFNs [Kawai, Akira, 2011].

2.2.2. RNA sensing pathways

The signaling ofviral infection can be initiated by the recognition of pathogenic RNA with RLRs and results in production of IFN I and/or other cytokines. Interaction between RIG-I and viral RNA in the ATP-dependent manner leads to RIG-I movement along RNA molecule and oligomerization. Then, RIG-I is ubiquitinated with tripartite motif protein 25 (TRIM25). Inhibition of ubiquitination prevents interferon signaling [Gack et al., 2010; Nistal-Villan et al., 2010]. After ubiquitination, the entire complex translocates from cytoplasm to mitochondrial membrane and interacts with the membrane-bound mitochondrial antiviral signaling adaptor protein (MAVS) through CARD interactions [Kawai et al., 2005].

MDA-5 binds dsRNA through internal DExD/H-box helicase domain and C-terminus. The C-terminal helix of MDA-5 interacts with the phosphate backbone of the RNA through

strong electrostatic interactions on the major groove of RNA [Li et al., 2009; Wu et al., 2012]. After interaction, the N-terminal CARD of MDA-5 undergoes dephosphorylation. Lin et al. found that 14-3-3η chaperone interacts with N-terminal CADR domain of MDA5 and stimulates its oligomerization which results in a ring formation around RNA [Lin et al., 2019]. After that, MDA-5 translocates from the cytoplasm to the mitochondrial membrane and interacts with MAVS, as RIG-I.

MAVS plays a role of adaptor protein, which works downstream of RNA sensors and links them to upstream proteins. MAVS (also called VISA, CARDIF, or IPS-1) has N-terminal CARD-like domain, which is very similar to CARDs of RIG-I and MDA-5, proline-rich region in the middle part and hydrophobic transmembrane domain at C-terminus [Seth et al., 2005]. The transmembrane domain of MAVS attaches protein to the outer mitochondrial membrane. Loss of this domain completely abolishes production of IFN-β and turns MAVS into soluble cytosolic protein, whereas full-length MAVS is found in a membrane pellet. Mislocalization of MAVS to ER or plasma membrane due to mutations in the transmembrane domain inhibits its activity [Seth et al., 2005]. Interestingly, Dixit et al. found MAVS in peroxisomes of MEF cells, mouse macrophages and human hepatocytes. Peroxisomal MAVS was unable to induce IFN-β response during reovirus (which induces RIG-I and MDA5 signaling pathways) and influenza virus infection but promotes expression of interferon stimulated gene, viperin. Authors suggest that during reovirus infection, activation of both mitochondrial and peroxisomal MAVS occurs. The activation results in maximal antiviral gene expression [Dixit et al., 2010]. Kawai et al. demonstrated that RIG-I and MDA-5 interact with MAVS through their N-terminal CARD domains. Absence of these domains results in a weak interplay [Kawai et al., 2005]. During viral infection, direct interaction between CARDs of RNA sensors and MAVS results in a formation of large MAVS aggregates which activate IRF3 [Hou et al., 2011; Peisley et al., 2013; Wu et al., 2012].

Then, MAVS interacts either with i) Tank binding kinase-1 (TBK1), TNF receptor-associated factor (TRAF) 3 and inhibitor of κB kinase (IKK) ε, and thus ensures phosphorylation of IRF3 that leads to production of IFN I, or ii) with IKKα/β/NEMO complex that results in upregulation of proinflammatory genes dependent on nuclear factor kappa-light-chain-enhancer of activated B cells (NF-kB) (Figure 11) [Belgnaoui et al., 2011].

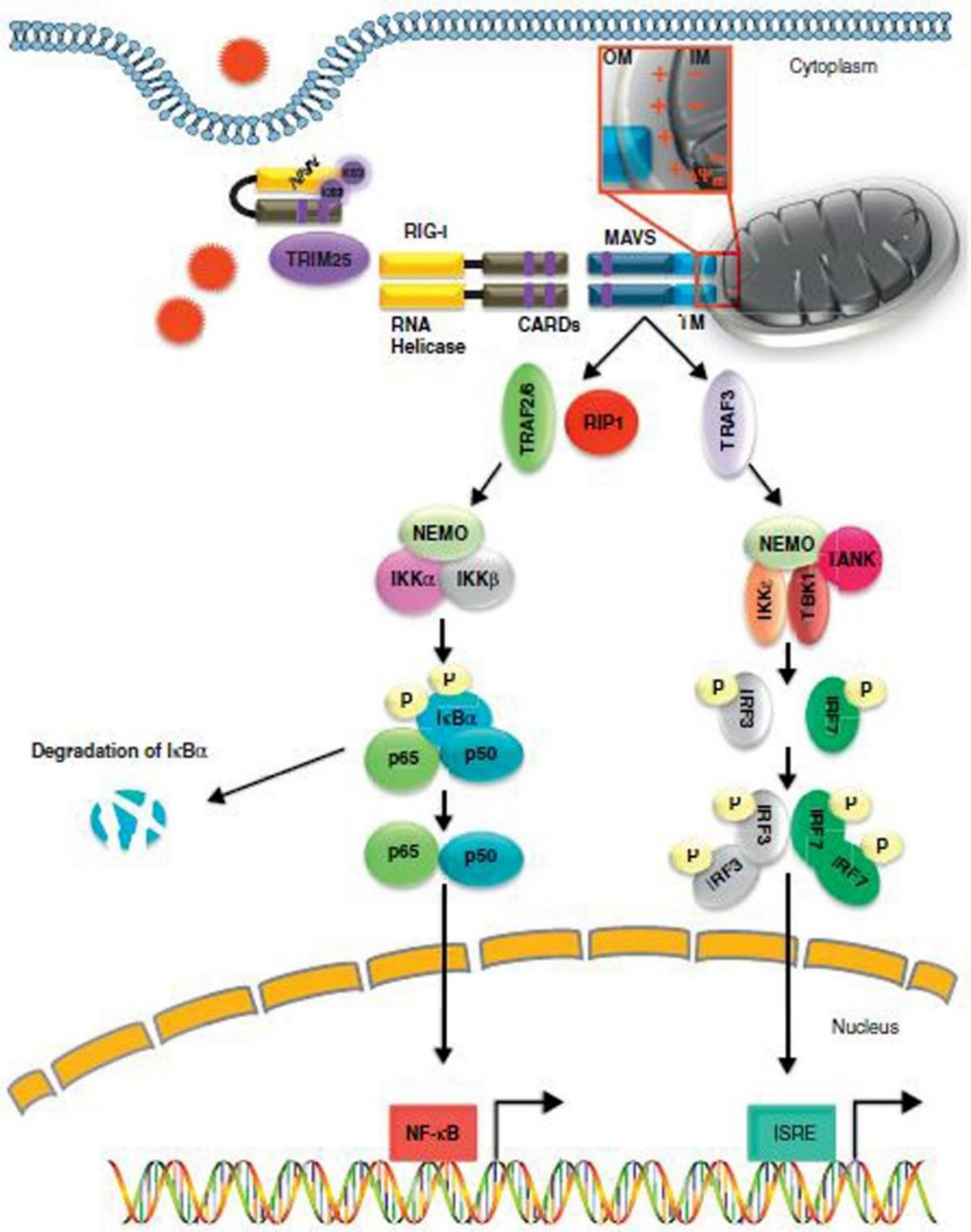

Figure 11. Schematic representation of the RIG-I signaling pathway. RIG-I is shown in a closed conformation and upon detection of intracellular viral RNA, several molecular events occur — protein unfolding, ubiquitination of the CARD domain by TRIM25, dimerization and interaction with the adaptor molecule MAVS at the mitochondrial outer membrane (OM). MAVS function is dependent on a normal mitochondrial membrane potential (DCm) at the inner membrane (IM). MAVS dimerizes and recruits adaptor proteins that activate transcription factors NF-kB, IRF3 and IRF7. Induction the NF-kB pathway occurs via the recruitment of TRAF2/6 and RIP1, followed by the activation of the IKK complex that will phosphorylate the inhibitor of NF-kB (IkBa), causing its proteasomal degradation, release and translocation of active NF-kB dimers to the nucleus. In the IFN arm of the RIG-I pathway, TRAF3 interacts with MAVS which leads to the recruitment of the TANK/NEMO/IKKε/TBK1 complex and subsequent phosphorylation, dimerization and translocation of both IRF3 and IRF7 to the nucleus. IRF3 and IRF7 dimers bind ISRE (Interferon Stimulated Response Elements) promoters to induce IFN regulated genes. Figure is taken from Belgnaoui et al., 2011.

i) Firstly, TBK1 binds TRAF and IKKε, making a pre-assosiated complex, which can be detected in resting cells. After viral infection, this complex is recruted to MAVS and autophosphorylated [Fang et al., 2017]. Because the TBK1-TRAF-IKKε complex localizes in cytoplasm, there should be some adaptor molecule for its interaction with MAVS. One of such adaptors is IFIT3 (IFN-inducible protein with tetratricopeptide repeats), which colocalizes with a mitochondrion. Absence of IFIT3 results in a weak interaction of MAVS and TBK1. Additionally, silencing of IFIT3 inhibits transcription of IRF3 during Senday virus infection or Poly I:C treatment, while its induction increases IRF3 phosphorylation [Liu et al., 2011]. At the next stage, activated TBK1 binds IRF3 or IRF7, which is present in cytosol as inactive monomer. Interaction with TBK1 results in phosphorylation of S385 and S386 residues of IRF3 and its dimerization [Takahasi et al., 2003]. After dimerization, IRF3 or IRF7 translocates to the nucleus where it interacts with IFN I genes and stimulates its transcription [Taniguchi et al., 2001].

ii) In contrast to the first pathway, activation of proinflammatory genes requires MAVS interaction with TRAF2 and TRAF6. Then, in cooperation with receptor-interacting serine/threonine-protein kinase1 (RIP1), TRAF activates IKKα/β/NEMO complex, resulting in IkB phosphorylation and degradation. That results in NF-kB release and translocation to the nucleus where it activates inflammation genes [Hayden, Ghosh, 2012].

RNA recognition with TLRs stimulates downstream signaling cascades that initiate activation of type I IFN and/or other cytokins. TLR3 activates TIR-domain-containing adapter-inducing interferon-β (TRIF) - dependent pathway, while TLR7 and TLR8 activate myeloid differentiation primary response 88 (MyD88) - dependent pathway [Kawasaki, Kawai, 2014].

During TRIF signaling pathway, TRIF either: 1) activates production of IFN I or, 2) synthesis of different cytokines.

1) After binding to TLR3, TRIF protein interacts with TRAF3 and recrutes nucleosome assembly protein 1 (NAP1). This stimulates binding of TBK1/IKKi for phosphorylation of different IRFs, which dimerize and translocate from cytoplasm to the nucleus, and induce IFN I genes expression (Figure 12) [Akira et al., 2006; Thwaites et al., 2014].

2) TRIF interacts with RIP-1 which stimulates activation of NF-kB followed by its delivery to the nucleus and cytokines production (Figure 12) [Akira et al., 2006; Thwaites et al., 2014]. The engagement of TLR7 and 8 with RNA induces recruitment of MyD88 protein and interaction with IL-1 receptor-assosiated kinases IRAK1 and IRAK4. Activation of IRAK proteins results in their association with TRAF6 (in case of signaling through TLR8) or

3) TRAF6/TRAF3 (during signaling through TLR7). Interaction of TRAF6 with IKK complex leads to NF-kB activation and cytokines production while TRAF6/TRAF3 binds IRF proteins and stimulates IFN I synthesis (Figure 12) [Yamamoto et al., 2002].

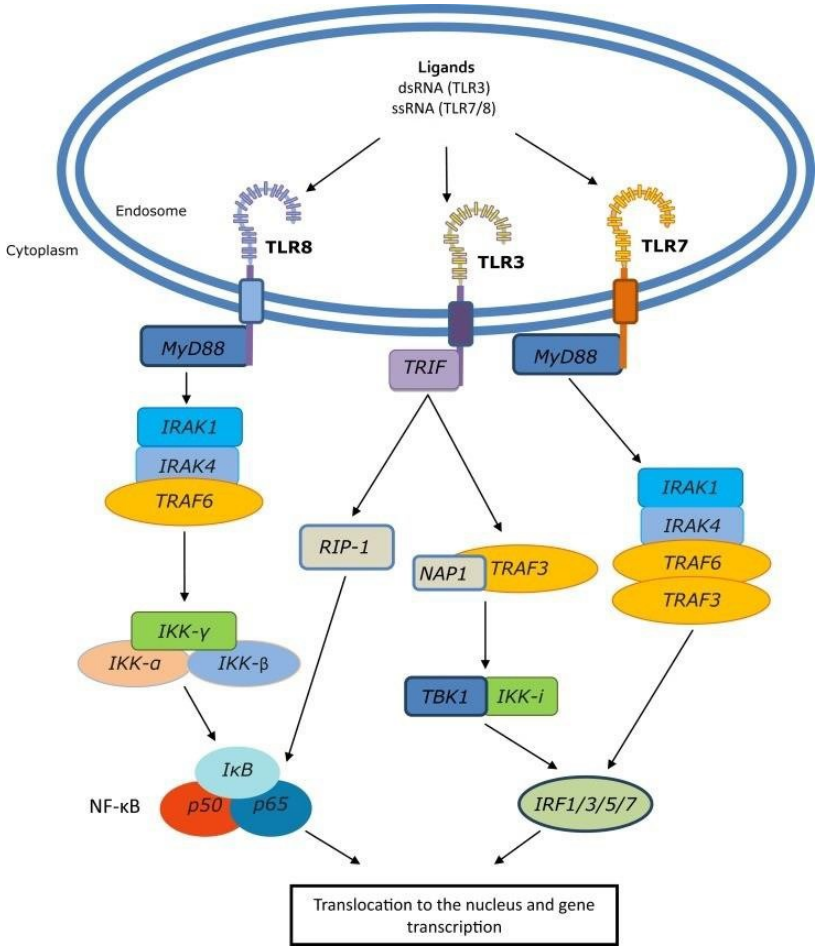

Figure 12. Endosomal signaling from TLR3, TLR7 and TLR8. Following RNA binding, TLR7 and TLR8 activate MyD88 - dependent pathway. For TLR8, it leads to activation of NF-kB through IRAK1, IRAK4, TRAF6 and IKK complex proteins, whereas TLR7 engages IRAK1 and IRAK4 with TRAF6 and TRAF3 for activation of IRF family members and IFN I production. TLR3 signaling through the TRIF molecule leads to either cytokine production by binding RIP-1 protein or IRF-mediated transcription through TRAF3-NAP1-TBK1-IKK-i proteins. Figure is taken from Thwaites et al., 2014.

2.2.3. DNA sensors

Detection of pathogenic DNAs by innate immune system is particullarly important for activation of protective response to virus infections. This process depends on DNA sensors and initiates production of IFNs and cytokines. DNA sensors are localized in endosomes, cytoplasm and the cell nucleus.

To date, we know only one endosomal sensor - TLR9. TLR9 recognizes unmethylated 2′-deoxyribo cytidine-phosphate-guanosine (CpG) DNA motifs that are presented in viruses

and bacteria. TLR9 is produced in macrophages and pDCs [Hemmi et al., 2000]. Different researchers demonstrated that TLR9 senses HSV-1 and adenovirus in DCs [Hochrein et al., 2004; Zhu et al., 2007]. Additionally, TLR9 recognizes malaria pigment hemozoin and activates production of different cytokines and chemokines [Coban et al., 2005].

At least, fifteen sensors were found in cytoplasm. They include interferon gamma inducible protein 16 (IFI16), DNA dependent activator of IFN regulatory factors (DAI), absent in melanoma 2 (AIM 2), RNA polymerase III, DEAH box polypeptide 9 (DHX9), DEAH box polypeptide 36 (DHX36), DExD/H-box helicase 41 (DDX41), DExD/H-box helicase 60 (DDX60), cGAS, Ku70/Ku80 complex, leucine-rich repeat flightless-interacting protein 1 (LRRFIP1), LSm14A, Sox2, hnRNPA2B1 and interferon-inducible protein X (IFIX) [Xia et al., 2016; Li et al., 2016; Diner et al., 2015]. Three of these sensors - IFI16, IFIX, hnRNPA2B1 - were described to sense DNA also in the cell nucleus [Stratmann et al., 2015; Diner et al., 2015; Zhang et al., 2019]. Interestingly, cGAS described as the cytosolic sensor, was found in both, nucleus and cytoplasm. IFI16 and cGAS are the most crucial and best characterized DNA sensors.

IFI16 and its mouse analogue, p204, belongs to a family of HIN200 proteins and have pyrin domain on its N-terminus and two DNA-binding HIN-200 domains (HIN A and HIN B) on C-terminus (Figure 13) [Zhao et al., 2015; Yan et al., 2008]. These proteins are involved in many processes such as modulation of transcription, cell proliferation and differentiation, protein degradation, senescence, activation of immune response [Ding, Lengyel, 2008; Zhao et al., 2015]. Moreover, Rolle et al. found that p204 stimulates mouse cytomegalovirus replication [Rolle et al., 2001]. IFI16 prefers to interact with quadruplex DNA rather than with double stranded DNA and enhances quadruplex formation and stabilization [Hároníková et al., 2016]. Stratmann et al. demonstrated that IFI16 scans along the dsDNA and binds it non-linearly and sequence independently [Stratmann et al.,2015]. Morrone et al. showed that FI16 cooperatively binds dsDNA in a length-dependent manner. They found that with the DNA binding footprint of ~15 bp for ona full–length IFI16 molecule there are required 10 copies of the protein for optimal oligomeric assembly [Morrone, et al., 2014]. The minimal length of exposed dsDNA required for IFI16 binding is 50-70 base pairs. According to Stratmann et al., chromatiniszation of DNA should be a key factor for recognition of self-DNA from a pathogenic one [Stratmann et al., 2015]. Size of DNA linker between two nucleosome was described to be about 20 to 30 base pairs [McGhee et al., 1983]. Longer DNA (300 base pairs and more) allows binding of more IFI16 molecules with higher efficiency [Stratmann et al., 2015].

IFI16 has a nuclear localization signal and shuttles between the nucleus and cytosol.

Its cellular localization depends on the cell type and post-translational modifications [Veeranki, Choubey, 2012; Choubey, Lengyel, 1992; Li et al., 2012]. Li et al. found that the cellular localization of IFI16 is regulated by acetylation of its NLS motifs with p300 [Li et al., 2012]. As was shown for HSV-1, interaction between viral DNA and IFI16 stimulated IFI16 acetylation and translocation to cytoplasm. Blocking of nuclear export with Leptomycin B did not affected IFI16 acetylation but prevented its cytoplasmic translocation [Ansari et al., 2015].

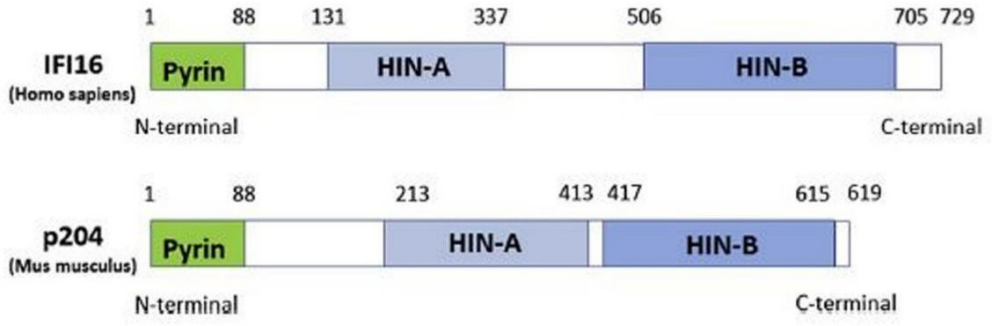

Figure 13. Molecular structure of IFI16 and p204 proteins. Both, IFI16 and p204 contain pyrin (PYD) domain at N-terminus, and HIN-A and HIN-B domains. Picture is taken from Zhao et al., 2015.

DNA sensor cGAS interacts with pathogenic or host dsDNA to activate innate immunity. cGAS is composed of N-terminus domain and catalytic domain localized at C-terminus. The catalztic domain of cGAS is conserved from fish to human (Figure 14) [Wu, Chen, 2014].

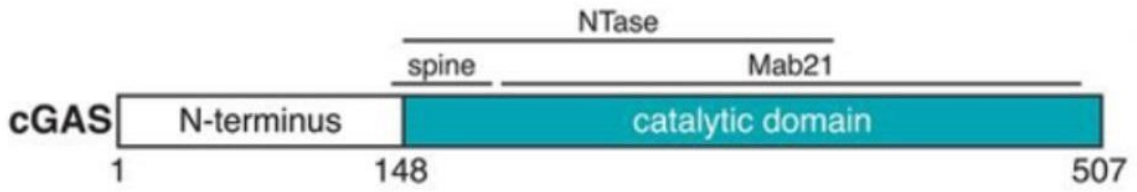

Figure 14. Molecular structure of mouse cGAS. cGAS has N-terminus domain and catalytic domain. Figure is adapted from Boyer et al., 2020.

Both, N-terminus and catalityc domain have DNA binding activity. However, truncation of N-terminus does not abolish the ability to activate IFN-β production [Sun et. al., 2013]. The catalytic domain has two lobes with the active site at their interface, which is not active in free cGAS. DNA binding induces conformational changes in cGAS resulting in appearance of activation loop between two lobes. The conformation changes required for binding adenosine triphosphate (ATP) and guanosine triphosphate (GTP) to cGAS [Gao et al., 2013; Civril et al., 2013]. For the stabilization of active conformation, cGAS needs to assemble into a dimer with two DNA strands between two cGAS protomers. Each protomer of the dimer

has three DNA binding sites A, B and C. Two DNA molecules are bound by site A of one protomer and site B of another protomer (Figure 15) [Hopfner and Hornung, 2020]. Site C stabilizes active dimers [Michalski et al., 2020].

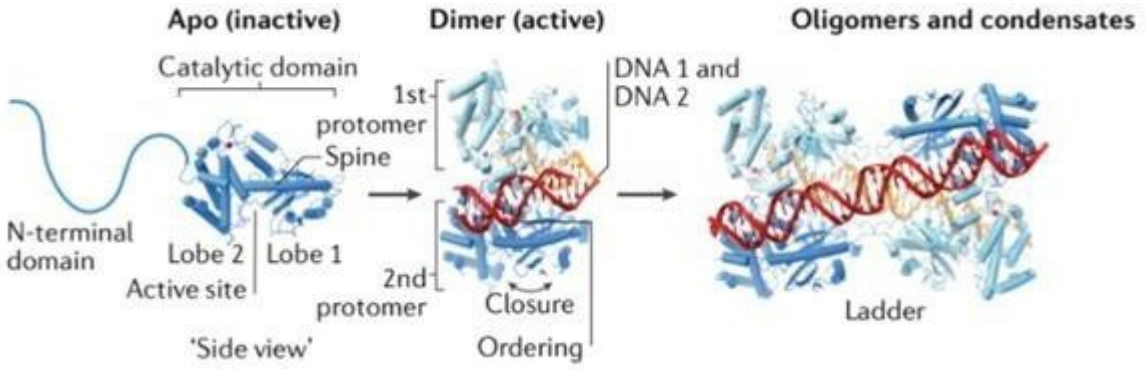

Figure 15. Mechanism of cGAS activation. First, the structure of inactive (apo) human cGAS with two lobes and active site between them is shown. Then, DNA-bound cGAS dimer with two protomers is demonstrated. At the end, oligomeric state is presented. Figure is adapted from Hopfner and Hornung, 2020.

cGAS interacts with B-form of dsDNA in a sequence independent, but length dependent manner through contact with sugar-phosphate backbone [Kranzusch et. al., 2013]. cGAS molecules form a ladder-like network with DNA resulting in sensing. Interestingly, binding of dsDNA with one cGAS dimer is not effective but required for DNA binding of subsequent cGAS molecules [Sun et al., 2013; Andreeva et al., 2017]. Additionally, cGAS binds single-stranded DNA (ssDNA) but affinity to these molecules is significantly lower than that to dsDNA [Kranzusch et al., 2013].

After binding to dsDNA, cGAS catalyzes the production of the second messenger cyclic guanosine monophosphate–adenosine monophosphate (cGAMP) in the presence of GTP and ATP. 2'-3'-cGAMP containing 2'-5' and 3'-5' phosphodiester bonds is required for activation of IFN-β production in mammalian cells [Wu et al., 2013; Ablasser et al., 2013]. Gentili et al. and Bridgeman et al. showed that different viruses (HIV-1, murine cytomegalovirus, modified vaccinia Ankara virus and herpesvirus) can encapsidate cGAMP and transfer it to non-infected cells [Gentili et al., 2015; Bridgeman et al., 2015]. It can be also transferred by exosomes [Urbanelli et al., 2019]. Moreover, mouse and human cells can transfer cGAMP to neighbouring cells through gap junctions and thus can promote activation of immune response in them [Ablasser et al., 2013].

cGAS was found to localize on the plasma membrane, in cytoplasm and the nucleus [Volkman et al., 2019; Barnett et al., 2019; Yang et al., 2017; Gentili et al., 2019; Liu et al., 2018]. In cytoplasm, cGAS can interact with viral and bacterial DNA, or with cytosolic

fragments of cellular chromatin trapped in micronuclei which are generated during DNA damage in senescent and cancer cells. Micronuclei consist of chromatin fragments surrounded by the nuclear membrane. The disruption of their fragile membrane leads to cGAS accumulation and IFN-β production [Glück et al., 2017; Mackenzie et al., 2017]. Moreover, it can interact with mitochondrial DNA in cytosol upon mitochondrial stress [West et al., 2015]. To prevent the detection of mitochondrial DNA and production of type I interferon, dengue virus NS2B protease cofactor promotes cGAS lysosomal degradation during infection [Aguirre et al., 2017]. Although most of studies describe cGAS as a cytosolic DNA sensor, it was found in the nucleus [Yang et al., 2017]. Some authors found it even as predominantly nuclear protein, regadless of cell cycle phase or cGAS activation status [Volkman et al., 2019, Sun et al., 2021].

Nevertheless, the mechanism that prevents the recognition of cellular DNA in the nucleus should exist. 3D structural analysis of cGAS revealed three sites A, B and C. All of them are in the catalytic domain of cGAS and play a role in binding histones of nucleosome and/or free dsDNA. B site of cGAS binds H2A, H2B histones on nucleosomes. This interaction prevents formation of active cGAS dimers and DNA binding, which is mediated by sites A and B. (Figure 16) [Michalski et al., 2020; Pathare et al., 2020; Zhao et al., 2020].

The cellular localization, stability, DNA binding and enzymatic activity of cGAS are regulated by different post-translational modifications, such as phosphorylation, glutamylation, ubiquitylation, sumoylation and acetylation. For example, phosphorylation of serine 291 of mouse cGAS suppresses its enzymatic activity and increases herpes simplex virus 1 (HSV-1) replication [Wu et al., 2020].

Liu et al. and Jiang et al. found that cGAS inhibits homologous reparation of double-stranded breaks. For that, cGAS binds broken DNA and interacts with Poly (ADP-ribose) polymerase 1 (PARP1), preventing the PARP1-Timeless complex formation and as a result, suppresses homologous recombination [Liu et al., 2018; Jiang et al., 2019].

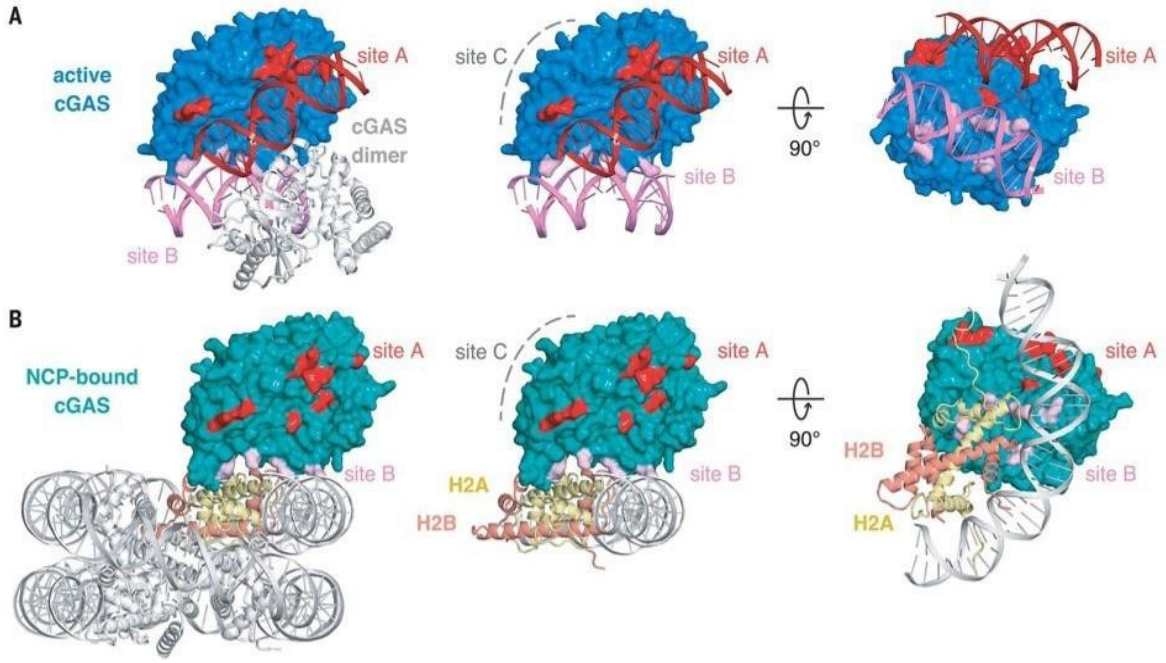

Figure 16. Binding to nucleosome inhibits cGAS activity. (A) Structure of active cGAS-DNA complex. cGAS sites A, B and C are shown in red, pink and gray respectively. On the middle and the right pictures are presented side and bottom views on the cGAS-DNA complex. **(B)** Structure of nucleosome core particle (NCP)-cGAS complex. cGAS DNA binding sites are highlighted by red, pink, and grey. Interactions between cGAS and H2A, H2B histones are shown in yellow and orange colours. Figure is adapted from Boyer et al., 2020.

2.2.4. DNA sensing pathways

DNA sensing by endosomal TLR9 occurs through MyD88-dependant pathway. Interaction between TLR9 and CpG DNA leads to TLR9 dimerization and binding to MyD88. Then, MyD88 recrutes IRF1. IRF1 translocates to the nucleus and activates transcription of IFN I inducible genes. Additionally, TLR9 stimulation leads to NF-kB pathway activation and production of cytokines (Figure 17) [Briard et al., 2020]. Hayashi et al. found that TLR9 activation can be assosiated with autophagy system [Hayashi et al., 2018]. Upon stimulation with pathogenic DNA, the autophagy component, light chain 3 (LC3), and autophagy-related protein 5 (ATG5) bind to the endosome containing TLR9. This association is provided by a non-canonical process called “autophagy associated with LC3 protein” (LAP). Further, the signal is transdused through inhibitor of NF-κB kinase subunit α (IKKα) and IL-1 receptor-associated kinase 1/4 (IRAK1/4). The LC3/IKKα complex interacts with TRAF3 and IRF7, which in turn leads to the induction of type I IFNs [Hayashi et al., 2018].

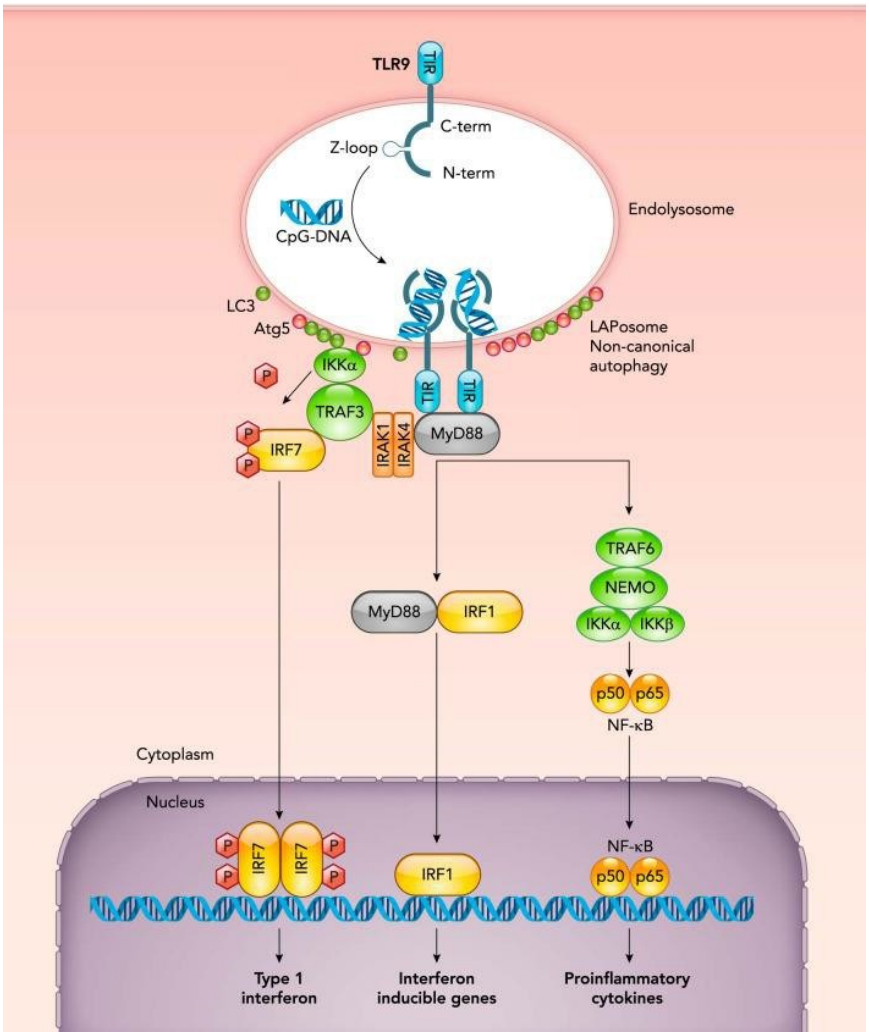

Figure 17. Signaling pathway through TLR9. Binding of CpG DNA to TLR9 (through its N and C termini) results in recrutment of MyD88 adaptor protein and activation of three possible signaling pathways. The first one leads to transcription of IFN inducible genes (through IRF1). The second one activates synthesis of cytokines through NF-kB pathway. The third signaling pathway results in recrutment of LC3 and ATG5 proteins to endosome and assambly of IKKα/IRAK1/IRAK4/TLR9/MyD88/TRAF3/IFR7 complex, which stimulates production of type I IFN. Picture is taken from Briard et al., 2020.

For cGAS DNA sensing, a pathway leading through STING has been described. Upon DNA binding, cGAS dimerizes and starts to produce cGAMP using ATP and GTP. Then, cGAMP binds to STING. STING is expressed in many tissues and localizes on the outer membrane of ER [Ishikawa, Barber, 2008]. Crystallization of STING indicated that the activated form of the protein exists as a dimer on ER membrane preserved after interaction with cGAMP [Shang et al., 2012]. Interaction between STING and cGAMP induces STING inward rotation and formation of a deep pocket for anchoring of cGAMP [Zhang et al., 2013]. Also, it leads to STING trafficking from ER to the endoplasmic-reticulum–Golgi intermediate compartment (ERGIC). There, STING recruits and activates TBK1. TBK1 represents a compact dimer, activation of which is regulated by phosphorylation of serine 172 and

subsequent conformational changes [Larabi et al 2013; Kishore et al., 2002].

According to Almine et al. and Jønsson et al., STING complex includes also DNA sensor, IFI16. IFI16 recruits the TBK1 to cGAMP stimulated STING. This double binding is critical for the full activation of STING and induction of IFN-β production [Almine et al., 2017; Jønsson et al., 2017]. Almine at al. showed that IFI16 deficient human immortal keratinocytes exhibit weak production of chemokine mRNA after transfection with synthetic 2'-3'-cGAMP, in comparison with the production in wild type cells. Additionally, IRF3 phosphorylation and chemokine gene expression induced by using of a non-hydrolysable analogue of cGAMP was affected by the absence of IFI16. [Almine et al., 2017].

TBK1 recruited to the STING complex mainly induces phosphorylation of IRF3 (and probably, in lesser extent, NF-kB activation), which results in its nuclear translocation. In the nucleus, IRF3 activates IFN-I gene expression (Figure 18) [Hopfner and Hornung, 2020].

However, Diner at al. demonstrated that IFI16 is not required for activation of STING-TBK1-IRF3 pathway. They showed that IFI16 represses HSV-1 gene expression and induces cytokines production. Knockout of IFI16 in human primary fibroblasts did not affect activation of TBK1 by phosphorylation while knockout of cGAS or STING significantly decreased it [Diner et al., 2016]. Further research is needed to evaluate the role of IFI16 in cGAS induced IFN-β production.

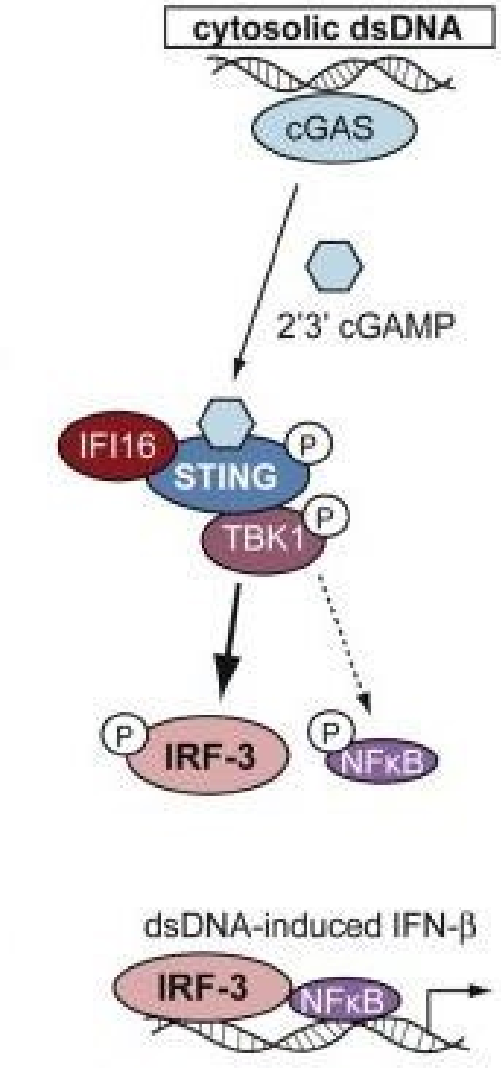

Figure 18. cGAMP-STING-IFI16 DNA sensing pathway. Interaction between cellular DNA and cGAS induces cGAMP production and binding to STING. At the same time, activated IFI16 binds STING complex too. STING dimerizes, translocates from ER to ERGIC, binds TBK1, and activates it. After that recruitment and phosphorylation of IRF3 (and much less of NF-kB) occurs. IRF3 stimulates transcription of IFN-β and other immunomodulatory genes. Adapted from Dunphy et al., 2018.

Non-canonical immune response was detected after etoposide induced DNA damage response (DDR). According to Dunphy et al., innate immunity activated by DDR in human keratinocytes resulted in predominant phosphorylation of NF-kB rather then IRF3. This pathway starts from the recognition of double-stranded breaks in the cell nucleus with PARP1 and ataxia telangiectasia mutated (ATM) kinase proteins. PARP1 protein is essential for initiation of DNA repair and regulation of gene expression [Ko, Ren, 2012]. ATM recruites to double stranded breaks and induces activation of DNA damage ckeckpoint and as a result, cell cycle arrest, DNA reparation or apoptosis [Khanna, et al., 2001] ATM-dependent NF-κB activation was found after using an ionizing radiation, etoposide and

during replication stress [Miyamoto, 2011].

On the next stage, ATM phosphorylates p53, which, as was shown by Liao et al,. interacts with IFI16 [Dunphy et al., 2018; Liao et al., 2011]. At the same time, ATM - PARP1 complex stimulates TRAF6 activation. As a result, alternative complex STING – TRAF6 - IFI16 - p53 assembles in cytoplasm. TRAF6 catalyzes STING ubiquitinylation that leads to NF-kB phosphorylation and gene expression. Additionally, authors showed that etoposide also induces low level of STING trafficking from ER to perinuclear foci and weak IRF3 activation (Figure 19) [Dunphy et al., 2018].

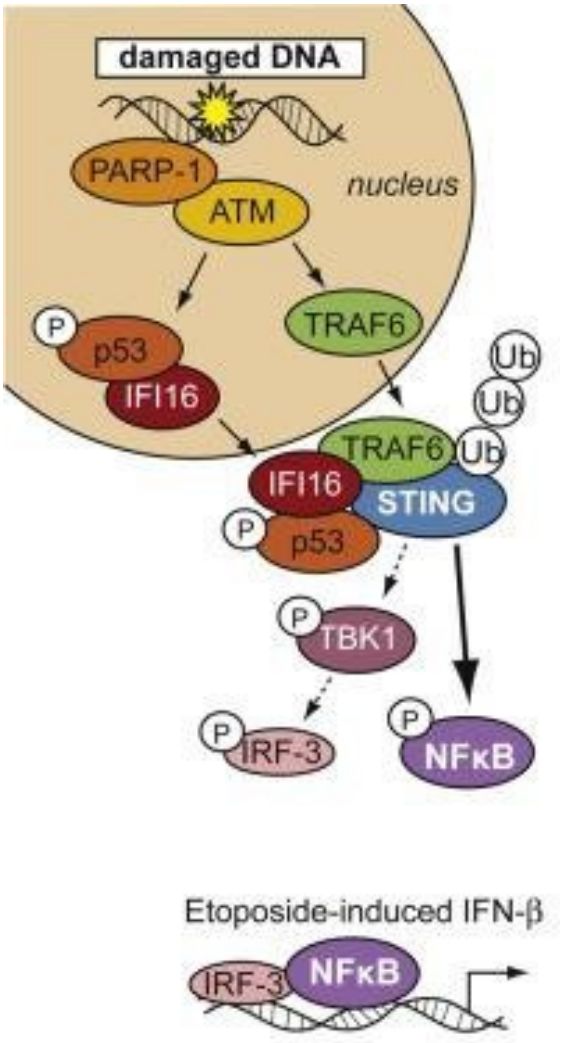

Figure 19. Non-canonical DNA sensing pathway. The induction of DNA damage in the nucleus by etoposide and its recognition with ATM, PARP1 and IFI16 proteins result in assembly of STING signaling complex which includes phosphorylated tumor suppressor p53 and the E3 ubiquitin ligase TRAF6. TRAF6 catalyzes the formation of K63-linked ubiquitin chains on STING, leading to the activation of the transcription factor, NF-κB, and induction of ubiquitinated STING-dependent induction IFN production. Adapted from Dunphy et al., 2018.

3. Aims

Previously, our laboratory studied polyomavirus trafficking from the cell membrane towards the nucleus. Despite extensive research, it is still not clear how polyomaviruses deliver their genomes from ER into the cell nucleus. Therefore, in the first part of the thesis, we investigated the pathway of MPyV trafficking from cytoplasm to the cell nucleus.

The role of the immune system in polyomavirus reactivation is very important, since the virus-induced pathology mainly occurs in immunocompromised individuals. However, there is a little information about the role of innate immunity in protection against polyomaviruses. In the second part of thesis, we aimed to investigate whether and when polyomavirus genomes are sensed by DNA sensors and prospective mechanisms of activation of innate immunity response.

Specific aims are:

1. To elucidate the way used by MPyV for delivery of its genomes into the nucleus.

- To prove the role of importin β1 in the nuclear entry of the mouse polyomavirus.
- To determine the role of NLS sequences of VP1 and the minor capsid proteins VP2 and VP3 in virus translocation from cytoplasm to the cell nucleus.

2. To reveal the mechanism of IFN-β induction during MPyV infection.

- To find out when polyomavirus infection induces interferon β in infected cells.
- To determine the possible role of cGAS and p204 DNA sensors in the induction of interferon response.

4. Material and Methods

4.1. Cell lines

Mouse fibroblasts NIT 3T6 (ATCC; CCL-96), NIH 3T3 (ATCC), Mouse embryo fibroblasts (MEF), immortalized MEF STING wild type (STING wt) and MEF STING knockout cells (STING KO), primary MEF cGAS wild type (cGAS wt) and MEF cGAS knockout cells (cGAS KO) (kindly provided by Dr. Jonh Cambier, University of Colorado, USA and Dr. Jan Rehwinkel, University of Oxford), primary MEF p53 wild type (p53 wt) and MEF p53 knockout cells (p53 KO) (kindly provided by Prof. T. Stopka, First medical faculty at Biocev, Charles University, Czech Republic) were grown in Dulbecco's modified Eagles medium with high glucose – DMEM (Sigma-Aldrich) supplemented with 10% fetal bovine serum (FBS) (Invitrogen) at 37ºC in humidified incubator with a 5% CO2 atmosphere.

4.2. Virus production

MPyV BG strain, was isolated from infected 3T6 mouse fibroblasts according to Mahy et al. and purified by CsCl and sucrose gradient ultracentrifugation [Mahy et al.., 1985]. The quality of preparation was confirmed by electron microscopy (negative staining) and hemagglutination assay.

4.3. Negative staining

Viral suspensions were adsorbed by placing a drop of a sample on a formvar-carbon-coated 400 mesh copper grid for a negative staining. Next, the grid was washed twice with deionized water and further stained with 2% phosphotungstic acid (pH 7.0) for 1 minute The samples were observed with a JEOL JEM (Akishima) 1200EX electron microscope operating at 80 kV. Fine structure measurements/observations were performed using a Veleta camera and iTEM 5.1 software (Olympus Soft Imaging Solutions GmbH).

4.4. Hemagglutination assay

The total number of viral particles (both full and empty) can be estimated by using hemagglutination test (in HAU - hemagglutination units). This method is based on the ability of VP1 capsid protein bind to sialic acid on the cell membrane. Thus, viral particles agglutinate erythrocytes and the level of agglutination depends on the number of particles.
0.2% bovine serum albumin (BSA) in 1x phosphate-buffered saline (PBS) was added to the round bottom 96 well plate and then, viral sample was added to the first well. After mixing, 50

µl of solution was transferred to the next well, mixed and again, 50 µl of solution was transferred to the next well continuing till the last one. Then, to all wells, 0.4% guinea pig erythrocytes in 0.2% BSA were added. The plate was stored in a fridge, and the results were read after 2 hours. The hemagglutination titer was defined as the reciprocal of the highest virus dilution showing hemagglutination.

4.5. Viral infection

Cells were seeded on 13-mm glass coverslips, in 24-well, 6-cm or 10-cm plates (to have 50-70% of confluence) and grown for the time periods indicated in each experiment. At the day of infection, cells were incubated with wild type (wt) MPyV or mutants diluted in serum-free medium for 1 hour on ice (co-immunoprecipitation and proximity ligation assay) or at 37°C. After virus adsorption, medium with serum was added, and cells were incubated at 37°C in humidified incubator with a 5% CO2 atmosphere. The infection start was measured from the time of cell transfer to 37°C.

4.6. Co-immunoprecipitation and cross-linking

The antibody against importin β1 or nonspecific immunoglobulin G (IgG) control antibody were diluted in 0.02% Tween-20 in 1xPBS (final concentration 5 µg/200 ml). Then, they were incubated with 20 µl of protein G dynabeads (Invitrogen) on a mixing rotor at 4°C for 30 minutes After incubation, beads were separated and washed once with 0.02% Tween-20 in 1xPBS. The antibody was crosslinked to the beads by using a disuccinimidyl suberate (DSS) crosslinker (final concentration 1.25 mM) (Fisher Scientific) for 30 minutes and then washed 2 times. Next, 230 µl of cell lysate (from the 3-cm plate) was prepared in modified RIPA buffer ((10 mM Tris/HCl, pH 7.4, 1 mM EDTA, 150 mM NaCl, 1% P-40, 1% sodium deoxycholate (without SDS)) supplemented with a protease inhibitor cocktail (Roche). Aliquots (30 µl) of whole cell lysates were saved as input controls. The rest (200 µl) was added to beads-antibody complexes and incubated with rotation overnight at 4°C. After incubation, the beads (containing antibody-protein complexes) were washed three times with 1xPBS. Then, beads were divided into two fractions: fraction one was used for suspension in a 50 µl of 1xLaemmli buffer and analyzed using SDS-PAGE (10% gel) followed by western blot. The second fraction was used for DNA isolation.

4.7. SDS polyacrylamide (SDS-PAGE) electrophoresis and western blot analysis

Cells were harvested at indicated times and washed with 1xPBS, then resuspended in ice-cold cell lysis buffer (10 mM Tris/HCl, pH 7.4, 1 mM EDTA, 150 mM NaCl, 1% P-40, 1% sodium deoxycholate, 0.1% SDS) supplemented with a protease inhibitor cocktail (Complete Mini EDTA free, Roche). Cell lysis was carried per 30 minutes on ice. Cell debris was removed by centrifugation. Cellular proteins were resuspended in 5xLaemmli buffer and applied to 10% acrylamide gel for SDS-PAGE. The samples were blotted to a nitrocellulose NC45 membrane and detected by immunostaining with selected antibodies. For detection of minor proteins in samples after co-immunoprecipitation, we used ultra-sensitive enhanced chemiluminescent substrate "Super Signal West Femto" (Thermo Fisher Scientific). Proteins were visualized using Amersham imager 600 (GE Healthcare).

4.8. PCR detection of DNA isolated from immune complexes

Samples containing antibody-antigen complexes bound to dynabeads were washed five times in 1xPBS and then, resuspended in 500 µl of 1xPBS containing 5 µl of Proteinase K (100 µg/ml) (Roche) and 5 µl of 10% SDS. Next, samples were heated at 55°C for 30 minutes and DNA was isolated by treatment with phenol-chloroform-isoamyl alcohol (25:24:1) and precipitated with acetate/ethanol overnight at 4°C. After precipitation, samples were centrifuged; the precipitate was dried and resuspended in a sterile water. The samples were subjected to polymerase chain reaction (PCR) for amplification of a fragment of MPyV genomic DNA using "Illustra^{TM} TempliPhi 100" amplification kit according to manufacturer instructions. Primers used for the reaction were: forward 5′-TGATTCTTCGGGATTTG-3′ and backward 5′-GTGGCGTTGCATT-3′. The expected product should be 250 bp long.

4.9. Agarose gel electrophoresis

Samples for DNA detection were run in 0.8% agarose gel stained by "GelRed TM Nucleic Acid Gel Stain" (Biotium) according to the standard procedure.

4.10. Proximity ligation assay (PLA)

We used a Duolink kit (Sigma-Aldrich) according to the manufacturer's instructions. Infected cells were fixed at 6 and 8 hpi with 4% paraformaldehyde (PFA) in 1xPBS for 10 minutes, permeabilized for 5 minutes with 0.5% Triton X-100, 3 times washed with 1xPBS,

(10 minutes each wash) and incubated with blocking solution at 37°C for 30 minutes. Then, samples were incubated for 1 hour at room temperature with different combinations of antibodies: mouse antibody against VP1 with rabbit antibody against importin β1, mouse antibody against VP1 with rabbit antibody against VP1 (used as a control), rabbit antibody against p204 with mouse antibody against T antigens or rabbit antibody against p204 with mouse antibody against acetylated lysine. After washing, cells were incubated with secondary anti-mouse minus (DUO92004) and anti-rabbit plus (DUO92002) antibodies tagged with PLA oligoprobe. Then, the ligation reaction was performed. For detection of ligation products, *in situ* PCR was carried out and the products visualized by the hybridization of fluorescently labeled oligonucleotides (λ_{ex} = 594 nm and λ_{em} = 624 nm). The signal was detected by fluorescence microscopy. Images were captured using a LSM 880NLO confocal microscope, Carl Zeiss (Oberkochen, Germany). Calculation of obtained results was done using plug-in for Image J software.

4.11. NLS sequence analysis

Sequences of the VP2/VP3 and VP1 capsid proteins of wt, mutant 1, mutant 2 and mutant 3 of MPyV were analyzed using the NucPred program, available online [Brameier et al., 2007].

4.12. Plasmids

pMJG - plasmid [Krauzewicz et al., 1990] containing the entire genome of MPyV, strain BG opened and inserted into the bacterial plasmid pMJ1 (a 2.266-base-pair derivative of pAT153 plasmid) in the unique EcoRI site was used as a source of wt MPyV.

pMJG-P2 – plasmid was used for production of MPyV with one substitution in NLS sequence of VP1 (lysine (K6) by glutamine (Q6)) and one substitution in VP2/VP3 (lysine (K315) by alanine (A315)). The construct was prepared in our laboratory by Sandra Huerfano.

pMJG-P1P2 – plasmid was used for production of MPyV carrying one substitution in VP1 (K6Q) and two mutations in VP2/VP3 (K314A, K315A). A construct was prepared in our laboratzory by Sandra Huerfano.

pMJG-P1P2P4 - plasmid was used for production of MPyV with three mutations in VP2/VP3 (K314A, K315A, and K317A) and three mutations in VP1 (K6Q, S7R and G8R). The construct was prepared in our laboratory by Sandra Huerfano.

pwPVP1-P1 and pwVP1-P1P2P4 – plasmids were used for production of VP1 capsid protein with one and three amino acid changes in NLS. Plasmids were prepared using pwVP1 plasmid encoding MPyV VP1 from LID strain with inactivated GFP (provided by Lenka Hornikova). Mutations were introduced by using a GENEART® Site-Directed Mutagenesis System (Invitrogen) kit, according to the manufacturer's instructions.

Primers (synthesized by KRD)
pwPVP1-P1 forward
5'-TAC CGT GGT TTC GCG GTC AGA CCC CAG TCG-3'
pwPVP1-P1 backward
5'-ATG GCA CCA AAG CGC CAG TCA GGG GTC AGC-3'
pwPVP1-P1P2P4 forward
5'-TAC CGT GGT TTC GCG GTC GCT GCC CAG TCG TTT A-3'
pwPVP1-P1P2P4 backward
5'-ATG GCA CCA AAG CGC CAG CGA CGG GTC AGC AAA T-3'

pwPVP2-P1, pwPVP2-P1P2, pwPVP2-P1P2P4 – plasmids, used for production of VP2 capsid protein with one, two and three mutations in NLS. These plasmids were prepared using ph2pΔG plasmid encoding MPyV VP2 from LID strain with inactivated GFP (provided by Lenka Hornikova).

Primers (synthesized by KRD)
pwPVP2-P1 forward
5'-TG CCC GGT GTC TTC CGC TTT GCG TCC AAG AC-3'
pwPVP2-P1 backward
5'-AC GGG CCA CAG AAG GCG AAA CGC AGG TTG TG-3'
pwPVP2-P1P2 forward
5'-CTC CTG CCC GGT GTC CGC CGC TTT GCG TCC AAC ACT-3'
pwPVP2-P1P2 backward
5'-GAG GAC GGG CCA CAG GCG GCG AAA GC AGG TTG TGA-3'
pwPVP2-P1P2P4 forward
5'-GGT GTC CGC CGC TTT CGC TCC AAC ACT ACG AT-3'
pwPVP2-P1P2P4 backward
5'-CCA CAG GCG GCG AAA GCC AGG TTG TGA TGC TA-3'

4.13. Introduction of mutations in individual proteins VP1 and VP2

The plasmid pVP1 encoding for MPyV VP1 from LID [Horníková et al., 2011] and ph2pΔG encoding for MPyV VP2 -from LID strain [Huerfano et al., 2013] were used for introduction of mutations in the NLS coding sequences of the capsid proteins, VP1 and VP2. Mutations were introduced by using GENEART® Site-Directed Mutagenesis System (Invitrogen) kit, according to manufacturer's instructions. The following protein variants were produced: VP1/K6Q, VP1/K6Q-S7R-G8R, VP2/K315A, VP2/K314A-K315A and VP2/K314A-K315A-R317A.

4.14. Cell transfection

The transfection of 3T6 and 3T3 cells was performed by electroporation in a Nucleofector™ device using Nucleofector V solution (Lonza) according to the manufacturer's instructions. Briefly, $4x10^6$ exponentially growing cells were mixed with 5 µg of plasmid DNA and 100 µl of Nucleofector V solution and electroporated (program T-030 and U-030 respectively).

4.15. Viral genome quantification

Viral particles isolated by CsCl were cleaned from extracellular DNA by treatment with DNase I (0.4 U/µl) for 1 hour at 37°C. After DNase inactivation with 0.5 M EDTA and heatingfor 10 minutes at 80°C, capsids were degraded by treatment with proteinase K (20 mg/ml) (Roche) for 1 hour at 60°C. Then, samples were incubated with 0.5 M dithiothreitol (DTT) (Sigma) for 30 minutes at 60°C and viral DNA was extracted by phenol-chloroform-isoamyl alcohol (25:24:1), followed by ethanol precipitation according to the protocol previously described [Orlando et al., 2000]. Viral DNA was quantified by real-time PCR assay using iQ™ SYBR® Green Supermix (Bio-Rad Laboratories) detection and amplified using primers set to fragments of VP1 and LT genes: VP1 5'-GCAAGAAGGCGACGAC-3' and 5'-TGGCCTCCCTCATAAGT-3' and LT 5'-GCTGACAAAGAAAGGCTGCT-3' and 5'-AGCCGGTTCCTCCTAGATTC-3'. Thermal cycling was performed in a Light Cycler 480 II from Roche. Values were obtained by comparison of samples with a standard curve of known viral DNA concentrations.

4.16. Infectivity assay

3T6 cells were seeded on coverslips to have 50% of confluence next day and incubated at 37°C in 5% CO2 atmosphere. Then, cells were infected with wt or mutated MPyV 1, 2 or 3 (strain BG) using virus equivalent representing $1.5x10^4$ genomes per cell. Infection was performed as described previously. At 24 hpi cells were fixed for 10 min with 4% PFA, permeabilized with 0.5% Triton X-100 for 5 minutes, blocked and stained for LT antigen and mounted in glycerol containing DAPI. Microscopy fields were photographed. The efficiency of infection was determined as the percentage of LT positive cells of all cells on glass.

4.17. Immunofluorescence with pre-extraction buffer

Cells were grown on coverslips. Then, medium was removed, and cells were incubated with cytoskeletal buffer containing 25 mM Hepes, 50 mM NaCl, 3 mM $MgCl_2$, 300 mM sucrose and 0.5% Triton X-100 (pH 7.4) for 5 minutes on ice. After that, cells were washed once with 1xPBS and fixed with ice-cold methanol for 10 minutes at - 20°C. Immunofluorescence was proceeded according to standard protocol. This procedure was performed for visualization of p204 nuclear localization [Hua, Ferland, 2017].

4.18. Immunofluorescence staining

Cells growing on coverslips were fixed with 4% PFA in 1xPBS for 10 minutes at room temperature or with ice-cold methanol at - 20°C for 10 minutes. Then, cells were permeabilized with 0.5% Triton X-100 in 1xPBS for 5 minutes, followed by three times washing in 1xPBS. After that, cells were blocked with 0.25% BSA and 0.25% porcine skin gelatin in 1xPBS for 30 minutes at room temperature. Immunostaining with the primary and secondary antibodies was carried out for 1 hour or overnight or 30 minutes with extensive washing in 1xPBS after each incubation. Staining of cells for visualization of p-STING was done with immunofluorescence application solutions kit (Cell Signalling). Images were made with a TCS SP8 confocal microscope (Leica) and LSM 880NLO confocal microscope (Carl Zeiss, Oberkochen, Germany).

4.19. Reverse transcription quantitative PCR

Total cellular RNA was extracted using High Pure RNA Isolation Kit (Roche) in accordance with the manufacturer's protocol. The RNA concentration and purity were

measured by a nanodrop spectrophotometer (Thermo Fisher Scientific). Reverse transcription was performed using the iScript cDNA synthesis kit (Bio-Rad Laboratories) in accordance with the manufacturer's instructions. cDNAs were amplified by PCR using the following primer sets: MX-1:5'-GGTCGGCTTCTGGTTTTGTA-3' and 5'-GAACAGGTCCACTTCCTCCA-3', GAPDH:5'-ATGACATCAAGAAGGTGGTG-3' and 5'-ATACCAGGAAATGAGCTTG-3', IFN-β: 5'-CCCTATGGAGATGACGGAGA-3' and 5'-CTGTCTGCTGGTGGAGTTCA-3', spliced LT: 5'-GAACCGGCTTCCAGGGCTC-3' and 5'-CTTAGGCGGCGACTGGTAG-3'.

The quantification of PCR products in real-time was performed in a Light Cycler 480 II (Roche) using the Light Cycler® 480 SYBR Green I Master kit (Roche) in accordance with the manufacturer's protocol. The quantification of target gene expression was performed using Light Cycler 480 II software based on the relative quantification method, which determined the concentration of target amplicons normalized to the reference gene GAPDH.

4.20. Cell stimulation with inducers of IFN

Polyinosinic:polycytidylic acid (Poly I:C) (GE Healthcare) was used to stimulate 3T6 cells; specifically, $2x10^6$ cells were transfected by TurboFect (Thermo Fisher Scientific) with 20 μg of Poly I:C. The cells were incubated for 16 hours and then collected for isolation of RNA or for the preparation of cell lysates. c-di-GAMP (InvivoGen), plasmid DNA (pDNA), CpG oligonucleotide (InvivoGen) or 26-mer DNA (G3-YSD, InvivoGen) were used to stimulate 3T6 cells as follows: cells ($4x10^6$) were transfected with 4 μg of c-di-GAMP, 6 μg of pDNA, or 4 μg CpG by Amaxa nucleofector (Lonza), incubated for a further 6 hours, and collected for the isolation of RNA.

4.21. Nuclear-cytoplasmic fractionation

We used either the nuclear and cytosol extraction kit to prepare cell fractions in accordance with the manufacturer's instructions (G-Biosciences) or performed extraction using NP-40 in accordance with the Cold spring harbor protocol [Nabbi and Riabowol, 2015]. In addition, when required, nuclear fractions were further separated into soluble and insoluble fractions. For that, nuclear fraction was resuspended in buffer B (3 mM EDTA, 0.2 mM EGTA, and 1 mM DTT, H_2O, protease inhibitor) and incubated on ice for 30 minutes. The soluble fraction was separated by centrifugation at 1700 g for 4 minutes at 4°C.

The pellet containing chromatin was washed with buffer B and lysed in RIPA buffer.

4.22. Fluorescence in situ hybridization (FISH) combined with immunofluorescence or EdU labeling

We performed FISH in combination with immunofluorescence in accordance with the protocol described by Solovei and Cremer [Solovei, Cremer, 2010]. Briefly, cells were grown on coverslips, fixed with 2% PFA for 10 minutes, permeabilized with 0.5% Triton X-100 for 10 minutes, incubated in blocking solution (1% BSA/PBS) for 1 hour, and stained by the selected antibodies or subjected to EdU Click chemistry. The cells were post-fixed with 4% PFA for 5 minutes, treated with RNase, and incubated with 20% glycerol/PBS for 1 hour. Then, five freeze-thaw cycles were performed in liquid nitrogen. The cells were then equilibrated in 50% formamide/2xsaline-sodium citrate (SSC) for 8 hours and hybridized with the MPyV DNA probe generated by nick translation using BioNick DNA Labeling System (Invitrogen). Denaturation and hybridization were performed as follows: 90°C - 2 minutes, 80°C - 2 minutes, 70°C - 2 minutes, 60°C - 2 minutes, 50°C - 2 minutes, 42°C - 1 hour and 37°C overnight. After hybridization, the cells were washed three times in 2xSSC at 37°C and twice for 5 minutes in 0.1xSSC at 60°C. Each wash step was performed for 10 minutes. After washing, the cells were incubated with blocking solution (1% BSA/PBS) for 1 hour and processed for the detection of biotin by using antibodies. Coverslips were stained with DAPI and mounted on droplets of Anti-Fade Fluorescence Mounted Medium (Abcam). Images were obtained using a LSM 880NLO confocal microscope (Carl Zeiss).

4.23. EdU click chemistry

The Click-iT EdU reaction was performed in accordance with the instructions for the Click-iT imaging kit (Invitrogen). In brief, a solution of 20 μM EdU was prepared in complete medium and added to growing cells on coverslips to a final concentration of 10 μM. After incubation for 30 or 24 hours (experiment with cGAS-EGFP) minutes, the cells were fixed, permeabilized, blocked in 3% BSA/PBS, and subjected to Click-iT reaction.

4.24. siRNA transfection

Sense and antisense siRNA for p204 were prepared in Lipofectamine in accordance with manufacturer's instructions (Thermo Fisher Scientific). The siRNA sequences were: 5'-GUUUCAUCAAGAUAUCAAAtt-3' and 5'-UUUGAUAUCUUGAUGAAAtg-3'. As a

control, the Silencer® Select Negative Control #1 siRNA (Thermo Fisher Scientific) was used.

4.25. 2'-3'-cGAMP detection by liquid chromatography-mass spectrometry (LC-MS)

For detection of 2'-3'-cGAMP, the cells were detached using trypsin and $4x10^6$ cells were collected and used for the experiment. The cells were washed five times with 1 ml of 1xPBS and lysed in lysis buffer (20% acetonitrile and 40% methanol in deionized water). Then, the lysates were heated for 10 minutes at 60°C and cooled for 10 minutes on ice. After cooling, the samples were centrifuged at 17,000 g for 10 minutes at 4°C, and the supernatant was collected in a clean Eppendorf tube (Supernatant A). The pellet produced in the previous centrifuge step was washed in 500 µl of H_2O and centrifuged at 17,000 g for 10 minutes at 4°C, and the supernatant was collected in a clean Eppendorf tube (Supernatant B). Supernatants A and B were combined and centrifuged at 17,000 g for 5 minutes at 4°C and transferred to a new Eppendorf tube. To prepare the samples for analysis by LC-MS, the samples were frozen at -80°C for 1 day, dried by vacuum centrifugation, and resuspended in 40 µl of H_2O.

As a control, an internal standard of 100 pmol of 2'-3'-cGAMP was spiked into the lysate of mock-infected cells or cells transfected with a plasmid DNA and collected after 2 hours.

2'-3'-cGAMP expression was measured using a Dionex Ultimate 3000RS LC system coupled to a TSQ Quantiva mass spectrometer (Thermo Fisher Scientific) using an ESI source in positive mode with the following ion source parameters: ion transfer tube temperature, 300°C; vaporizer temperature, 125°C; spray voltage, 3500 V; sheath gas, 35 arbitrary units (au); auxiliary gas, 5 au. A ZIC ® -HILIC column (150 mm x 2.1 mm, 5 µm) from Merck (Darmstadt, Germany) was used to separate the analytes. The column was maintained at room temperature, and an injection of volume of 2 µl was used per sample. A gradient elution was set from 15% B to 60% B (A: 95% acetonitrile and 5% 10 mM ammonium acetate pH 9.3, B: 10 mM ammonium carbonate in water, pH 9.3) in 7.3 minutes at a flow rate of 200 µl/min, followed by a washing phase (2.7 minutes of 60% B) and an equilibration phase (9 minutes of 15% B). For the targeted determination of 2'-3'-cGAMP, a selective reaction monitoring (SRM) assay was used, which was developed previously, comprising infusion of the pure compound, and monitoring the following seven transitions: 675.1>136.1, 675.1>524.1, 675.1>312.1, 675.1>506.0, 675.1>152.1, 675.1>476.0, and 675.1>330.0. The integration of 2'-3'-cGAMP peak areas was related to the transition 675.1>506, which provided appropriate signal intensity

and was less affected by the matrix effect.

4.26. 2'-3'-cGAMP ELISA detection

2'-3'-cGAMP ELISA was performed in accordance with the manufacturer's protocol using 2'-3'-cGAMP ELISA Kit (Arbor Assays). Briefly, mock-infected or infected cells ($1.5x10^6$) were used for fractionation with the kit described above. The fractions were handled on ice and immediately used for ELISA. The 2'-3'-cGAMP standards were prepared in the cytosolic and nuclear cell lysis buffers to achieve precise calculation of the 2'-3'-cGAMP concentration in the samples. The cell fractions or standards were added to the ELISA plates, followed by antibodies against 2'-3'-cGAMP and horseradish peroxidase (HRP)-labeled – 2'-3'-cGAMP for a competition assay. After incubation for 2 hours, the plates were washed; subsequently, the reaction was developed using TMB and stopped by HCl. The optical density (OD) was measured at 450 nm using a microplate ELISA reader (Tecan). The data were processed using the Four Parameter logistic (4PL) curve calculator available online (myassays.com) as recommended by the manufacturer.

4.27. Generation of 3T6 cell line expressing GFP-cGAS

For the production of N-terminally eGFP-tagged mouse cGAS, the plasmid pMSCVpuro-eGFP-mcGAS, coding for GFP-cGAS, was transfected using Lipofectamine into Phoenix Ecotropic cells for the production of the retrovirus. Then, the retrovirus was used for transduction of 3T6 cells in the presence of polybrene. Mouse cells were further selected for stable integration using 1–10 $\mu g/m^{-1}$ puromycin.

4.28. Antibodies

Mouse monoclonal anti-VP2/3, rabbit polyclonal anti-VP1 antibody, mouse monoclonal anti-VP1, rat monoclonal anti-LT (provided by B. E. Griffin, Imperial College of Science, Technology and Medicine at St. Mary's, London, UK), mouse monoclonal anti-importin β1 antibody (Fisher Scientific), rabbit anti-KPNB1 (Bioss Antibodies), normal mouse IgG (Upstate Biotechnology), normal rabbit IgG (Upstate Biotechnology), rabbit polyclonal against GAPDH (Sigma–Aldrich), rabbit polyclonal anti-phospho-IRF3 (Ser369) (4D4G) (Cell Signalling Technology), rabbit polyclonal anti-phospho-IRF3 (Ser369) (D601M) (Cell Signalling Technology), rabbit polyclonal anti-phospho-STING (Ser365) (D8F4W) (Cell Signalling Technology), rabbit polyclonal anti-phospho-STING

(Ser365)(D1C4T) (Cell Signalling Technology), rabbit polyclonal anti-phospho-NF-kB (Ser536) (93H1) (Cell Signalling Technology), rabbit polyclonal against IFI16/p204 (Elabscience), rabbit polyclonal anti STING/anti MPYS (Sigma), rabbit polyclonal anti-p53 (Cell Signalling Technology), rabbit polyclonal anti-phospho-p53 (Ser15) (Cell Signalling Technology), rabbit monoclonal anti cGAS (Cell Signaling Technology), rabbit polyclonal anti-biotin antibody (A150) (Bethyl Laboratories), mouse anti-acetylated lysine (Cell Signaling), mouse anti-γH2AX (Millipore), rabbit anti-p53BP1 (Abcam), Alexa Fluor® 488 donkey anti-mouse IgG (Thermo Fisher Scientific), Alexa Fluor® 488 goat anti-rat IgG (Thermo Fisher Scientific), Alexa Fluor® 546 donkey anti-rabbit IgG (Thermo Fisher Scientific), goat anti-rabbit IgG-HRP (Bio-Rad), and goat anti-mouse IgG-HRP (Bio-Rad), Cy3® goat anti-rabbit IgG (ThermoFisher Scientific), Alexa Fluor® 488 goat anti-rabbit IgG (ThermoFisher Scientific), goat anti-rat IgG-HRP (Bio-Rad), Alexa Fluor® 647 goat anti-rat IgG (ThermoFisher Scientific).

4.29. Statistical analysis

Student's t-test was performed using the GraphPad Prism software, version 6.0 (GraphPad Software).

5. Results

5.1. This result section refers to the results published in the paper: **Soldatova Irina**, Prilepskaja Terezie, Abrahamyan Levon, Forstová Jitka, Huérfano Sandra: **Interaction of the Mouse Polyomavirus Capsid Proteins with Importins Is Required for Efficient Import of Viral DNA into the Cell Nucleus.** Viruses. 2018; 10(4):165.

The contributions of the co-authors are presented for individual experiments throughout the text. The published paper is in the appendix 1.

5.1.1. MPyV particles interact with importin β1 at early times post infection

Previous studies showed that prior to appearence in the nucleus, MPyV released from ER to the cytosol. Therefore, we decided to prove the role of cellular importins in the traficking of MPyV to the nucleus. For that, 3T6 cells were infected with MPyV (multiplicity of infection (MOI)=2) and incubated for 3, 6 and 8 hpi. Samples were collected and used for co-immunoprecipitation with antibody against importin β1 or mouse IgG as a negative control. Presence of the major capsid protein, VP1, minor capsid proteins VP2 and VP3, and importin β1 in obtained complexes was verified by western blot (Figure 20A-D).

We found that complexes, containing both VP1 and importin β1 proteins can be precipitated at 3 and 6 hpi. Immunocomplexes obtained at 8 hpi did not contain VP1. Additionally, amount of VP1 capsid protein detected at 6 hpi was higher than that at 3 hpi (Figure 20A, 20B). Neither VP1 nor importin were detected in immunoprecipitates obtained with the nonspecific, control rabit IgG. Western blot of the minor proteins revealed that VP2 could be detected in precipitated complexes at 6 hpi, while VP3 is detected at 3 and at 6 hpi (Figure 20C, 20D). To prove that obtained complexes represent the full viral particles, we isolated MPyV DNA and amplified VP1 gene by PCR. Viral DNA was detected at 3 and 6 hpi in agreement with the results of the western blot (Figure 20E).

Additionally, to show interactions of MPyV virions with importins, we performed PLA assay. For that 3T6 cells were infected with 200 viral particles per cell, fixed at 6 and 8 hpi and incubated with antibodies against VP1 and importin β1. As a positive control, we made the staining of VP1 protein using mouse anti-VP1 and rabbit anti-VP1 antibodies (Figure 21A). Red spots represent products of oligonucleotide ligation, which takes place only when the oligoprobes are in a close proximity (< 40 nm). We found that number of dots, representing interaction between capsid protein VP1 and importin β1 was 1028 per 50 cells at 6 hpi, while

only 379 dots per 50 cells were detected at 8 hpi. The background number of dots observed in non-infected cells was 230 per 50 cells (Figure 21B).

Altogether, our results demonstrate that MPyV interacts with importin β1 at the early times post infection and this interaction mainly occurs at 6 hpi.

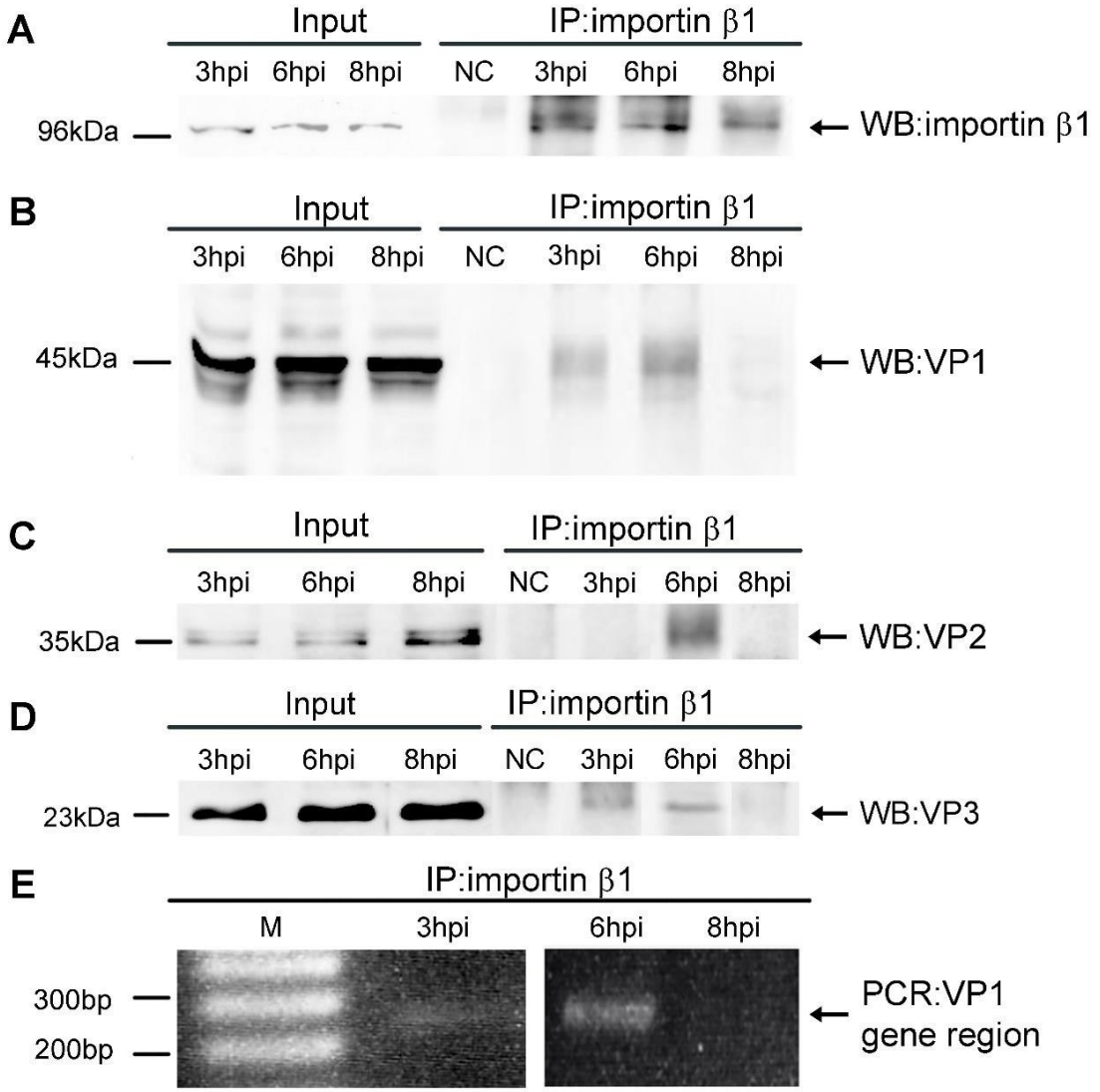

Figure 20. In vivo interactions between importin β1 and viral particles at early times post infection. Western blots of 3T6 cell lysates (labeled as Input) or complexes precipitated through antibody against importin β1 (labeled as IP) were performed with antibody against importin β1 **(A)**, VP1 **(B)** or VP2/VP3 **(C, D).** As a negative control (NC), samples precipitated through nonspecific anti-mouse IgG were used. The viral DNA was isolated from complexes and amplified by PCR at indicated times post infection **(E).**

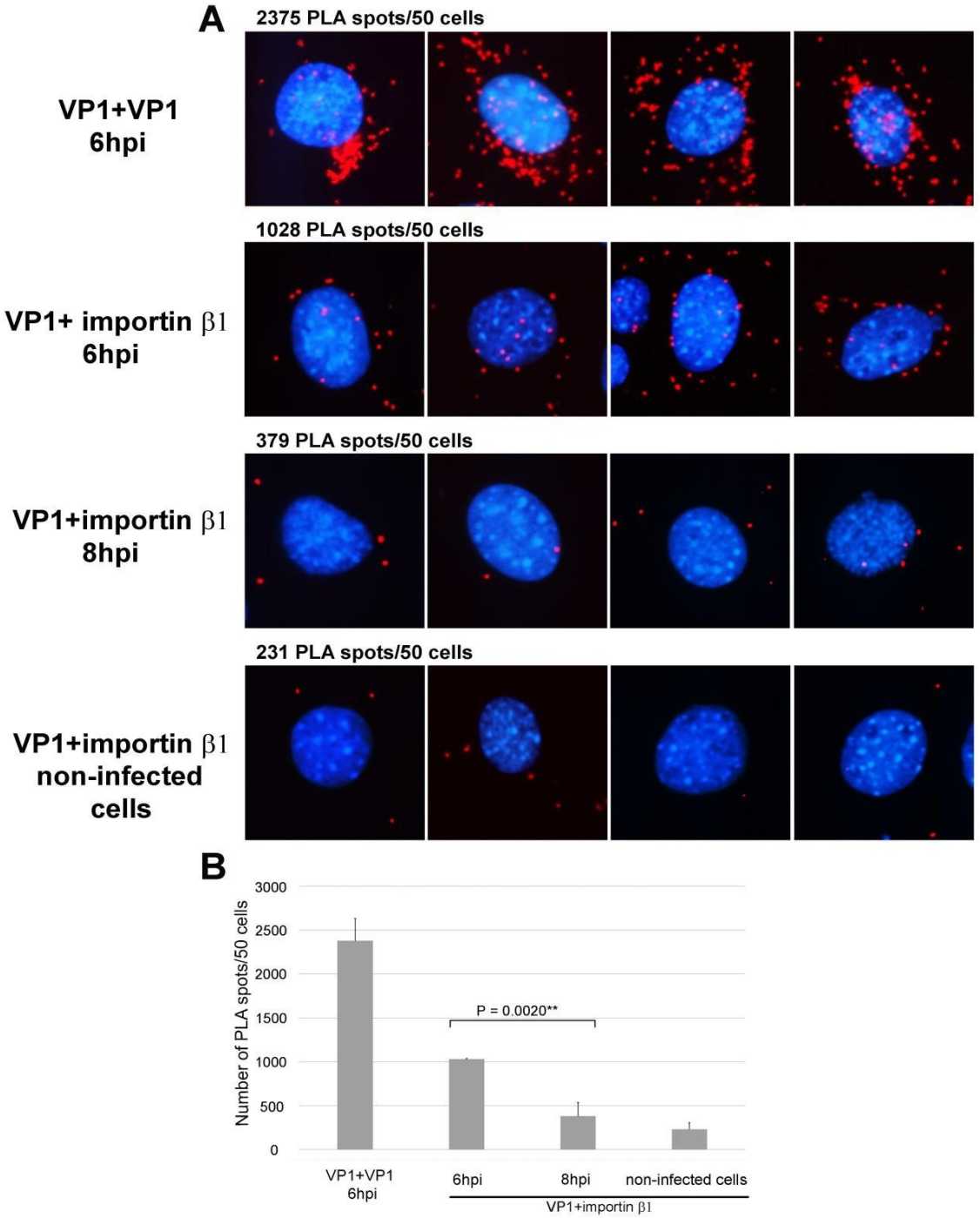

Figure 21. Proximity ligation assay of VP1 and importin β1 at 6 and 8 hpi. (A) PLA assay was performed on 3T6 cells infected with MPyV (200 virus particles per cell), using primary mouse and rabbit antibodies against VP1 or mouse antibody against VP1 and rabbit antibody against importin β1. Next, the oligoprobes tagged anti-mouse and anti-rabbit antibodies were used. Red spots represent the products of amplification after oligonucleotide ligation. DNA was stained by DAPI. As controls, the infected cells were stained with two antibodies (mouse and rabbit) against VP1 and non-infected cells were stained with anti-VP1 and anti-importin β1 antibodies. At the top of each image, the average numbers of the PLA spots quantified in three independent experiments are presented (for each experiment 50 cells were analyzed). The pictures were taken 20x magnification; **(B)** The graph represents the mean values of three independent experiments ± standart deviation (SD). Samples were compared by the Student's t-test. *P* values are given and asterisks represent statistically significant differences (**$p \leq 0.01$).

5.1.2. Creation of MPyV mutants with amino acid changes in NLS sequences of capsid proteins

Previously, eleven N-terminus amino acids (M_1APKRKSGVSK_{11}) of VP1 and twelve C-terminus amino acids (E_{308}EDGPQKKKRRL$_{319}$) of VP2/VP3 contain NLS sequences which are required for the importin mediated transport of these proteins to the cell nucleus for virion assembly were identified [Engel et al., 2011; Caruso et al., 2003]. Both these sequences are enriched with lysine (K) and arginine (R), which are essential for interaction of NLS with importins. Therefore, we decided to create mutant viruses, with substitution of basic amino acids (aa) in these sequences (to disrupt or weaken NLS) or with introducing of additional basic aa by substitution (to enhance NLS strength), and to analyze the ability of mutated virions to translocate from cytoplasm to the nucleus.

However, we met the serious problem that the N-terminus sequence of VP1 and the common C-terminus sequence of VP2 and VP3 proteins partially overlap (by 33 nucleotides). As a consequence, changes in NLS of VP2/VP3 affect the strength of NLS of VP1 and vice versa [Liebl et al., 2006]. Mutations were designed with respect to the minimum number of substitutions and based on nuclear localization prediction analyzes using NucPred software which gave results in a score. The score numbers between 0,1 and 1 mean that proteins can spend some time in the nucleus. The higher score most likely indicates that the protein is located in the nucleus [Griffith and Consigli, 1984].

Three mutant viruses were designed (*by Sandra Huerfano*). Mutant 1 and mutant 2 had one aa substitution in NLS of VP1 (lysine (K6) by glutamine (Q6)). One aa change was introduced into NLS of VP2/VP3 of mutant 1 (lysine (K315) by alanine (A315)), and two additional mutations (lysines (K314, K315) by alanines (A314, A315)) were introduced into VP2/VP3 proteins of mutant 2. Mutant 3 has three amino acid changes in NLS of VP1 (lysine (K6) by glutamine (Q6), serine (S7) by arginine (R7) and glycine (G8) by arginine (R8)) and three substitutions in NLS of VP2/VP3 (lysines (K314, K315) by alanines (A314, A315) and arginine (R317) by alanine (A317)). We expected that mutants 1 and 2 should have weakened both NLS of VP1 and VP2/3. Mutant 3 should have disrupted NLS of VP2/VP3 but NLS of VP1 should be retained, or even enhanced.

Sequences of wt and mutated VP1 (top) and VP2/VP3 (bottom) capsid proteins are given in a Figure 22. Basic amino acids are labeled with a red color and introduced mutations are shown in green. Results of NucPred measurements are presented on the right and the scores are in agreement with our expectations.

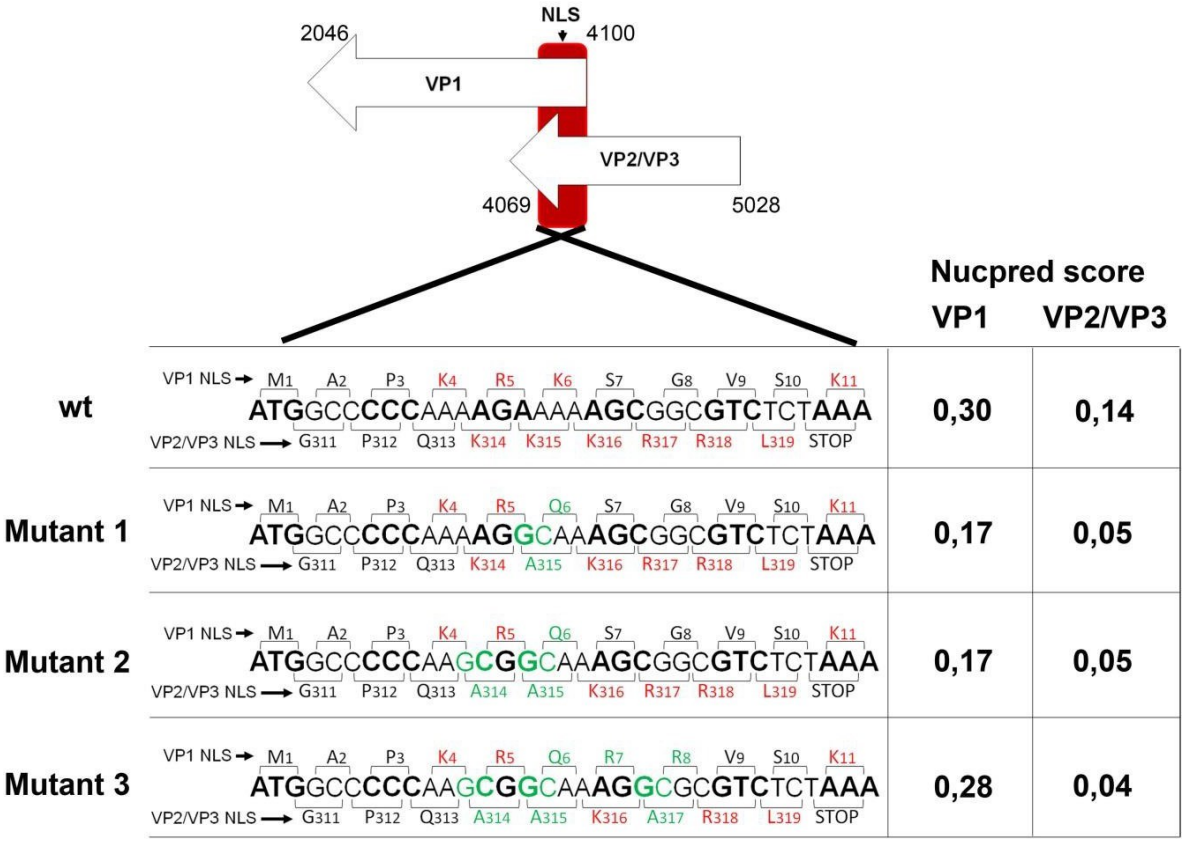

Figure 22. Mutagenesis design. Wild type MPyV overlapping coding sequences for VP1 and VP2/3 genes are displayed with the corresponding aa at the top of the nucleotide triplet for VP1 or at the bottom of the nucleotide sequence for VP2/3 (brackets show the codons). Positions of aa residues are given for VP1 (top) and VP2 (bottom) proteins, respectively. For better differentiation, codons for VP1 are alternate in bold and not bold letters. Mutants 1, 2, and 3 are also presented. For better display, the basic aa (K and R) are shown in red and the mutated nucleotides and corresponding aa are shown in green. NucPred score values for NLSs of VP1 and VP2/3 capsid proteins of the wt or mutated variants are presented on the right.

On the next stage, we created designed mutant viruses, using pMJG plasmid containing entire genome of MPyV strain BG as described in materials and methods (*performed by Sandra Huerfano*). Then, mutated genomes were transfected to 3T6 cells, and mutant viruses were isolated according to standard protocol (*mutant viruses were produced in cooperation with Sandra Huerfano and Terezie Prilepskaja*).

To verify the results of mutagenesis, viral DNA was isolated and sent for the sequencing. As a control, DNA isolated from wt virus was used (Figure 23A). Obtained results indicated that we produced a homogeneous populationof mutant viruses without any revertants. Additionally, we made the electron microscopy and found that mutations did not affect to the structure and size of viral particles. Western blot revealed that the binding of the minor proteins to the VP1 pentamers was not affected and the major capsid protein VP1 and the minor capsid proteins VP2 and VP3 were present in all 3 mutants. Their relative amount in mutant virions

was similar as their ratio in the wt virions (Figure 23B, 23C).

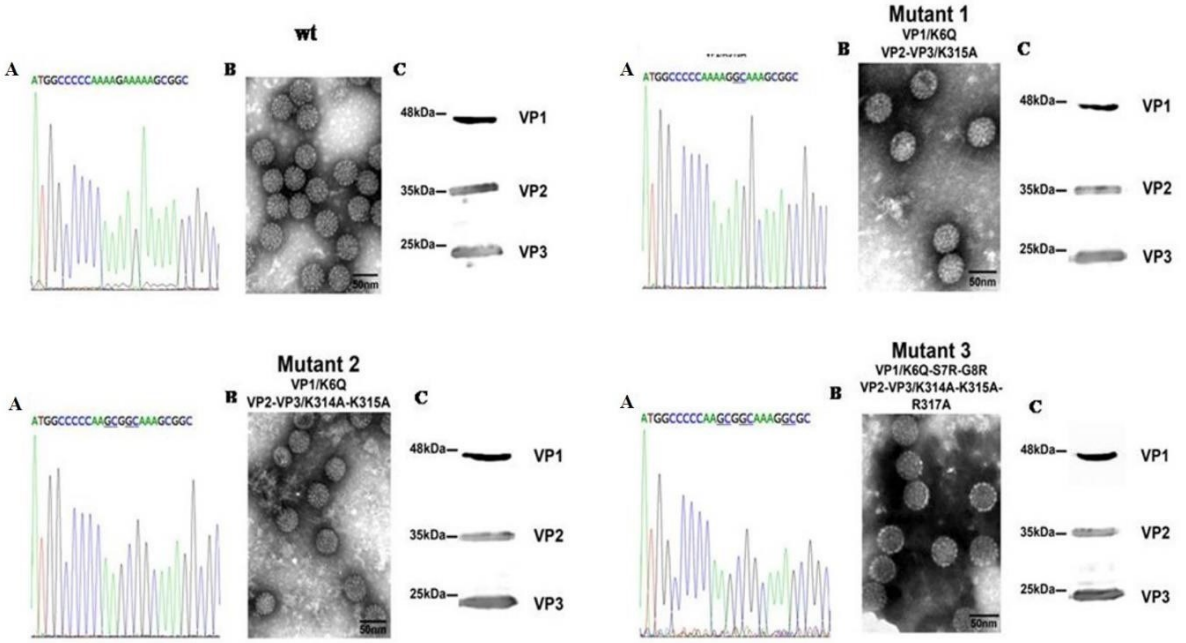

Figure 23. Characterization of designed mutants. **(A)** To verify the efficiency of mutations introduced into the genomes as well as to detect possible revertants we isolated DNA from virus preparations and sequenced regions of interest. Different nucleotides are shown with different colours. Introduced mutations are underlined. **(B)** WT and mutated viruses 1, 2 and 3 were produced in 3T6 cells, isolated and contrasted with phosphotungstic acid. Viral particles were visualized with electron microscopy (Bars=50 nm). **(C)** Presence of VP1, VP2 and VP3 proteins in produced viruses was detected by western blot analysis using specific antibodies against capsid proteins.

Infectivity assay performed in 3T6 cells infected with wt or mutant viruses (genome equivalent $1{,}5x10^4$ per cell) and fixed at 24 hpi, showed that disruption of NLS sequences of VP1 and VP2/VP3 capsid proteins affected the ability of mutants to infect cells (*made in cooperation with Sandra Huerfano*). Thus, mutant 1 with one amino acid change in NLS of VP1 and one amino acid change in NLS of VP2/VP3 has only 66% of infectivity in comparison with the wt virus. Mutant 2, with the same mutation in NLS of VP1 as mutant 1 and two basic aa substitutions in NLS of VP2/VP3 capsid proteins displayed only 25% of infectivity of the wt virus. Mutant 3 with newly enhanced NLS of VP1 and three amino acid changes in NLS of VP2/VP3, exhibited infectivity, comparable with the wt virus (Figure 24A).

To verify the ability of mutant 2 to interact with importin β1, we performed PLA assay. 3T6 cells were infected with mutant 2 or wt virus for 6 hours, fixed and stained (Figure 24B). Number of spots per 50 cells was quantified in two independent experiments (Figure 24C). As a positive control, in infected cells was visualized VP1 protein by using rabbit anti-VP1 and mouse anti-VP1 antibodies. Mock infected cells were used as a negative control. We found, that in cells, infected with mutant 2 the number of spots was 18% in comparison with

wt virus and very close to the negative control. This means, that mutant 2 almost does not interact with importin β1.

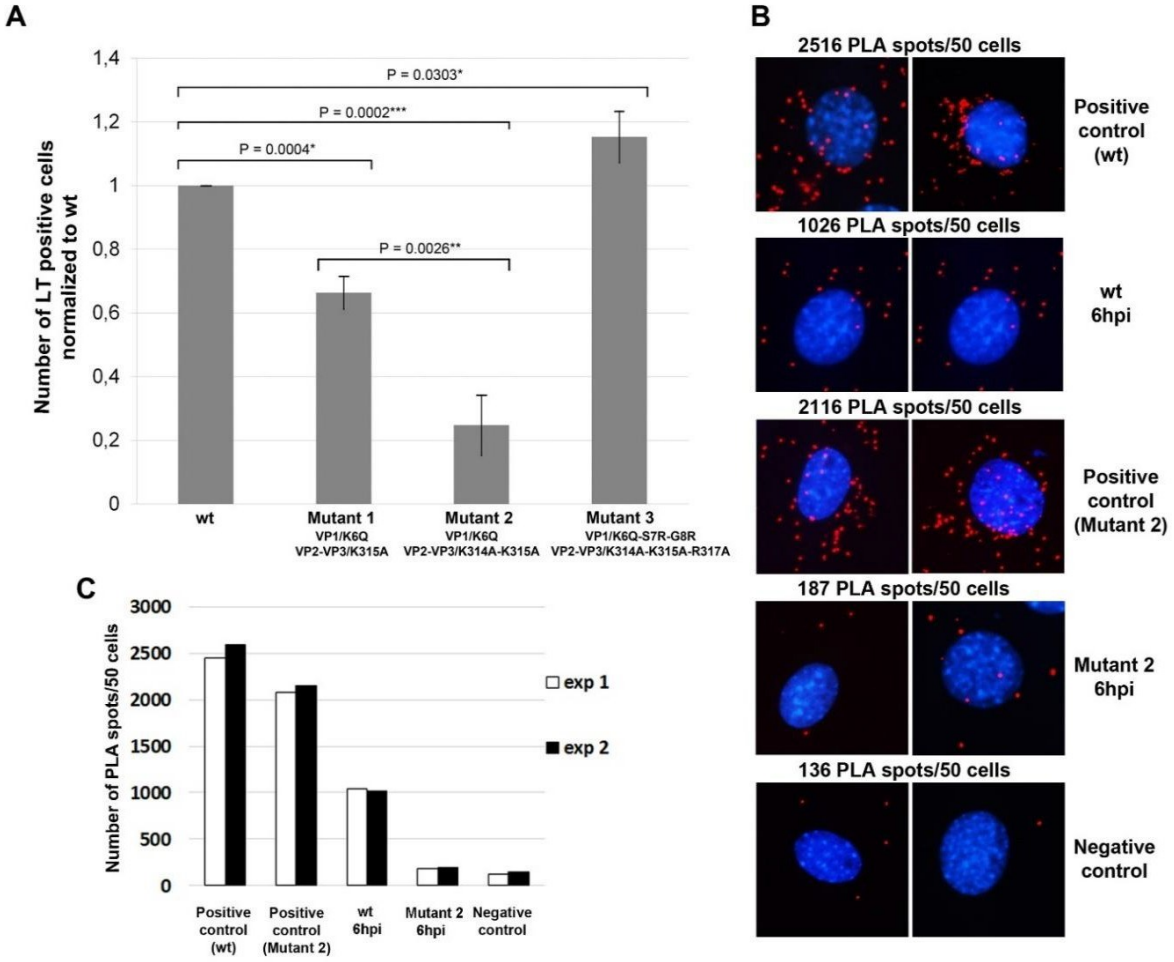

Figure 24. Effects of mutations in the NLS of VP1 and VP2/3 on viral infection and on binding of viruses to importin β1. (A) 3T6 cells were infected with wt or mutant viruses 1, 2, or 3 (using virus equivalent representing $1.5x10^4$ genomes per cell). Cells were fixed at 24 hpi and LT antigen was stained by specific antibody. The presented data correspond to the mean of three independent experiments ± SD. At least 300 cells were counted per experiment. Samples were compared by the t-test. *P* values are given and asterisks represent statistically significant differences (*$p \leq 0.1$, **$p \leq 0.01$ ***$p \leq 0.001$). **(B)** PLA assay was performed in 3T6 cells at 6 hpi with wt MPyV or the mutant 2 virus (200 virus particles per cell). For this experiment, we used primary mouse and rabbit antibodies against VP1 or mouse antibody against VP1 and rabbit antibody against importin β1. Next, the oligoprobes tagged with anti-mouse and anti-rabbit antibodies were used. Red spots represent the products of amplification after oligonucleotide ligation. DNA was stained by DAPI. As controls, the infected cells were stained with two antibodies (mouse and rabbit), both against VP1 and non-infected cells were stained with anti-VP1 and anti-importin β1 antibodies. At the top of each image, the average numbers of the PLA spots quantified in two independent experiments are presented (for each experiment spots in 50 cells were counted). The pictures were taken 20x magnification. **(C)** The graph represents the mean values of two independent PLA experiments.

All these results suggest that importins are used for delivery of MPyV genomes to the nucleus. NLSs of both VP1 and the minor capsid proteins VP2 and VP3 become exposed due to partial disassembly of virions in ER prior to their translocation to the cytosol. Also, results

indicate that the capsid proteins are apparently present in the MPyV complex translocating to the nucleus.

Then, we followed localization of newly synthesized capsid proteins. For that, 3T6 cells were infected with wt MPyV or mutant viruses 1-3 and fixed 24 hpi. Localization of VP1 and VP2/VP3 proteins was visualized by confocal microscopy (Figure 25). We found, that in cells infected with mutants 1 and 2, VP1 protein was localized in cytoplasm with microtubules (Figure 25b, 25f). Cells infection with mutant 3 showed nuclear localization of VP1 (Figure 25j). The same results were observed for wt virus (Figure 25n). VP2/VP3 capsid proteins of the mutants 1 and 2 were found in both, cytoplasm and the nucleus, while the minor capsid proteins of the mutant 3 were presented in the nucleus, similar to the wt virus (Figure 25c, 25g, 25k, 25o).

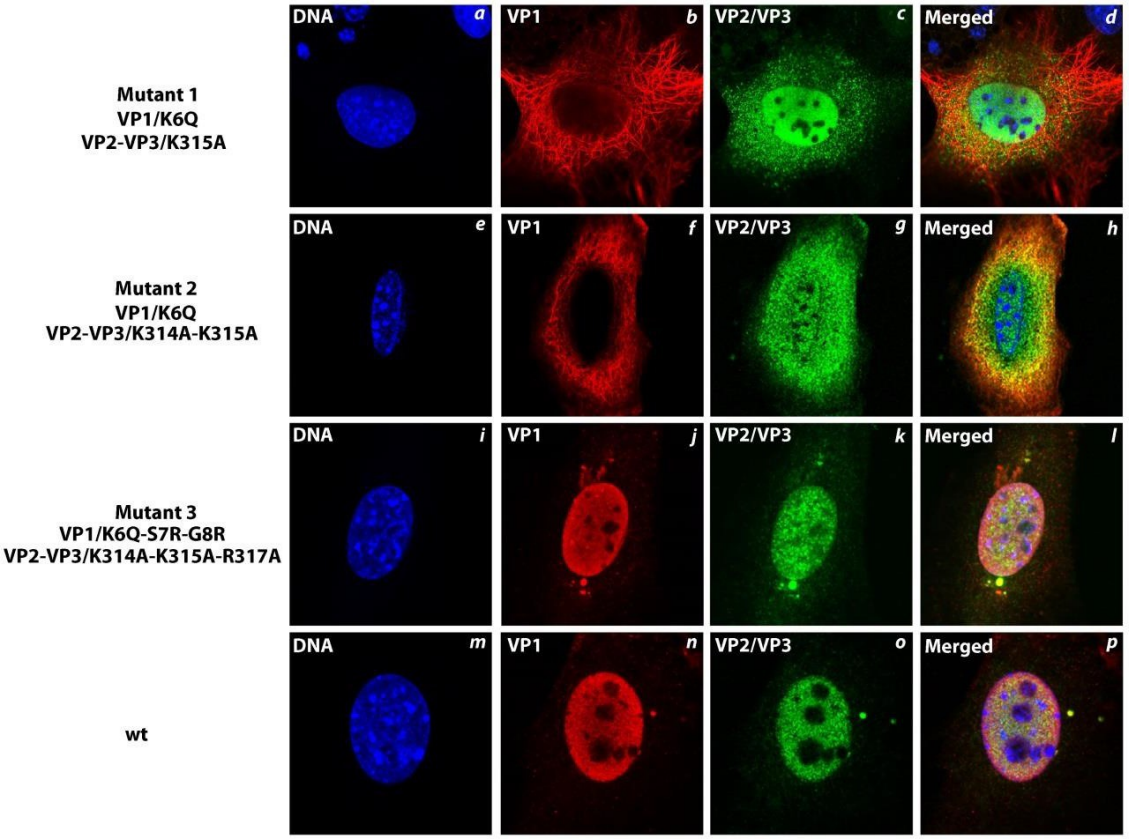

Figure 25. Effect of mutations in NLS of MPyV structural proteins VP1, VP2, and VP3 on their cellular localization during infection. Confocal sections of 3T6 cells infected with wt (m–p) or mutated viruses 1 (a–d), 2 (e–h), or 3 (i–l). Cells were fixed at 24 hpi and stained by antibodies against VP1 (red), VP2/3 (green), and DNA by DAPI (blue). Bars=5 μm.

These results indicate that one strong NLS is enough for the replacing a function of the others as it occurs in the mutant 3.

5.1.3. Studies of the cellular distribution of individually and co-expressed mutated capsid proteins VP1 and VP2

Based on the last result mentioned above, we considered two facts: i) First, localization of capsid proteins at the late times post-infection is influenced by formation of complexes of VP1 pentamers with VP2/VP3 in cytoplasm preceding transport to the nucleus and viral morphogenesis. Therefore, the effect of the mutations can be misleading in the context of infection. ii) Second, the possibility of passive diffusion of small capsid proteins VP2 and VP3 (35 and 23 kDa, respectively) also can lead to incorrect interpretation of results. Therefore, we prepared mutated capsid proteins, introducing the same amino acid changes which were made during production of mutant viruses into expression plasmids encoding individual MPyV-VP1 or MPyV-VP2 genes.

Then, 3T3 cells were transfected with wt or mutant proteins and fixed at 24 hours post transfection (hpt) for VP1 and at 5 hpt for VP2 staining (Figure 26A and 27A, respectively). Fixation of cells with VP2 protein was performed at earlier time due to the high toxicity of the minor proteins when they are expressed without VP1. Cellular distribution of proteins was analysed in 50 cells for each wt or mutant variants (Figure 26B and 27B).

Confocal microscopy sectioning revealed two cellular populations of wt VP1 distribution: 1) VP1 localized either in both cytoplasm and the nucleus (47,2% from 50 analysed cells) (Figure 26i), or 2) predominantly localised in cytosol (52,8%) (Figure 26ii). VP1 protein, containing one amino acid substitution (mutants 1 and 2) localized exclusively in cytoplasm (Figure 26iii). Interestingly, very often we observed fiber patterns made by these mutants (in 80% of analyzed cells). VP1 protein of the mutant 3 with three amino acid changes, resulted in creation of a new NLS, was localized 1) in the nucleus and cytosol of infected cells as wt VP1 (59,2%) (Figure 26iv), or 2) in cytoplasm only (13%), or 3) predominantly in the nucleus (27,8%) (Figure 26v). Therefore, we made a conclusion, that VP1 of the mutant 3 has NLS stronger than that of the wt VP1.

A

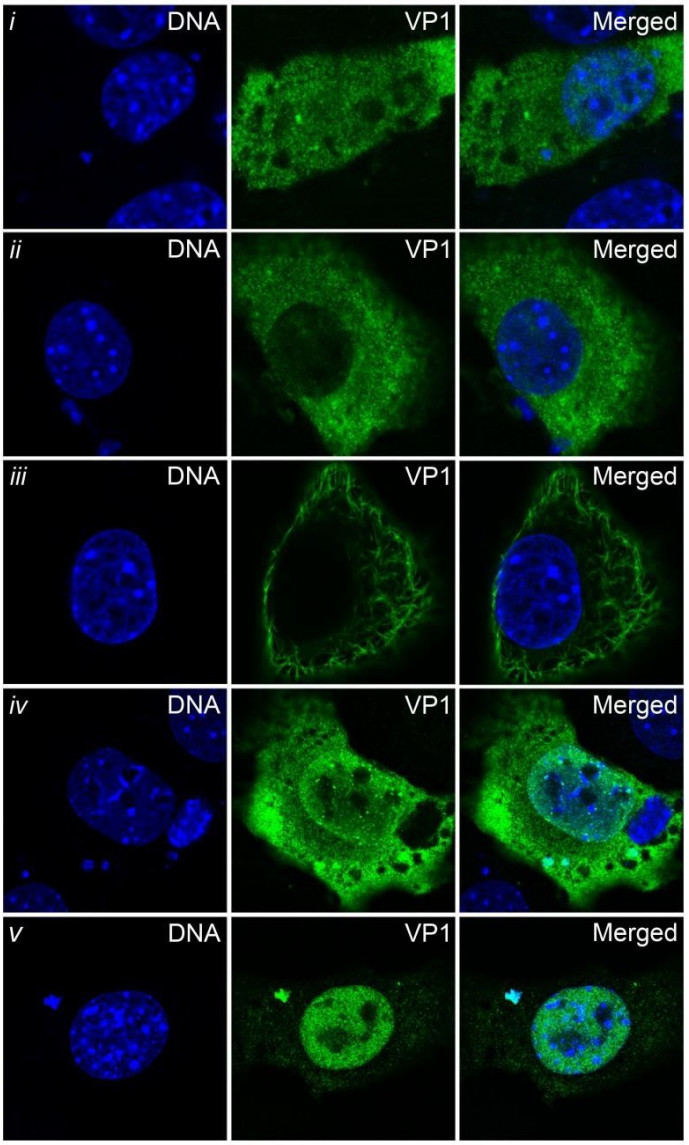

B

Protein	% of cells with protein localized:		
	Predominantly in nucleus	Abundant in nucleus and cytosol	Predominantly in cytosol
wt VP1	0%	47,2%	52,8%
Mutant VP1 K6Q	0%	0%	100%
Mutant VP1 K6Q-S7R-G8R	27,8%	59,2%	13%

Figure 26. Subcellular distribution of wild type or mutated VP1 capsid proteins. Confocal sections of 3T3 cells expressing wt or mutated VP1 proteins. Cells were fixed at 24 hpt and stained with anti-VP1 antibody (green) and DNA by DAPI (blue) **(A)**. For analysis of subcellular distribution of wt (i–ii) or mutated proteins (iii–v), 50 cells were examined for each variant. Bars = 5 μm. Scores are given as percentage **(B).**

Analysis of VP2 localization showed that wt VP2 protein was localized: 1) mainly in cytoplasm and the nucleus of transfected cells (79% of 50 counted cells), or 2) predominantly

in the cell nucleus (21%). One amino acid substitution in NLS of VP2 resulted in: 1) predominantly cytoplasmic localization of the protein (79%), and 2) nuclear and cytoplasmic distribution (21%). Two amino acid changes lead to mainly cytoplasmic localization of the protein (81%of cells) (mutant 2), while 3 amino acid substitutions made the protein exclusively cytosolic (100% cells) (mutant 3) (Figure 27).

These results indicate that even changing of just one basic amino acid in NLS of capsid proteins significantly affects their cellular distribution. Neither wt NLS of VP1 nor wt NLS of VP2 are strong enough for efficient translocation to the nucleus when they are expressed individually.

A

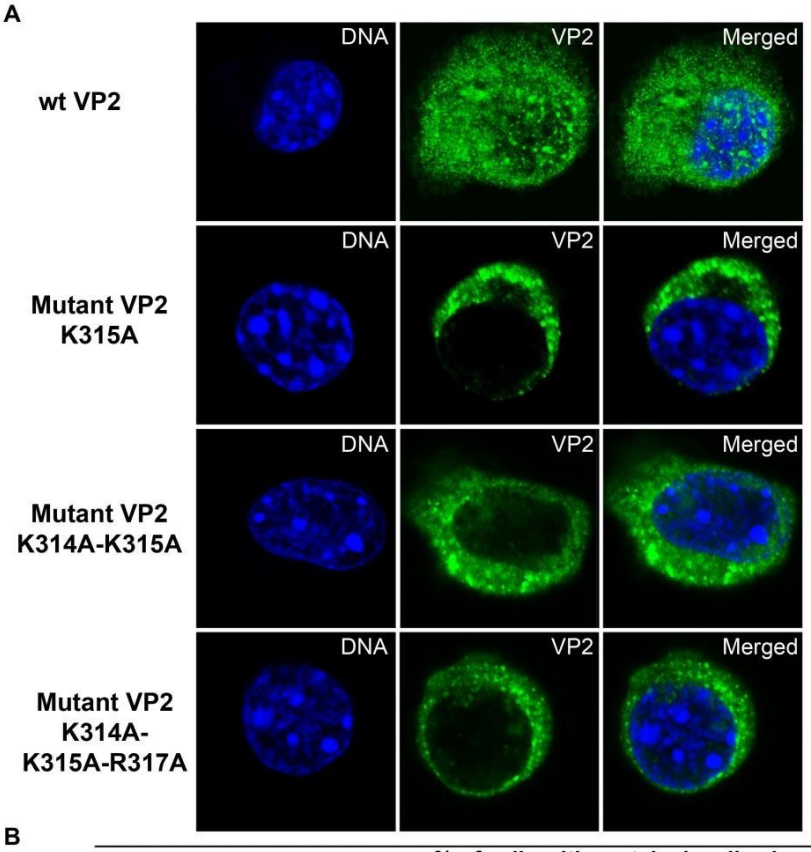

B

Protein	% of cells with protein, localized:		
	Predominantly in nucleus	Abundant in nucleus and cytosol	Predominantly in cytosol
wt VP2	21%	79%	0%
Mutant VP2 K315A	0%	21%	79%
Mutant VP2 K314A-K315A	8%	11%	81%
Mutant VP2 K314A-K315A-R317A	0%	0%	100%

Figure 27. Subcellular localization of wild type or mutated VP2 proteins. Confocal sections of 3T3 cells expressing wt or mutated VP2 proteins. Cells were fixed at 5 hpt and stained by antibodies against VP2 (green) and DNA by DAPI (blue). Bars=5 μm **(A).** Scores are given as percentage **(B).**

Next, we performed co-transfection of 3T3 cells with wt and mutated variants of VP1 and VP2 capsid proteins and followed their localization by confocal microscopy at 24 hpt (Figure 28). Per each combination of proteins, 50 cells were analysed. We found that all combinations of mutated VP2 and wt VP1 and vice versa resulted in efficient nuclear transport of both proteins. These results indicate, that one functional NLS either of VP1 or minor capsid protein is sufficient for successful transport of protein complexes to the cell nucleus, but not for productive trafficking of viral particles.

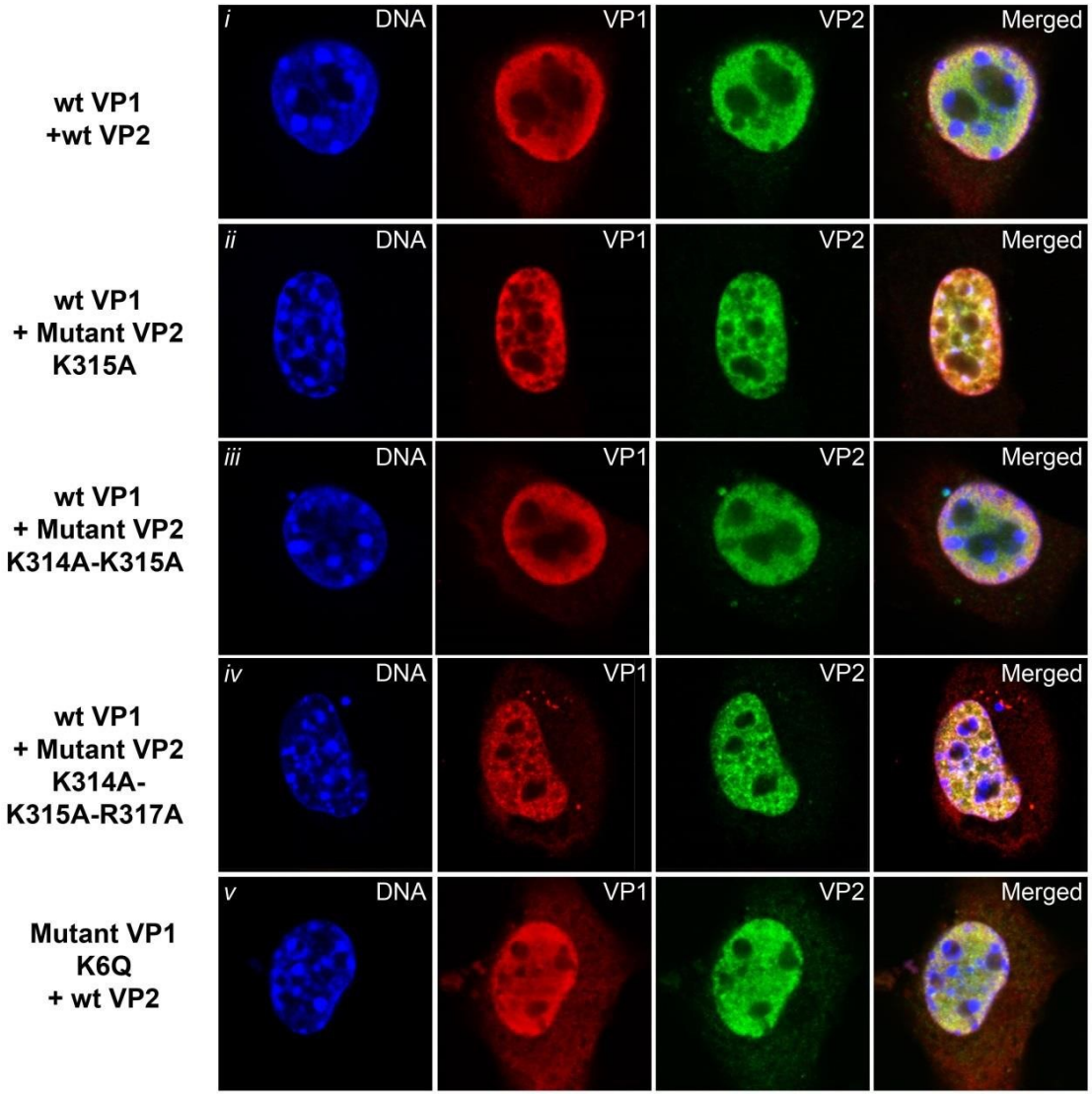

Figure 28. Nuclear entry of wt and mutant variants of the VP1 and VP2 proteins. Confocal sections of 3T3 cells co-expressing combinations of wt VP1 and wt VP2 (i) or wt VP1 and mutated variants of VP2 (ii–iv) or wt VP2 with the mutated variant of the VP1 (v). Cells were fixed at 24 hpt and stained with antibodies against VP1 (red) and VP2 (green). DNA was stained by DAPI (blue). Bars=5 μm.

Based on our findings, we can conclude that translocation of MPyV from the cytosol to the nucleus is mediated by importins. One strong NLS either of VP1 or VP2/VP3 is enough

for nuclear translocation of virions. However, the presence of all capsid proteins is required for importin binding, possibly due to formation of suitable surface conformation of virions or VP1 pentamer – VP2 (or VP3) complexes.

5.2. This result section presents an extended version of the results published in the paper: Ryabchenko Boris, **Soldatova Irina,** Sroller Vojtech, Forstova Jitka, Huerfano Sandra. **Immune sensing of mouse polyomavirus DNA by p204 and cGAS DNA sensors.** FEBS J. 2021 May 10. https://doi.org/10.1111/febs.15962

My contributions to this work is presented for individual experiments throughout the text. The paper is in the appendix 2.

In the previous chapter, we demonstrated that virions of MPyV, travelling in endosomal compartments throughout the cytoplasm to ER, appear naked and partially disassembled in the cytosol prior to their translocation into the nucleus. The C-terminus of the minor capsid proteins and the N-terminus of VP1, otherwise hidden within intact virions, become accessible for interactions with importins. Recently, Ravindran et al. found that additional disassembly of the related polyomavirus (SV40) taking place after virion release from ER before translocation through nucleopore [Ravindran et al., 2018]. Thereby, we were interested if MPyV can be sensed by DNA sensors.

5.2.1. MPyV activates IFN-β production at the late time post infection through STING and IRF3

Firstly, we decided to prove if MPyV infection can activate IFN-β production. For that, 3T6 cells were infected with MPyV (MOI=5 and MOI=30) and collected at 5, 10, 24 and 30 hpi. Mock infected cells were used as a control. RNA was isolated, and expression of *IFN-β* and IFN inducible gene, *MX-1*, were measured by quantitative real-time RT-PCR (qPCR). We found up-regulation of IFN-β and MX-1 transcription at 24 hpi, with strong increase at 30 hpi (Figure 29A, 29B). Interestingly, the levels of IFN-β and MX-1 mRNAs were higher in cells infected with MOI=30 (Figure 29B). Additionally, we decided to prove that 3T6 cells used in these experiments are able to activate IFN-β production to different stimuli. For that, cells were exposed with plasmid DNA (pDNA), CpG, Poly I:C and 2'-3'cGAMP and incubated for indicated times. RNA was isolated and the levels of IFN-β and MX-1 transcription was measured (Figure 29C, 29D). We found that different stimuli induce up-regulation of *IFN-β* from 4000 to 80 000 times in 3T6 cells. MPyV infection induced IFN-β overexpression only about 300 times (MOI=30). The levels of MX-1 induced by viral infection and some stimuli were comparable.

These results indicate that MPyV activates innate immunity and IFN-β production at the later stages of infection, at the time of replication of viral genomes in the nucleus. The response is weak in comparison with other stimuli and depends on MOI. The regulation of *MX-1* gene is probably tightly controlled in 3T6 cells.

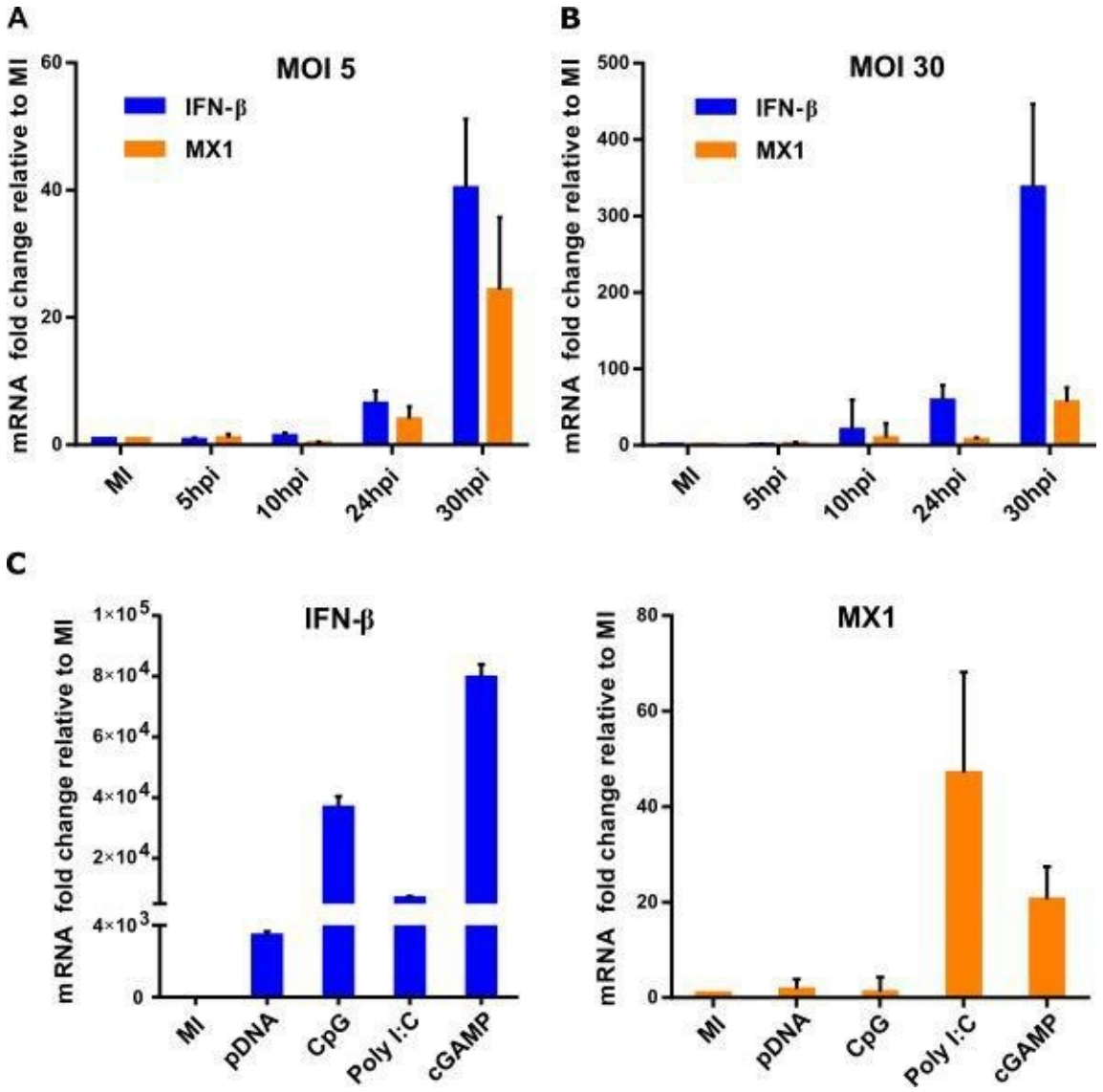

Figure 29. Kinetics of the IFN response during MPyV infection. (A, B) Mouse 3T6 fibroblasts were infected with MPyV at MOI=5 **(A)** or MOI=30 **(B).** After 5, 10, 24, and 30 hpi, the cells were collected, and RNA was isolated. **(C, D)** 3T6 cells were stimulated with pDNA, CpG, Poly (I:C), or 2'-3'cGAMP and collected at the indicated times (described in Materials and methods) for RNA isolation. For all samples **(A–D),** the levels of IFN-β and MX-1 RNAs were detected by qPCR and normalized to the GAPDH mRNA levels. The displayed data correspond to one representative experiment from at least three independent repeats (each experiment was performed with a different viral stock), and the presented values correspond to the mean of biological triplicate ± SD. Selected data were compared using Student's t-test. Asterisks indicate *p*-values representing statistically significant differences. For **(A)** IFN-β, $^{**}p = 0.0024$; for **(B)** IFN-β, $^{***}p = 0.0007$; for **(C)** IFN-β, $^{****}p = 0.0001$ and **(D)** MX-1, $^{**}p = 0.0074$. For the experiments, mock infected cells (MI) were used as the control.

Next, we followed activation of components known to be involved in signalling

pathway leading to IFN-β induction, transcription factor IRF3 and mediator of the IFN type I response to pathogenic intracellular DNA, STING protein.

For that, 3T6 were infected with MPyV (MOI=10) and collected at 6, 10, 15, 18, 24 and 30 hpi. Cell lysates were prepared and used for western blot analysis. Mock infected cells were used as a negative control. LT was detected as a control of viral infection and GAPDH was used as a loading control. We found that activation (by phosphorylation) of both, STING and IRF3, occured at 24 and 30 hpi, while in the earlier time it was not observed (Figure 30A). In agreement, confocal microscopy of infected cells confirmed presence of phospho-STING (p-STING) in cytoplasm at 24 hpi (Figure 30B) (*Experiment was performed by me*).

These results confirmed activation of signalling pathway of IFN-β and suggested that viral nucleic acids might be sensed first in the cell nucleus during MPyV genome replication.

To reveal the influence of STING on IFN-β production, we used MEF STING knockout cell line (STING KO). Parental MEF STING wild type (STING wt) and STING KO cells were infected with MPyV (MOI=20) collected at 30 hpi and used for subsequent analysis (Made by Sandra Huerfano). First, we confirmed the absence of STING in knockout cell line by western blot (Figure 30C). Then, we followed IRF3 phosphorylation and showed that it occurs only in STING wt cell line but not in STING KO cells (Figure 30C).

On the next stage, we measured levels of mRNAs of *IFN-β* and *MX-1* genes by qPCR. We found that infection of STING wt cells with MPyV stimulates transcription of IFN-β (188-fold) and MX-1 (48-fold). In contrast, we did not detect up-regulation of these genes in STING-KO cells (Figure 30D). Further, to characterize the ability of STING KO cells to activate IRF3 and produce IFN-β in response to other stimuli such as RNA, we treated them with Poly I:C (Figure 30E, 30F). We found that RNA stimulation of STINK KO cells induced phosphorylation of IRF3 and production of IFN-β and MX-1 mRNA. Thus, our results demonstrated that MPyV infection induces IFN production by activation of STING and phosphorylation of IRF3.

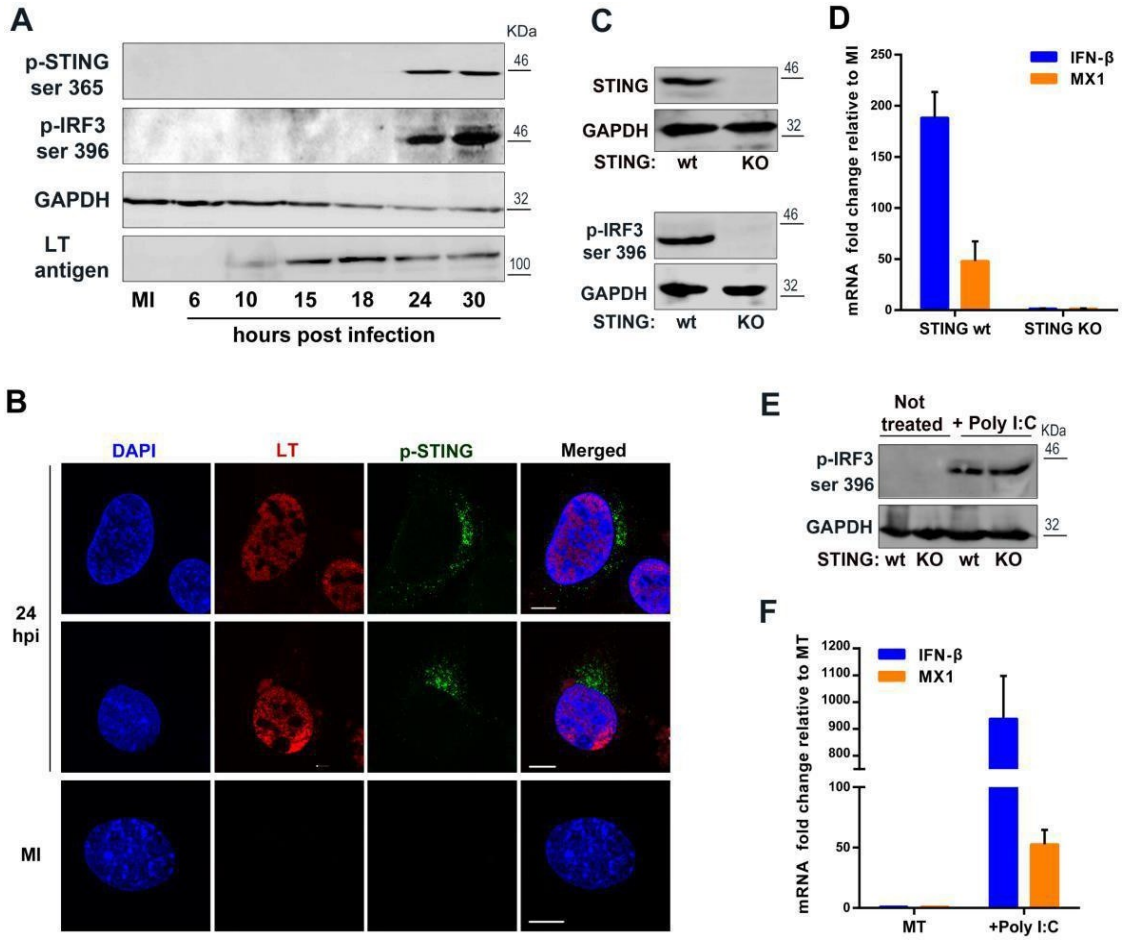

Figure 30. STING and IRF3 are involved in the IFN response induced by MPyV. (A) Mouse 3T6 fibroblasts were infected with MPyV (MOI=10). At the indicated times, cell lysates were prepared and phospho-IRF3 (p-IRF3), phospho-STING (p-STING), or GAPDH and LT antigen as controls, were detected by western blotting. **(B)** Mouse 3T6 fibroblasts were either mock-infected (MI) or infected with MPyV (MOI=3), fixed at 24 hpi, and stained by DAPI (blue) and by antibodies directed to MPyV early LT antigen (red) and p-STING (green). Confocal microscopy images of representative cell sections are presented. Bars=10 μm. **(C)** MEF STING KO or STING wt cells were infected with MPyV (MOI=20) and the cell lysates were prepared at 30 hpi. The samples were analyzed by western blotting for the presence of STING, pIRF3 and GAPDH as a loading control. **(D)** MEF STING KO and STING wt cells were mockinfected or infected with MPyV (MOI=20). At 30 hpi, RNA was isolated and subjected to qPCR for quantification of IFN-β, MX-1and GAPDH mRNAs, with values normalized to the transcripts in the mock-infected cells (MI). **(E, F)** MEF STING KO or STING wt cells were treated with Poly I:C (+) or mock treated (MT) and cells were collected after 16 h. Cell lysates were prepared and the presence of p-IFR3 and GAPDH (as a loading control) was followed by western blotting **(E).** RNA was isolated and the IFN-β, MX-1, and GAPDH mRNA levels were quantified by qPCR **(F).** For **(A)**, **(C)**, and **(E)**, each of the presented western blots is representative of at least two independent experiments. For **(D)** and **(F)**, the presented data correspond to the mean values of three independent experiments; the corresponding SD values are presented. Selected data were compared using Student's t-test. Asterisks indicate *p*-values representing statistically significant differences. For **(D)** IFN-β, ****$p = 0.0001$ for (F) IFN-β, ****$p = 0.0001$

5.2.2. Production of IFN-β induced by MPyV infection depends on the presence of viral genomes in the cell nucleus

To ensure that the nuclear phase of MPyV infection is essential for sensing of viral DNA, we used a mutated MPyV constructed in previous study (the mutant 2 described in the first part of the thesis). The mutated virus can enter cells with similar efficiency as the wt virus, travels in endosomal compartments and translocates from ER to cytosol on its productive pathway as the wt virus. However, this mutant cannot be delivered to the nucleus via nuclear pores due to mutations introduced into NLS of the capsid proteins. Its infectivity decreased by 80%. Mouse 3T6 cells were infected with wt or mutated MPyV (with MOI corresponding to 200 genomes per cell, quantified by qPCR), collected at5 and/or 30 hpi and used for measurement of STING and IRF3 activation and IFN-β production. As a control, mock infected cells were used. As expected, we found that phosphorylation of STING and IRF3 occurred at 30 hpi in cells infected with wt MPyV. Cells infection with NLS mutant exhibited markedly weaker activation of STING and IRF3 at 30 hpi (Figure 31A). Neither phospho-STING, nor phospho-IRF3 were detected at 5 hpi in both wt and mutant virus infected cells. Further, we measured the levels of IFN-β and MX-1 mRNAs. We detected their significant decrease (for IFN-β by 60% and for MX -1 by 70%) in cells infected with mutated MPyV in comparison to wt virus infected cells (Figure 31B).

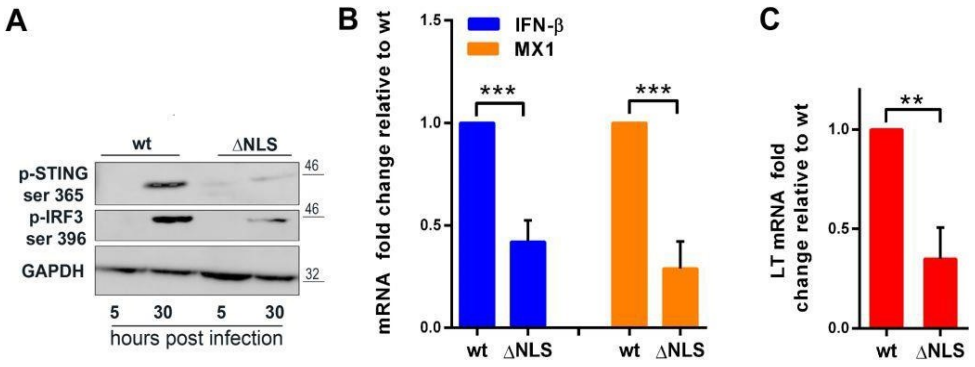

Figure 31. IFN response in MPyV-infected cells is strongly dependent on the presence of viral genomes in the cell nucleus. 3T6 fibroblasts were infected with MpyV wt (wt) or MpyV mutated in NLS (ΔNLS) with MOI corresponding to 200 genomes per cell, as quantified by qPCR. The cells were collected at 5 or 30 hpi for the preparation of cell lysates and at 30 hpi for isolation of RNA. **(A)** Cell lysates were subjected to western blotting and assayed for p-IRF3, p-STING, and GAPDH. The shown western blot is representative of two experiments. **(B)** RNAs were isolated and the mRNA for IFN-β, MX-1 **(B)**, or for LT **(C)** were measured by qPCR. For **(B)** and **(C)**, the presented data correspond to mean values of three independent experiments (performed with three different viral stocks); the corresponding SD values are given. For each experiment, the values were normalized to those of wt virus. The data were compared using Student's t-test. Asterisks indicate *p*-values representing statistically significant differences (IFN-β, ***$p = 0.0006$; MX-1, ***$p = 0.0007$; LT, **$p = 0.0021$).

Production of LT antigen was also reduced after infection with NLS mutant (by 70%) (Figure 31C).

This result confirms that induction of immune response by MPyV infection is associated with the late stages of viral infection and replication of viral genomes in the cell nucleus.

5.2.3. p204 participates in activation of IFN-β production

Based on the results showing induction of innate immune response in MPyV infected cells not sooner than at the time of viral genomes replication in the nucleus, we decided to investigate the involvement of DNA sensors that are known to be localized in both cytoplasm and the cell nucleus. Human DNA sensor IFI16 was described as the DNA sensor recognizing herpesvirus genomes in the nucleus and activating innate immunity [Ansari et al., 2015]. We focussed our attention to investigation whether the mouse protein, p204, analogous to human IFI16 participates in IFN-β induction provoked by MPyV. For that, 3T6 cells were treated with siRNA against p204 or control siRNA and incubated for 48 hours. Then, cells were infected with MPyV (MOI=20) and collected at 30 hpi. Efficiency of silencing was proved by western blot analysis. According to obtained results, production of p204 decreased by 60% in cells treated with p204 siRNA, while in a mock silenced cells or cells silenced with random siRNA no changes in p204 expression level were observed (Figure 32A). Transcription of *IFN-β* and *MX-1* genes after p204 silencing was measured by qPCR. We detected significant reduction of mRNA synthesis of both, *IFN-β* and *MX-1* genes (65% and 55% respectively) after p204 silencing in comparison with control cells (Figure 32B). Moreover, downregulation of p204 resulted in decreased phosphorylation of IRF3 (by 47%) (Figure 32C).

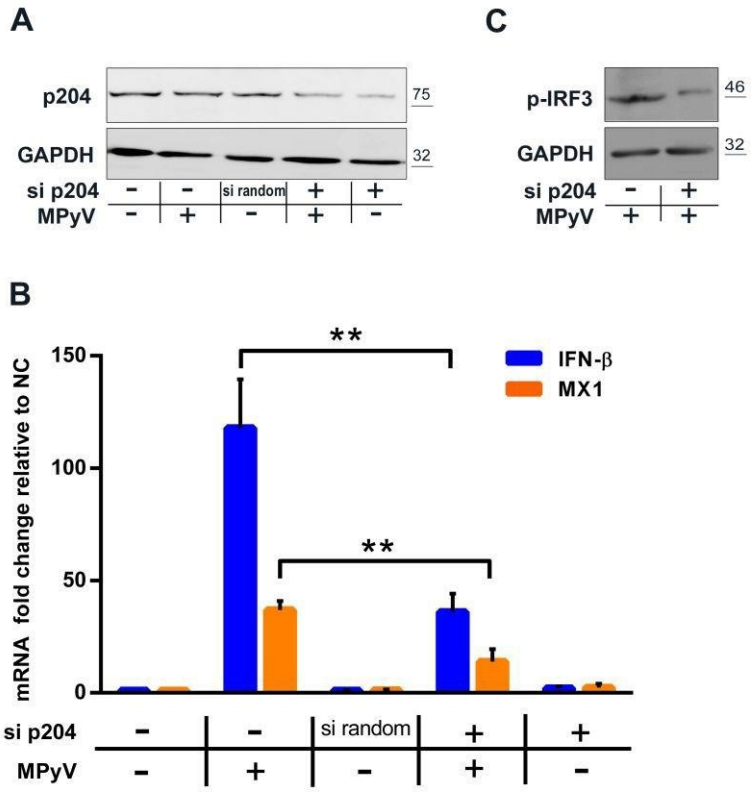

Figure 32. p204 plays a role in IFN induction during MPyV infection. (A–C) Mouse 3T6 cells were transfected with p204 siRNA. Random siRNA transfection or untransfected cells were used as the control. After 48 hours, cells were infected with MpyV (MOI=20) or mock-infected and incubated for 30 hours. **(A)** A representative western blot (of the three prepared) is presented. **(B)** IFN-β or MX-1 mRNA levels were measured by qPCR. The values were normalized to GAPDH mRNA levels. The data presented correspond to mean values of three independent experiments; the corresponding SD values are presented. Samples were compared by Student's t-test. Asterisks indicate *p*-values representing statistically significant differences (IFN-β, $^{**}p = 0.0053$; MX-1, $^{**}p = 0.0064$). **(C)** Cell lysates were prepared and subjected to immunoblotting for evaluation of the levels of p-IRF3 and GAPDH. A representative western blot (of the three prepared) is presented.

Further, we visualized localization of p204, LT antigen and MPyV DNA labeled with EdU. For that, MEF cells were infected with MPyV (MOI=5) and incubated for 24 hours. EdU was added 30 minutes prior to fixation. Then, cells we treated with cytoskeleton extraction buffer to uncover possible interactions between p204 and viral DNA, fixed and p204, LT and EdU labeled DNA were immunostained. Mock infected cells were used as a control. We found that p204 in the nucleus of infected cells concentrated on the viral replication/transcription foci, which overlap with EdU labeled replicating MPyV DNA and LT protein (Figure 33A). Importantly, the p204 was spread in whole nuclei in mock infected cells and very sporadically co-localized with EdU labeled cellular replicating DNA (Figure 33B) (*Experiment was performed in cooperation with Borys Ryabchenko*).

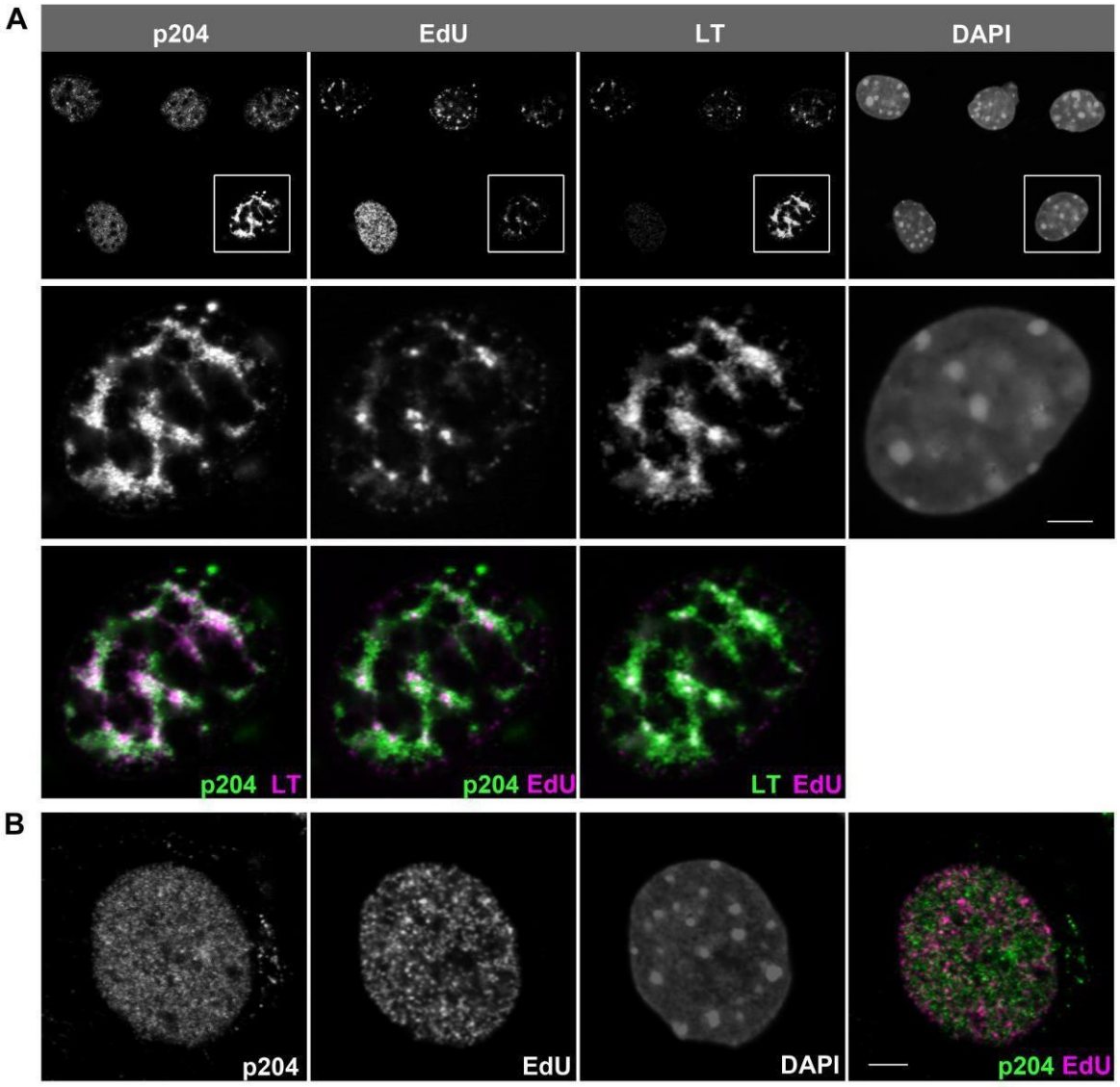

Figure 33. p204 accumulates in areas of MpyV DNA replication. MEF cells were infected with MPyV (MOI=5) **(A)** or mock-infected **(B)** and incubated for 24 hours. EdU was added for the last 30 minutes of incubation. Then, cells were treated for 5 minutes with pre-extraction buffer and fixed. For immunofluorescence, cells were stained with anti-p204 (green) and anti-MPyV LT (far red, displayed as magenta or green) antibodies. EdU was visualized by the Click-iT EdU reaction (red, displayed as magenta) and DNA was stained by DAPI (displayed as white). Representative confocal cell sections were analyzed. Scale bar=5 µm.

In addition (experiment and results are not included in the published manuscript), we examined whether interaction between p204 and viral DNA can induce p204 acetylation and translocation to cytosol for subsequent STING binding (*Experiment was performed by me*). For that, 3T6 cells were infected with MPyV (MOI=5) and incubated for 24 and 30 hours. Then, cells were fixed and staining with antibody against p204. As a control, mock infected cells were used. We found that a subpopulation of p204 was aggregated in bright clusters in cytoplasm of infected cells. Interestingly, at 24 hpi we detected more clusters than at 30 hpi (Figure 34).

A

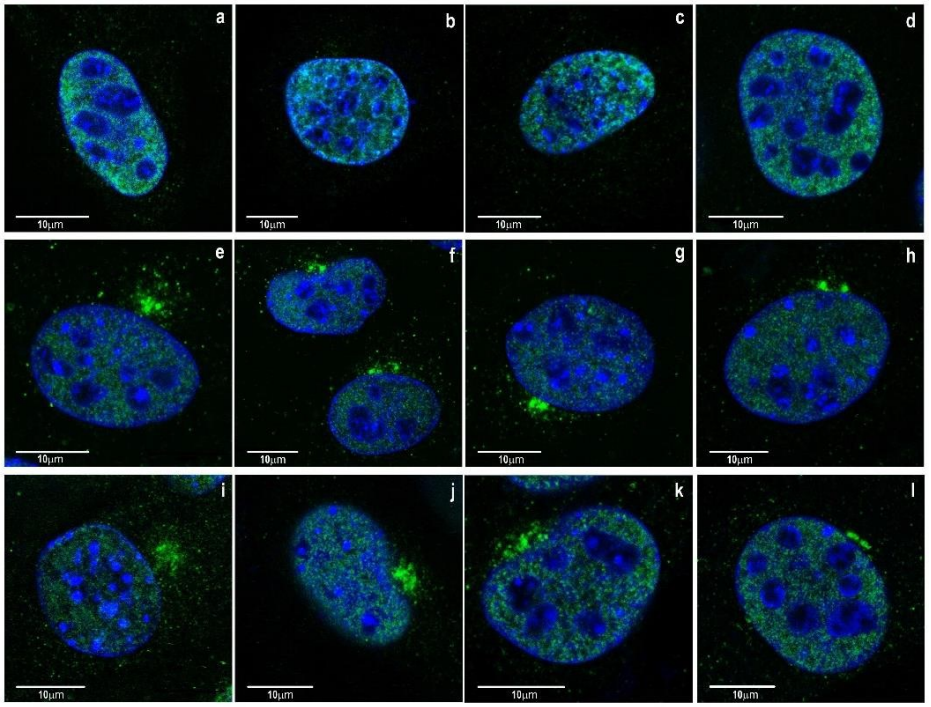

B

	% of cells with signal of IFI16 in cytosol
Mock infected	0%
24hpi	81%
30hpi	27%

Figure 34. p204 accumulates as clusters in cytoplasm of infected cells. (A) 3T6 cells were infected with MPyV (MOI=5) and incubated for 24 and 30 hpi. Cells were fixed and localization of p204 (green) was visualized. DNA was stained by DAPI (blue). As a control, mock infected cells were used. Confocal microscopy pictures of representative cell sections are shown. Scale bar=10 µm. **(B)** Evaluation of cytoplasmic localization of p204 protein was performed in fifty cells for each time post infection. The score is given as percentage.

To confirm that MPyV infection induces p204 acetylation, we aimed to prepare western blots of immunoprecipitates, but we met a problem with lack of suitable antibodies. Therefore, we performed preliminary experimnent (PLA assay) with antibodies against p204 and acetylated lysine (Figure 35). We found that at 24 and 30 hpi, p204 is either acetylated or closely associated with an acetylation protein and can be detected in both, cytoplasm and the nucleus (*Performed by me*).

Altogether, these results suggest that p204 participates in the recognition of MPyV DNA in the cell nucleus and after translocation to the cytoplasm, in a further activation of IFN-β production.

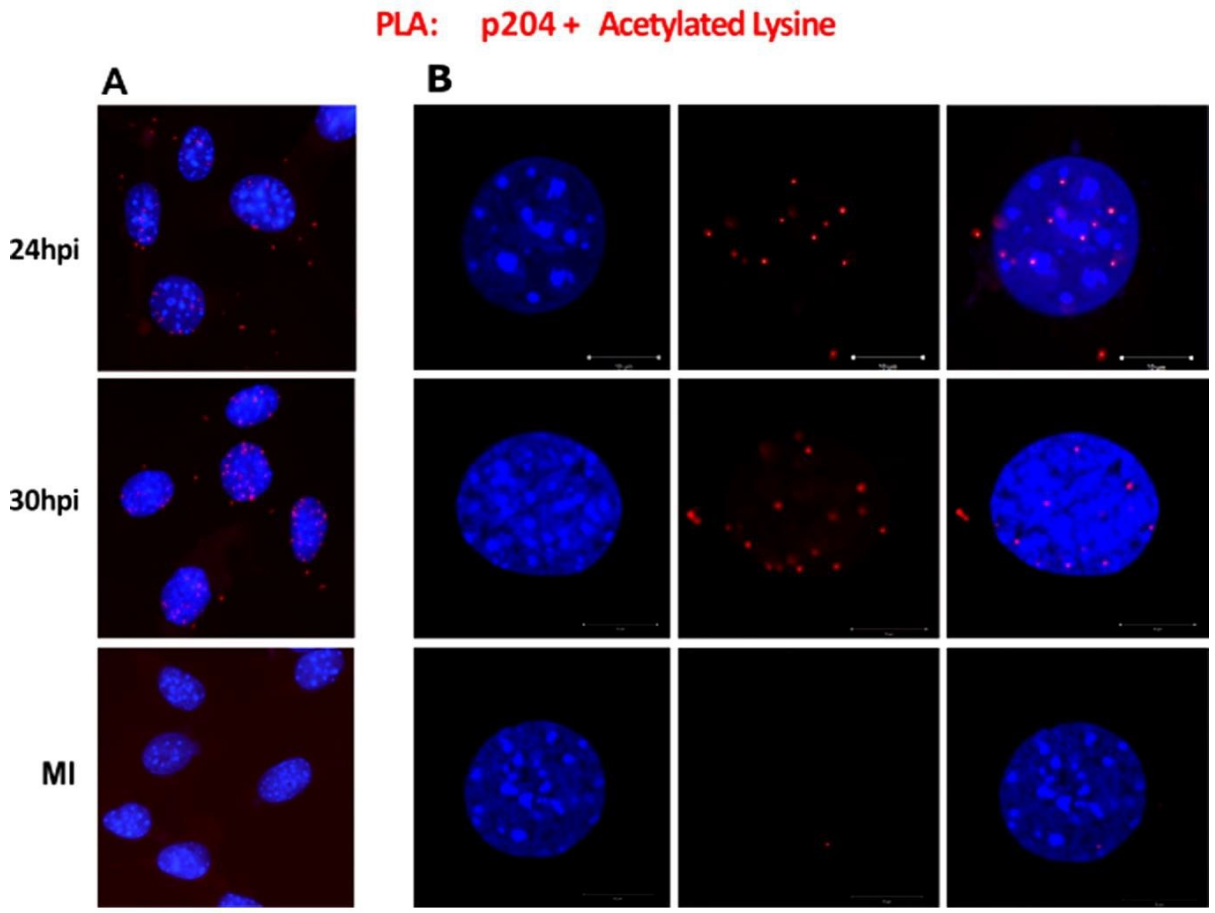

Figure 35. Figure 28. MPyV infection induces p204 acetylation and/or interaction with acetylated protein in the cell nucleus. 3T6 cells were infected with MPyV (MOI=3) and incubated for 24 and 30 hpi. As a control were used mock infected cells (MI). Then, cells were fixed and subjected to PLA. Rabbit anti-p204 and mouse anti-acetylated lysine primary antibodies were used. Oligoprobe-tagged anti-mouse and anti-rabbit antibodies were used for detection. Red spots represent the products of amplification after oligonucleotide ligation. DNA was stained by DAPI. **(A)** Representative images of cells visualized by immunofluorescence microscopy. **(B)** Representative confocal cell sections. Scale bar=10 μm.

5.2.4. cGAS is essential for production of IFN-β during MPyV infection

Next, we investigated a possibility of participation of another DNA sensor, cGAS in induction of IFN-β synthesis during MPyV infection. Next, we investigated a possibility of participation of another DNA sensor, cGAS in induction of IFN-β synthesis during MPyV infection. This enzyme is described as the key cytosolic sensor, which although presented in the cell nucleus. First, we followed the cellular localization of cGAS in infected cells by cellular fractionation. For that, MEF cells were infected with MPyV (MOI=3) and collected at 24 hpi. As controls mock infected cells (MI) and mock infected cells treated with etoposide (Et) were used. Etoposide, upon forming a ternary complex with DNA and topoisomerase II, causes breaks in dsDNA. It has been shown that during DNA damage, cytosolic cGAS translocates to

the nucleus [Liu et al., 2018]. The cells were fractionated into three fractions: cytosolic, nuclear-soluble, and nuclear-insoluble, and cGAS distribution was detected by western blot (Figure 36A).

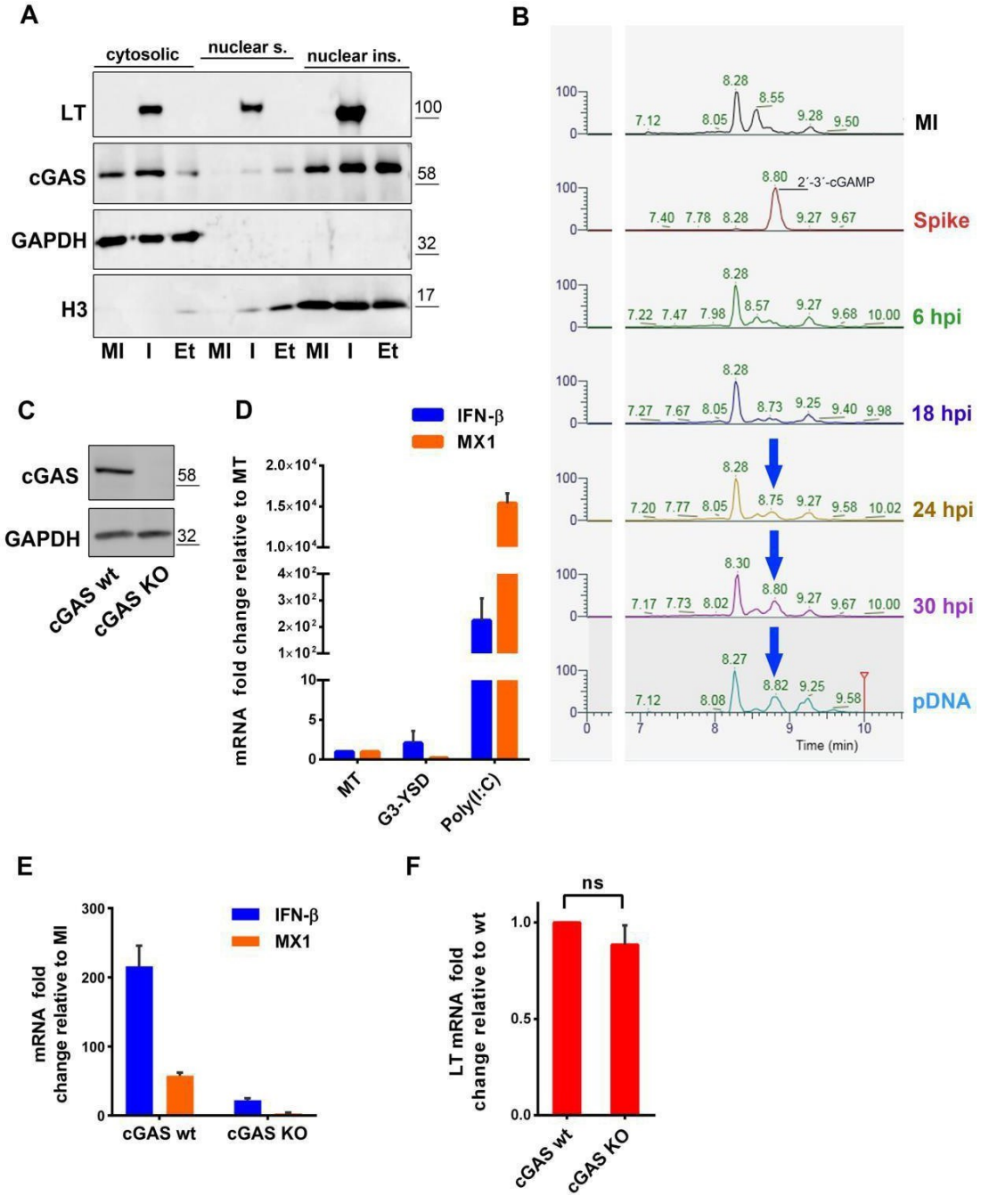

Figure 36. cGAS is activated during MPyV infection. **(A)** Mouse 3T6 cells were mock-infected (MI) or infected (I) with MPyV (MOI=3) for 24 hours or treated with etoposide (Et) for 6 hours. Then, the cells were collected and subjected to subcellular fractionation. The fractions 9cytosolic and nuclear-soluble (s), and nuclear-insoluble (ins)0 were immunoblotted and stained with antibodies against cGAS or, as controls, against GAPDH, Histone 3 (H3), or LT. **(B)** Mouse 3T6 fibroblasts were infected with MPyV (MOI=5), and at the indicated times, dinucleotides were extracted from the cells, and samples were analyzed by LC-MS for detection of 2'-3'-cGAMP. Mock-infected cells or transfected cells were included as controls. In addition, an internal control of commercial 2'-3'-cGAMP was spiked into the

lysate of mock-infected cells. Specific transitions for 2'-3'-cGAMP (675.1>136.1, 675.1>524.1, 675.1>312.1, 675.1>506.0, 675.1>152.1, 675.1>476.0, 675.1>330.0) were used to detect 2'-3'-cGAMP. In the graph, transition 506.0 is shown. 2'-3'-cGAMP (retention time: 8.75–8.82 min) is shown in the spike and indicated by arrows in the samples when present. **(C)** MEF cGAS KO or wt were cultivated for 24 hours. Than, cell lysates were prepared and subjected to western blotting for detection of cGAS. GADPH was visualized as the control. **(D)** MEF cGAS KO cells were either mock-transfected (MT) or transfected with 26-mer DNA (G3-YSD) or with Poly I:C. After 16 hours, cells were collected, and RNA was isolated. IFN-β, MX-1, and GAPDH mRNA levels were quantified by qPCR. **(E, F)** MEF cGAS KO and cGAS wt cells were infected with MPyV (MOI=5) and incubated for 30 hours before collection for RNA preparation. RNAs were isolated and used to measure IFN-β, MX-1 **(E)**, and LT **(F)** mRNA levels by qPCR. **(D–F)** The presented data correspond to mean values of three independent experiments; the corresponding SD values are presented. Selected data were compared using Student's t-test. Asterisks indicate *p*-values representing statistically significant differences. For **(D)** IFN-β, ***p= 0.0004; for **(E)** IFN-β, ***p= 0.0002; for **(F)** the obtained *p*-value did not show statistically significant differences, denoted as ns, p= 0.0807.

We found that during infection, as well as in mock infected cells, cGAS was present in both the cytosolic and nuclear-insoluble fractions. Treatment of MEF cells with etoposide stimulated cGAS re-distribution from the cytoplasm to the nucleus.

Then, we measured the production of the cGAS second messenger – 2'-3'-cGAMP 3T6 cells were infected with MPyV (MOI=5) or mock infected (MI) and incubated for 6, 18, 24 and 30 hpi. After that, cells were collected; cGAMP was isolated and measured by liquid chromatography–mass spectrometry (LC-MS). As controls, we used mock infected cells treated with 100 pmol (final concentration) of commercial 2'-3'-cGAMP (Spike) and cells transfected with pDNA for 2 hours. We detected the first 2'-3'-cGAMP production at 24 hpi and its production substantially increased at 30 hpi (Figure 36B) (*Done by me*).

Further, we used MEF cGAS knockout (cGAS KO) and MEF cGAS wild type (cGAS wt) cell lines for measurement IFN-β production during MPyV infection. First, we verified the cGAS knockout by western blot (Figure 36C) (*Performed by me*). Then, we proved that cGAS KO cells responded to RNA stimuli (cells were transfected with Poly I:C) and did not produce IFN-β in response to stimuli with DNA (cells were transfected with cGAS agonist G3-YSD, a short DNA sequence identified as a minimal motif sufficient for cGAS activation). Measurement of IFN-β and MX-1 transcription revealed its upregulation in cGAS KO cells after treatment only with Poly I:C, while in cGAS wt cells this effect was detected for both, Poly I:C and G3-YSD stimuli (Figure 36D).

We found that during infection, as well as in mock infected cells, cGAS was present in both the cytosolic and nuclear-insoluble fractions. Treatment of MEF cells with etoposide stimulated cGAS re-distribution from the cytoplasm to the nucleus.

Then, we measured the production of the cGAS second messenger – 2'-3'-cGAMP

3T6 cells were infected with MPyV (MOI=5) or mock infected (MI) and incubated for 6, 18, 24 and 30 hpi. After that, cells were collected; cGAMP was isolated and measured by liquid chromatography–mass spectrometry (LC-MS). As controls, we used mock infected cells treated with 100 pmol (final concentration) of commercial 2'-3'-cGAMP (Spike) and cells transfected with pDNA for 2 hours. We detected the first 2'-3'-cGAMP production at 24 hpi and its production substantially increased at 30 hpi (Figure 36B) (*Done by me*).

Further, we used MEF cGAS knockout (cGAS KO) and MEF cGAS wild type (cGAS wt) cell lines for measurement IFN-β production during MPyV infection. First, we verified the cGAS knockout by western blot (Figure 36C) (*Performed by me*). Then, we proved that cGAS KO cells responded to RNA stimuli (cells were transfected with Poly I:C) and did not produce IFN-β in response to stimuli with DNA (cells were transfected with cGAS agonist G3-YSD, a short DNA sequence identified as a minimal motif sufficient for cGAS activation). Measurement of IFN-β and MX-1 transcription revealed its upregulation in cGAS KO cells after treatment only with Poly I:C, while in cGAS wt cells this effect was detected for both, Poly I:C and G3-YSD stimuli (Figure 36D).

After that, we measured the levels of IFN-β and MX-1 mRNA in infected and mock infected cells (*Performed in cooperation with Boris Ryabchenko*). Both, cGAS wt and cGAS KO cells were infected with MPyV (MOI=5) and incubated for 30 hours. Cells were collected and RNA was isolated. qPCR measurement showed that knockout of cGAS resulted in dramatic decrease of IFN-β and MX-1 transcription during MPyV infection (9-folds) (Figure 36E).Changes in viral transcription detected by measurement the levels of LT mRNA in cGAS KO and wt cells at 30hpi were not significant (Figure 36F).

Altogether, our results indicate that cGAS plays an important role for activation of IFN-β production during MPyV infection. Altogether our results indicate that cGAS plays an important role for activation of IFN-β production during MPyV infection. Absence of cGAS does not abolish immune response completely. This can mean that MPyV infection activates simultaneously several pathways resulted in IFN production: sensing of viral genomes through p204 and in parallel, sensing through cGAS.

5.2.5. cGAS senses micronucleus-like bodies and DNA leaked from the nucleus to cytoplasm

On the next stage, we tried to identify in which cell compartment cGAS is activated to produce cGAMP during MPyV infection. Unfortunately, no usable antibody directed to mouse

cGAS is currently available. Therefore, 3T6 cells, expressing cGAS-EGFP were prepared. These cells were infected with MPyV (MOI=3) and incubated for 24 hpi. Then, cells were fixed and subjected for FISH with probe for MPyV genome. We found that cGAS-EGFP colocalized with polyomavirus DNA in different cellular compartments. Interestingly, there was a cell subpopulation where cGAS strongly colocalized with viral DNA in the nucleus and a cell subpopulation where cGAS colocalized with MPyV DNA in cytosol probably leaked from the nucleus (Figure 37A-C). Moreover, we found colocalization between cGAS and micronucleus-like bodies (Figure 37D). Comparison of numbers of micronucleus-like bodies in cells infected with MPyV (MOI=3) for 24 hpi and in mock infected cells showed that MPyV infection significantly increased number of micronucleus-like bodies in cytosol (Figure 37E).

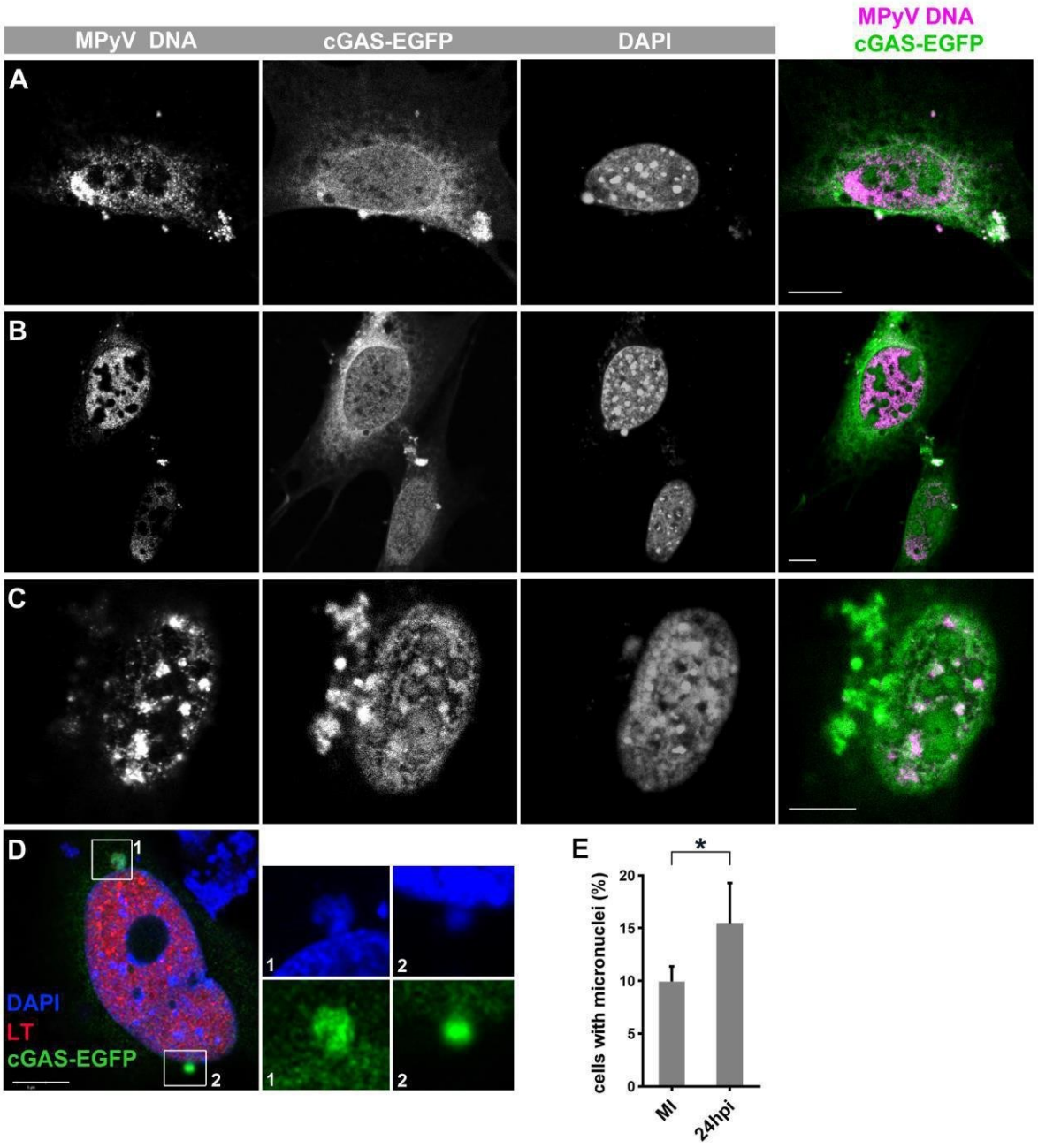

Figure 37. cGAS colocalizes with MPyV genomes and micronucleus-like bodies. (A–D) 3T6 cells expressing GFP-cGAS were infected with MPyV (MOI=3) and fixed at 24 hpi. **(A–C)** Cells were stained with anti-GFP (green) to enhance the signal, and then subjected to FISH with MPyV DNA probe labeled with biotin, followed by staining with anti-biotin antibody (magenta). Confocal sections of the cells displaying colocalization of GFP-cGAS with MPyV genomes are presented. Bars=10 μm. **(D)** Cells were stained with anti-LT antibody (red), cGAS-EGFP was visualized by anti-GFP (green), and DNA was labeled by DAPI (blue). Confocal sections of the cells displaying micronucleus-like structures colocalizing with GFP-cGAS are presented. Bars=10 μm. **(E)** Mouse fibroblasts infected with MpyV (MOI=3) or mock infected were fixed at 24 hpi and DNA was labeled by DAPI. Cells were scored for the presence of micronucleus-like bodies; the results are summarized in the graph. The data presented correspond to mean values of three independent experiments (At least 250 cells in each experiment were examined); the corresponding SD values are presented. Student's t-test was performed. Asterisks indicate *p*-values representing statistically significant differences (**p* = 0.0152).

Further, to confirm the leakage of viral DNA from the nucleus, we infected MEF cells with MPyV (MOI=3) and immediately added EdU to growing medium and incubated cells for 24 hpi. Then cells were fixed and used for FISH and click chemistry. We detected MPyV DNA with EdU incorporated into it during replication not only in the nucleus but also in cytoplasm of infected cells (Figure 38). As can be seen on the figure 31, not all EdU labeled DNA appearing in cytoplasm colocalized with MPyV probe, suggesting that host cell DNA also can leak from the nucleus during MPyV infection.

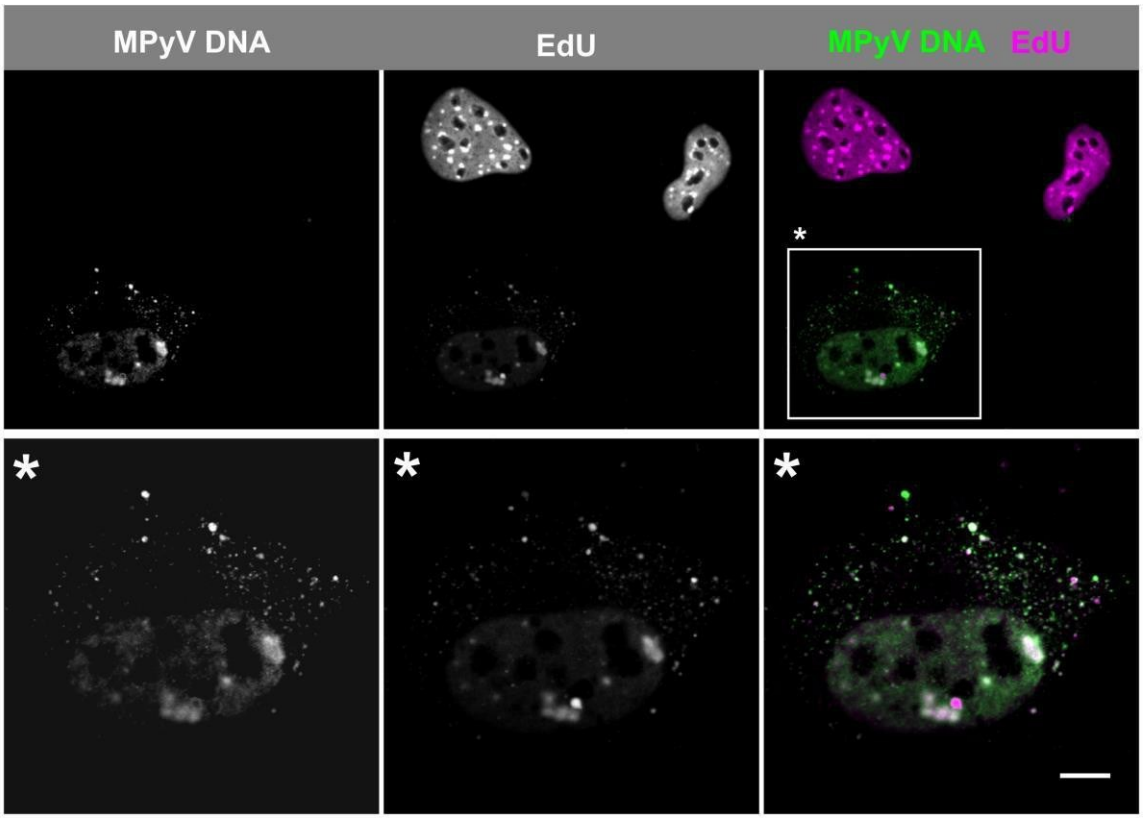

Figure 38. Leakage of DNA to cytosol during MPyV infection. MEF cells were infected with MPyV (MOI=3) in presence of EdU. After 24 hours, the cells were fixed, the Click-iT EdU reaction was performed, and the cells were used for FISH with MPyV DNA probe labeled with biotin and detected with anti-biotin antibody. Representative confocal section of cells displaying EdU DNA (magenta) and viral DNA (green). A white asterisk is used to highlight the infected cell among the uninfected ones. Bar=5 μm.

We also addressed the question whether interaction between cGAS and viral genomes in the cell nucleus resulted in cGAMP production (*Made in cooperation with Sandra Huerfano*). For that, MEF cells were infected with MPyV (MOI=5) and incubated for 30 hpi. Then, cells were fractionated to the nuclear and cytoplasmic fractions and used for cGAMP isolation. As a control mock infected cells were used. The efficiency of fractionation was verified by western blot (GAPDH and lamin A/C were used as markers for cytosolic and nuclear fractions

respectively) (Figure 39A). Two methods, LC-MS and competitive ELISA (by using special kit) were used for 2'-3'-cGAMP detection We found cGAMP in cytoplasmic fraction of infected cells. However, no traces of cGAMP were found in the nuclear fraction (Figure 39B). Interestingly, LC-MS of the samples from infected nuclei detecteded the presence of small amount of unknown dinucleotide with different spectra (Figure 39C).

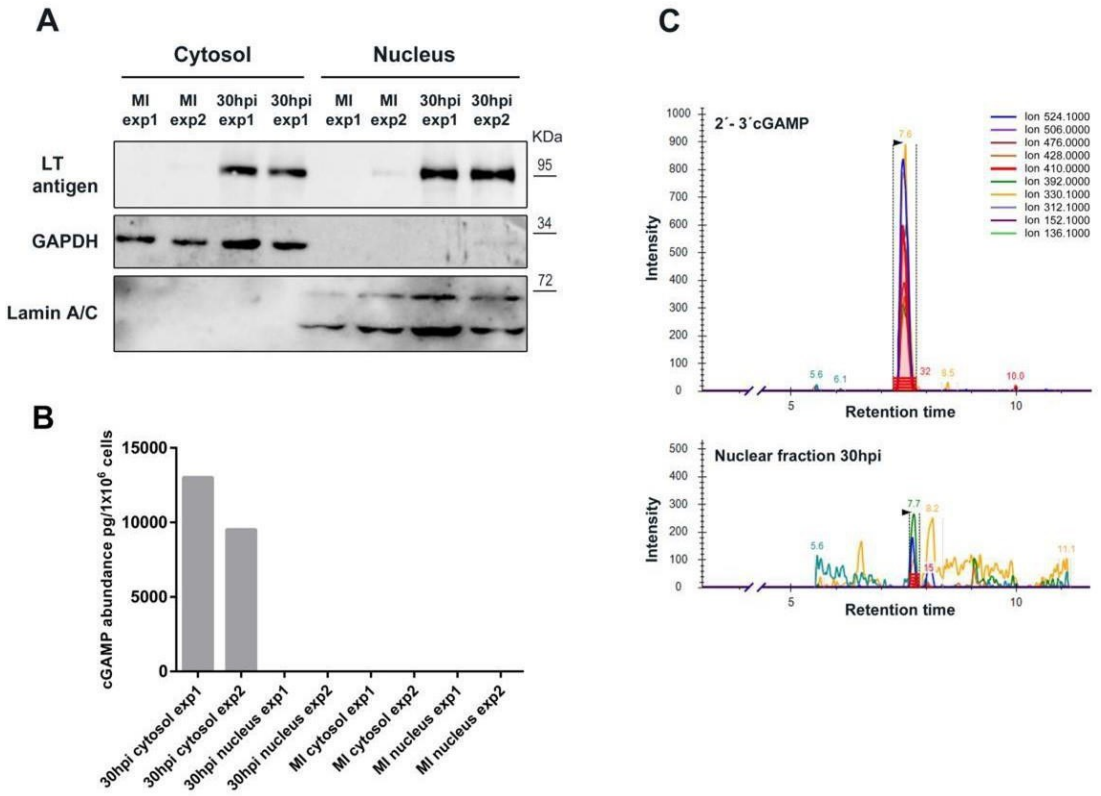

Figure 39. 2'-3'-cGAMP is detected only in the cytosolic fraction of infected cells. Mouse fibroblasts were infected with MPyV (MOI=5) or mock-infected (MI). After 30 hours, the cells were fractionated. Two independent experiments were performed. **(A)** The fractions were verified by western blotting using antibodies against lamin A/C for the nuclear fractions, GAPDH for the cytosolic fraction, and LT (to verify infectivity). One of two representative experiments is displayed. **(B)** The cell fractions were used for detection of 2'-3'-cGAMP by competitive ELISA. Standards were prepared in the cell lysis buffers. Two independent experiments are displayed (exp1 and exp2). **(C)** Nuclear fractions were analyzed by LC-MS. Specific transitions for 2'-3'-cGAMP (675.1>136.1, 675.1>524.1, 675.1>312.1, 675.1>506.0, 675.1>152.1, 675.1>476.0, 675.1>330.0) detection were used. One of two representative experiments is displayed. As the spike, commercial 2'-3'-cGAMP was used.

Our results indicate that cGAS recognizes MPyV DNA leaked from the nucleus into the cytoplasm and also DNA in micronucleus-like bodies, thus activating IFN production. The role of cGAS in the nucleus during MPyV infection is not clean and is apparently independent of innate immunity.

5.2.6. Absence of cGAS affects neither the level of p204 sensor, nor its interaction with MPyV genomes in the cell nukleus

Recently it was reported that cGAS can stabilize IFI16 on the genomes of herpes virus by preventing its proteasomal degradation [Orzalli et. al., 2015]. Therefore, we decided to prove if mouse cGAS has the same effect on p204 during MPyV infection. For that, cGAS KO cells were infected with MPyV (MOI=3) and incubated for 24 hours. After that, cells were fixed and stained with antibodies against LT and p204. We observed that even in the absence of cGAS, p204 still colocalizes with LT foci on replicating MPyV DNA in the cell nucleus (*Performed by me*) (Figure 40A).

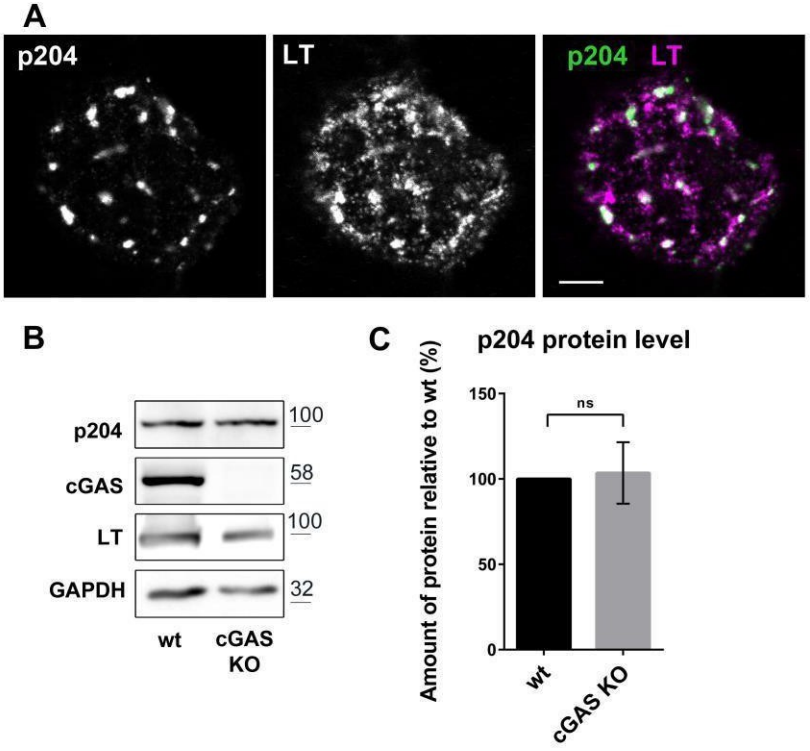

Figure 40. Absence of cGAS did not affect either the interaction of p204 with the MPyV genomes or its level in cells. (A) MEF cGAS KO cells were infected with MPyV (MOI=3) and incubated for 24 hours. The cells were treated for 5 minutes with pre-extraction buffer and then fixed. Next, cells were stained with anti-MPyV LT antigen (magenta) and anti-p204 (green) antibodies. The image shows a confocal section of the nucleus of the infected cell. Scale bar=5 μm. **(B, C)** MEF wt and cGAS KO cells were infected with MPyV (MOI=5). At 30 hpi, cell lysates were prepared and analyzed by western blotting to follow the p204 levels. As a control, antibodies against cGAS, GAPDH, and LT antigen were used. Three independent experiments were performed **(B)**. The graph represents comparison of levels of p204 (related to levels of GAPDH loading controls) in MEF cGAS wt and MEF cGAS KO cell lysates. The data presented correspond to mean values of three independent experiments; the corresponding SD values are presented. Student's t-test was performed. The *p*-value obtained did not show statistically significant differences, denoted as ns, $p = 0.85$ **(C)**.

Further, we confirmed obtained results by western blot (*Made in cooperation with Boris Ryabchenko*). cGAS KO and wt cells were infected with MPyV (MOI=5) and incubated

for 30 hours. Then, cells were collected and used for analysis. We found that the level of p204 production was comparable in both, cGAS KO and wt cells (Figure 40B-C). The obtained results indicate that cGAS does not affects to p204 stabilization on MPyV genomes. More data need to be obtained to understand the relationship between these two DNA sensors.

5.2.7. Pilot experiments for studies whether MPyV infection induces activation of non-canonical pathway of IFN-β production

Induction of double-stranded breaks can result in the activation of innate immunity through non-canonical pathway [Dunphy et al., 2018]. Therefore, we decided to test the presence of DDR markers in MEF cells. For that, cells were infected with MPyV (MOI=3) and fixed at 18 and/or 30 hpi. Presence of phosphorilated H2A histone family member X (γH2AX), phospho-p53 (p-p53) and p53BP1 (tumor suppressor p53-binding protein 1) was visualized with confocal microscopy. These proteins participate in a recognition of double stranded breaks and activation of the reparation [Sharma et al., 2012; Rappold et al., 2001; Lakin, Jackson, 1999]. As a control, mock infected (MI) cells were used (Figure 41A) (*Experiments were performed in cooperation with Boris Ryabchenko*). We found that all these proteins are presented in infected nuclei at indicated times.

Further, we investigated the participation of p53 in an activation of immune response during MPyV infection. For that, MEF p53 wild type (p53 wt) and MEF p53 knockout (p53 KO) cells, kindly provided by T. Stopka [Basova et al., 2014] were used. First, we verified p53 knockout by western blot (Figure 41Ba). Then, p53 wt and p53 KO cells infected with MPyV (MOI=5) and incubated for 30 hpi. Cells were collected and RNA was isolated. Transcription of IFN-β was measured by qPCR. We detected reduction of IFN-β mRNA level in p53 KO cells by more than 50% in comparison with its level in wt MEF (Figure 41Bb). The expression of LT antigen mRNA was similar in both cell lines (Figure 41Bc) (*Done by me*). Our preliminary results comfirmed activation of DDR in our cell system and indicated a role of phosphorylated p53 in IFN-β production. Examination of the participation of individual components of non-canonical pathway in MPyV induced IFN I expression will be the subject of a further research.

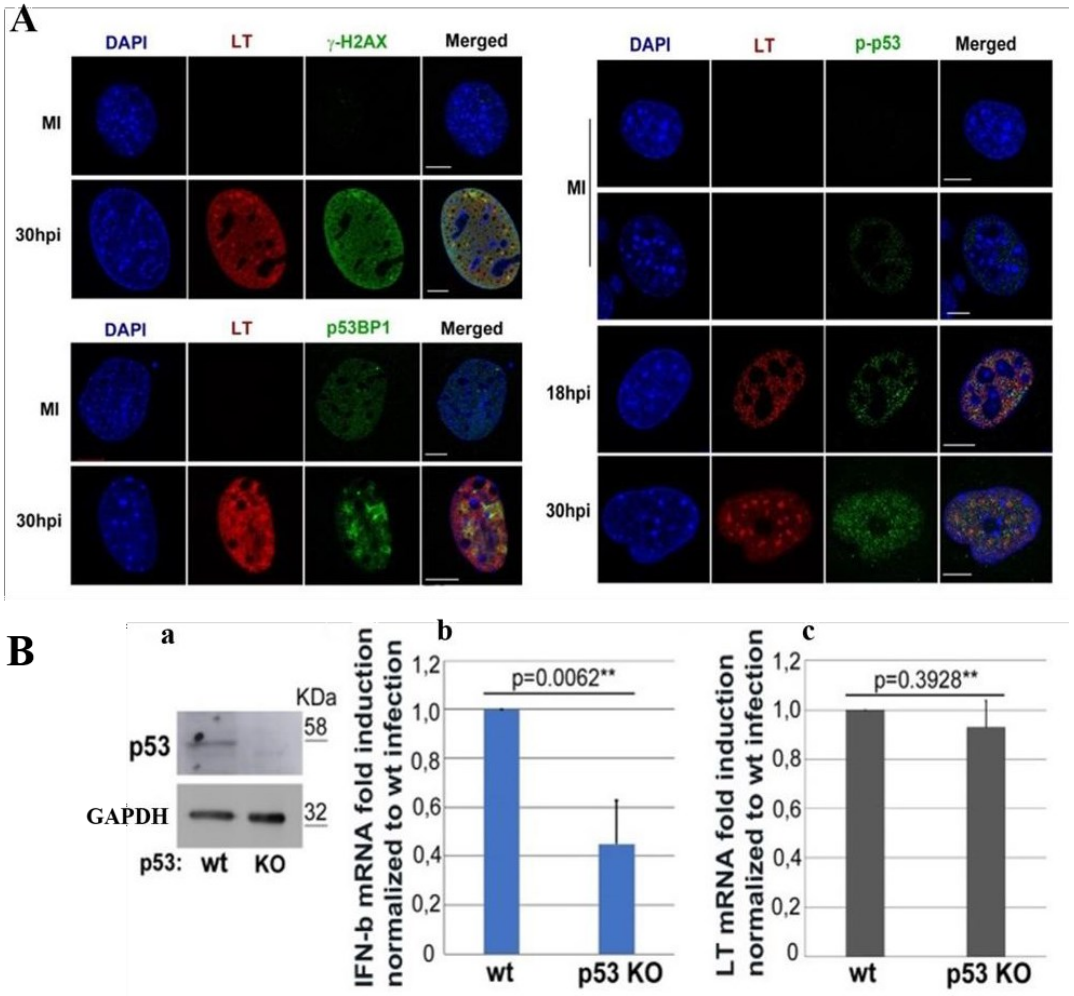

Figure 41. A. Activation of DDR markers by MPyV infection. MEF cells were infected with MPyV (MOI=3) and incubated for 18 and/or 30 hpi. Then, cells were fixed and presence of DDR marker proteins – γH2AX, p-p53 and p53BP1 was visualized by confocal microscopy. As a control mock infected (MI) cells were used. γH2AX, p-p53 and p53BP1 are green, LT antigen is red and DNA was labeled by DAPI (blue). **B. Absence of p53 in MEF cells leads to decrease of IFN-β production. (Ba)** Presence of p53 protein in MEF 53 wt (p53 wt) and MEF 53 knockout (p53 KO) cells was verified with immunoblotting. Results were normalized to GAPDH. **(Bb-Bc)** p53 wt and p53 KO cells were infected with MPyV (MOI=5) and incubated for 30 hpi. Then, cells were collected and used for RNA isolation. The expression of IFN-β and LT mRNAs was measured by qPCR. Values were normalized to GAPDH. The presenting data correspond to mean values of three independent experiments. The corresponding SD values are given. *P*-values are shown, and asterisks represent statistically significant differences (**$p \leq 0.01$).

6. Discussion

6.1. Nuclear trafficking of MPyV

During productive infection, polyomaviruses pass from the cell surface to the nucleus through different organelles and compartments [Richterová et al., 2001; Liebl et al., 2006]. Previously, direct fusion of monopinocytic vesicles carrying the virus with nuclear membrane was suggested on the base of electron microscopy studies [Hummeler et al., 1970; Mackay and Consigli, 1976]. Later, was accepted hypothesis that once reaching the ER, virions penetrate inner nuclear membrane and translocate directly to the nucleus. Thus, Butin-Israeli et al. demonstrated that SV40 infection induces deformations and fluctuations in the nuclear membrane on the level of lamin A/C, suggesting its penetration by the virus that accumulates in ER [Butin-Israeli et al., 2011]. Concurrently, several studies revealed that polyomavirus particles undergo conformational changes and partial disassembly in ER which leads to expose of the minor capsid proteins and escape virions to cytosol [Magnuson et al., 2005; Rainey-Barger et al., 2007; Geiger et al., 2011; Inoue, Tsai, 2011; Inoue et al., 2015; Huerfano et al., 2017]. Then, using canonical route of translocation through the nuclear pore complex with involvement of importins polyomaviruses delivered to the cell nucleus [Bennet, 2014].

We found that once in cytosol, MPyV utilizes importins mediated trafficking as the main pathway for productive infection. Interaction between capsid proteins of viral particles and importin β1 is time dependent process and occurs from 3 to 6 hpi. Binding of MPyV by importin β1 is not detectable at 8 hpi. This time interval corresponds to the massive virus release from the ER (5 hpi) and appearance of the first detectable transcripts in the nucleus (6 hpi) [Huerfano et al., 2017; Chen, Fluck, 2001].]. PLA assay confirmed results of co-immunoprecipitation and demonstrated that only small amounts of viral particles can interact with importins. The reasons can be i) the fact that only subpopulation of entering virions is sortied to the productive pathway, ii) fast process of virions translocation to the nucleus, or iii) proteasomal degradation. Interestingly, Nakanishi et al. showed that increasing multiplicity of SV40 used for infection does not affect to the amount of VP1 and VP3 proteins in complexes with importins α/β [Nakanishi et al., 2007]. This is in an agreement with the observation made in our laboratory that regardless of multiplicity of infection, only a minor subpopulation of MPyV virions reach the cell nucleus [Mannová, Forstová, 2003]. Also, problems with the virus trafficking can arise on the stage of translocation to the ER. Zila et al. and Qian et al. found that main amount of polyomavirus stacks in late endosomes, caveolin enriched vesicles, or in recycling endosomes and only a small part is delivered to ER [Zila et al., 2014; Qian et al., 2009]. Moreover, transport through the nuclear pore can be aborted with misdelivery of

partially disassembled viral particles, their improper docking and mechanical or chemical stress [Wang et al., 2013; Flatt, Greber, 2015].

Examination of the role of capsid proteins in the nuclear trafficking of MPyV revealed that VP1 or both VP1 and VP2/VP3 NLSs are involved in this process. Infectivity of mutant 1 with one amino acid substitution in overlapping NLSs of VP1 and VP2/VP3 (both NLSs were weakened) decreased to 66% in comparison with wt virus. One more change in NLS of VP2/VP3 that did not affect the NLS of VP1 (mutant 2) resulted in 25% infectivity of wt MPyV. These results confirmed the importance of NLS of the minor capsid proteins for delivery of polyomavirus into the cell nucleus. In contrast, infectivity of mutant 3, with destroyed NLS of VP2/VP3 and recovered NLS of VP1 was slightly higher than that of the wt virus. Thus, strong NLS of VP1 can be sufficient for successful trafficking of virions to the nucleus. Confocal microscopy confirmed results of infectivity assay and showed that cells infected with mutants 1 and 2 had inefficient transport of newly synthesized proteins to the nucleus, while infection with mutant 3 resulted in nuclear localization of capsid proteins as in a case of wt virus. Interestingly, Bennett et al. demonstrated that BK polyomavirus uses NLSs of VP2 and VP3 capsid proteins for the nuclear trafficking [Bennett S. M. et al., 2015]. Similar observations were made for SV40. Nakanishi et al. found that SV40 enters to the nucleus via interaction between NLS of VP3 and importins [Nakanishi A. et al., 2002]. This observation is in a contrast with the findings of Bennett et al. and Nakanishi et al. which demonstrated that NLS of the minor proteins VP2 and VP3 is used for the transport of BKPyV and SV40, respectively to the nucleus [Bennett et al., 2015; Nakanishi et al., 2002]. The reason for this discrepancy can be the difference in the common C- terminus of VP2 and VP3 proteins of primate polyomaviruses and murine polyomavirus. Primate polyomaviruses have an additional sequence of basic amino acids in the C-terminus. NucPred programme predicted substantially higher strength (around 0.50 – 0,60) for BKPyV, JCPyV and SV 40, while the score for MPyV was only 0.14. (Supplemented table 1 of enclosed manuscript Soldatova et al., 2018).

The remains question is how the mutant 2 with disrupted NLS of VP2/VP3 and partially inactivated NLS of VP1 enters to the cell nucleus because PLA assay revealed non-significant interaction with importin β1. One obvious possibility is that the virus translocates to the nucleus during cellular mitosis. Also, we cannot exclude a variant, that after escape from ER some virions can be further degraded, and the released minor proteins can employ their viroporin properties and cause local disruptions of nuclear membrane. The third option is that viral minichromosomes can be delivered to the nucleus via interaction between of histones' NLSs and importins [Mosammaparast et al., 2001; Mosammaparast et al., 2002; Wagstaff et

al., 2007].

Experiments with individual expression of capsid proteins showed that their nuclear transport was very inefficient. In contrast, studies of BKPyV and SV40 trafficking revealed that during individual expression their minor proteins VP2 and VP3 were localized exclusively in the nucleus [Bennett et al., 2015; Ishii et al., 1994]. As explained above, their NLS is stronger than the NLS of MPyV VP2 and VP3 proteins. On the other hand, NLS of MCPyV VP2 is weak – 0.18, similar as MPyV and cannot provide its nuclear trafficking during individual expression [Schowalter and Buck, 2013]. Comparison the strengths of VP1 NLS revealed that MPyV and SV40 have close values (0.30 and 0.38 respectively). However, wt VP1 of MPyV localized mainly in cytosol, while SV40 VP1 found in the nucleus [Ishii et al., 1994].

Co-expression of wt and mutated capsid proteins showed that wt VP1 can transport VP2 with completely disrupted NLS to the nucleus and, vice versa, wt VP2 with functional but weak NLS can deliver VP1 with not functional NLS to the nucleus. This observation can be explained by the fact that importin β1implements nuclear import of proteins via interaction with adaptor protein importin α [Goldfarb et al., 2004]. Sankhala et al. found that for interaction with importin α3, the three-dimensional structure of NLS of protein is more important than its amino acid sequence [Sankhala et al., 2017]. Therefore, that the presence of the minor capsid proteins in the central cavity of VP1 pentamers is essential for the transport of virions to the nucleus, even if their NLS is abolished by point mutations.

Altogether, these results indicate that NLS of both the major and minor capsid proteins interact with importin in concert. They also demonstrate that the conformation of the capsid protein complexes plays important role in their delivery to the nucleus.

6.2. Activation of immune response during MPyV infection

Invasion of viruses to cells induces activation of innate immunity, which recognizes viral components by different pattern recognition receptors (PRRs). These receptors stimulate production of IFNs and other proteins with antiviral properties. Over the past twenty years, many new PRRs were discovered, and some mechanisms of pathogens sensing were revealed. Using MPyV as a model, we investigated whether and when cells infection with polyomavirus can induce immune response and mechanism of its activation. We found that stable activation of IFN-β and IFN stimulated gene, MX-1 expression starts at the late stage of infection, from 24 hpi, when the replication of viral genomes is occurs. We did not detect any convincing upregulation of IFN-β at the early times post infection when the virus travels from the plasma

membrane towards the cell nucleus. This suggests that the virus is hidden from the recognition by immune system from the time of cell entry till the replication. We expected that at that time when virus escapes from ER and its virions appear partially disassembled in cytosol, viral DNA might be accessible to sensors. However, that was not the case. The reason can be that polyomavirus DNA forms nucleocore firmly condensed with histones and VP1 and its partial release occurs in the cell nucleus [Carbone et al.,2004]. Also, the virus particles travelling by non-productive pathway can accumulate in caveolar compartments and late recycling endosomes or become degraded in endolysosomal compartments.

At the time of interferon production, we detected phosphorylation of IRF3 and STING, which are essential for activation of IFN, and interferon stimulated genes [Au et al., 1995; Hopfner and Hornung, 2020]. Moreover, experiments with STING KO cells showed that knockout of this protein abrogates IRF3 phosphorylation and IFN-β, MX-1 transcription during MPyV infection. Similar results were observed during BKV infection in RPTE and LVEC cells. IFN-β production and IRF3 phosphorylation were detected at 3 and 5 days post infection, but not earlier [An et al., 2019]. Also, Popik et al. found that IFN-β expression was correlated with BK virus replication and increased from 24 to 96 hours during infection in podocytes and mesangial cells [Popik et al., 2019]. All these results indicate that sensing of MPyV occurs on the late stages of infection during massive replication of viral genomes. Experiments with the virus, which has mutated NLSs of the capsid proteins (mutant 2) and is almost unable to translocate to the nucleus, induced very weak immune response, confirming obtained results.

Synthesis of IFN-β at the late time post infection suggests recognition of viral minichromosome with DNA sensors. One of such sensors which can recognize viral genomes in both cytoplasm and the nucleus is IFI16 [Li et al., 2012; Ansari et al., 2015]. Therefore, we evaluate the role of p204 (mouse protein related to IFI16) in an activation of IFN-β production during MPyV infection. Silencing of p204 resulted in significant decrease of IFN-β and MX-1 transcription. In agreement with down regulation of IFN, we observed decrease of IRF3 phosphorylation. Similar observations were made during herpesvirus infection. Unterholzner et al. showed that transient knockdown of IFI16 results in decrease of IFN production and reduced IRF3 activation during HSV-1 infection and DNA ligands transfection [Unterholzner et al., 2010]. Confocal microscopy revealed that p204 co-localizes with LT and MPyV replicating DNA, labeled by EdU in the cell nucleus at 24 hpi. Stratmann et al. demonstrated that IFI16 can bind dsDNA by scanning along the duplex and it requires 50-70 bp fragment free of histones for successful recognition [Stratmann et al., 2015]. SV40 minichromosome, isolated at 30 minutes post infection contains significantly less nucleosomes in positions 5223 and 363 in

comparison with minichromosome isolated from viral particles [Kumar et al., 2017]. That means, that regulating region of polyomavirus DNA might be available for IFI16 recognition [Saragosti et al., 1980; Jakobovits et al., 1980; Varshavsky et al., 1979]. Herpesvirus genomes chromatinized after they entry to the nucleus. They are occupied by nucleosomes with lower frequency and irregularly leaving free DNA clusters long enough for IFI16 sensing [Herrera, Triezenberg, 2004; Oh, Fraser, 2008]. Apart of regulatory region of MPyV, partial removal of histones from genomes during replication, transcription, or repair processes, could contribute to p204 sensing.

Posttranslational modifications, such as acetylation and phosphorylation of IFI16 regulate its subcellular localization [Li et al., 2012; Cristea et al., 2010; Dell'Oste et al., 2014]. We found that in non-infected cells, p204 was presented mainly in the nucleus, while MPyV infection induced accumulation of its clusters in cytoplasm. We suggest that these clusters can represent acetylated p204 which interact with STING and trigger IRF3 – mediated IFN production. However, PLA assay performed with antibodies against p204, and acetylated lysine cannot distinguish whether p204 itself is acetylated or p204 is in a close contact with unknown acetylated protein. Surprisingly, we detected substantially higher number of clusters at 24 hpi than at 30 hpi - the time of higher IFN production. Recently, Li et al. demonstrated that STING interacts with IFI16 not only to induce IFN production but also facilitates its degradation via ubiquitin-proteasome pathway, thus mediating negative feedback to restrict IFN overproduction during HSV-1 infection [Li et al., 2019].

Further research is required to fully understand the mechanism of IFI16 sensing, the role of its post translation modifications and other possible functions. Moreover, mouse p204 protein has not identical structure with human IFI16 and therefore, their functions can differ [Zhao et al., 2015].

Next, we investigated the role of another DNA sensor cGAS, which although named “a cytosolic DNA sensor” its substantial subpopulation is present in the cell nucleus. cGAS is crucial for induction of IFN-mediated antiviral response. Its knockout results in significant decrease of IFN transcription and massive virus production [Li et al., 2013; Schoggins et al., 2014; Lahaye et al., 2013]. Infection of MEF cGAS KO cells with MPyV confirmed these findings and exhibited 9 times lower transcription of *IFN-β* and *MX-1* gene t in comparison with that of wt cells. Also, we detected production of cGAMP at the time of IFN-β induction during polyomavirus infection. Despite the fact, that we found cGAS in both cytoplasm and the cell nucleus (in complex with viral genomes) of infected cells, further experiments revealed that cGAMP synthesis occurs only in cytoplasm. These results are fully consistent with

previously published data [Abblaser et al., 2013; Mackenzie et al., 2017; Glück et al., 2017; Chen et al., 2016; Zierhut et al., 2019]. On the other hand, Gentili et al. demonstrated, that overexpression of cGAS fused with NLS resulted in production of small amount of cGAMP in the cell nucleus. We found that MPyV infection induced synthesis of a dinucleotide different from 2'-3'-cGAMP in a very tiny concentration and similar (but not identical) spectrum. Its structure and function are unknown and require further research. Presence of cGAS in the cell nucleus in complex with MPyV DNA can be explained by its possible participation in inhibition of double-stranded break reparation. As was shown by Liu et al. nuclear cGAS interacts with PARP1 preventing formation of complexes PARP1-Timeless protein, thus suppressing homologous recombination [Liu et al., 2018]. Moreover, Jiang et al. found, that interaction of cGAS with DNA double-stranded breaks inhibits recruitment of RAD51 [Jiang et al., 2019].

Polyomavirus infection induces activation of host DNA damage response to prolong the S-phase required for successful viral replication [Dahl et al., 2005; Sowd et al., 2013; Orba et al., 2010; Tsang et al., 2014]. This results in rearrangement, remodeling lamina and increase the size of the nucleus. Moreover, the minor capsid proteins, VP2 and VP3, have viroporin properties and could be responsible for the local disruption of the nuclear membrane [Huerfano et al., 2010; Huerfano et al., 2017]. As a result, we detected a leakage of cellular and viral DNA from the nucleus to cytosol. This DNA can be recognized by cGAS and stimulate IFN I production [Zhou et al., 2019]. Also, cells can display chromatin herniation, DNA double-stranded breaks and lamina alterations, which result in the formation of micronuclei or nuclear blebs (micronucleus-like bodies). Micronucleus membranes are fragile and can be easily disrupted making internalized DNA accessible to cGAS sensing [Mackenzie et al., 2017]. We found that the number of micronuclei and micronucleus-like bodies increased with the progression of MPyV infection. Confocal microscopy revealed relocalization of cGAS to micronuclei and micronucleus-like bodies. Thus, leaked viral and cellular DNA, and DNA of micronucleus-like bodies can be sensed by cGAS in the cytosol leading to cGAMP production and induction of *IFN-β* gene expression via STING pathway.

On the model of herpes virus, it was shown that cGAS can bind IFI16 and stabilize it on the viral DNA by protecting from proteasomal degradation [Orzalli et al., 2015]. However, we found that the absence of cGAS does not affect to the p204 stability and interaction with MPyV genomes. Nevertheless, we cannot exclude a possibility that p204 and cGAMP cooperate during STING activation as it was demonstrated by Almine et al. [Almine et al., 2017].

Recently, non-canonical pathway of immune response has been described [Dunphy et

al., 2018]. According to the authors, activation of DNA damage results in p53 phosphorylation, interaction with IFI16, and activation of TRAF6. These proteins translocate to cytoplasm and bind STING, stimulating its ubiquitination (but not phosphorylation as detected in the classical pathway). The signaling of the non-canonic pathway results in predominant activation of NF-kB and minor activation of IRF3.

During polyomavirus infection, host cell DNA instability and DNA damage response is induced by viral early antigens. LT antigen induces the ATM response and intra-S-phase checkpoint. Infected cells accumulate in S and G2, to ensure production of progeny virus. To examine possible imvolvement of non-canonic pathway in IFN induction during MPyV infection, we performed some pilot experiments. We folowed DDR markers (phosphorylated p53, p53BP1 and γH2AX) and detected their colocalisagtion with LT antigen. To evaluate the contribution of non-canonic pathway to MPyV induced IFN response, further research is needed. The problem is that LT antigen on the one hand activates DDR, on the other hand it also has the ability to inhibit downstream effectors of non-canonical signaling pathway, e.g. by binding phosphorylated p53. Examination the presence of ubiquitinylated STING in polyomavirus infected cells and participation of TRAF6 (we recently obtained TRAF6 KO cells) in ubiquitination of STING can bring progress in this study.

7. Conclusions

1. **Elucidation of the way used by MPyV for delivery its genomes into the cell nucleus.**

    - Co-immunoprecipitation and proximity ligation assay were used to demonstrate interaction of MPyV with importin β1. Virions bind importin in a time dependent manner, with a peak of interaction at 6 hpi, when virions are released from ER and appear naked and partially disassembled in cytosol.
    - Three mutant viruses with substitutions introduced into overlapping NLS sequences of the major capsid protein VP1 and the minor capsid proteins VP2 and VP3 (that have the same NLS present at their common C-terminus sequence) were designed and constructed. The mutated viruses were purified from cells transfected with mutated genomes.
    - Mutation analysis revealed that only when the NLSs of both VP1 and VP2/VP3 were disrupted, the mutated virus did not bind importin β1 and its infectivity decreased by 80%. Mutated virus with abolished NLS of the minor proteins and with recovered NLS of VP1 exhibited infectivity similar to that of the wt virus.
    - Neither wt VP1 nor wt VP2 were targeted into the nucleus, when produced individually. Their co-expression lead to efficient entry VP1 – VP2 complexes into the cell nucleus. The complexes VP1 – VP2 were efficiently delivered to the nucleus even when one NLS, either VP1 or VP2 was disrupted.
    - **All these results indicate that entry of MPyV into the cell nucleus through nucleopores mediated by importins is the main way of delivery of MPyV genomes to the cell nucleus. For binding importins, virions can use VP1 and/or VP2/VP3 NLSs in concert or, individually (when they are strong enough). For importin binding, not only NLS sequence, but also conformation of surrounded structure plays the important role.**

2. **Induction of IFN-β by MPyV infection and the participation of DNA sensors, p204 and cGAS, in sensing viral genomes.**

    - The absence of IFN-β induction in mouse fibroblasts at early times post infection suggests that the virus is hidden or invisible for the immune system when sorted through the endosomal compartments to ER.

- Interferon response was detected at late stages of the MPyV infection, during replication of viral genomes.
- Production of IFN-β induced by MPyV infection was dependent on the activation of STING and IRF3 by phosphorylation.
- Induction of IFN-β by the virus mutated in NLSs of both VP1 and VP2/3 capsid proteins (exhibiting a defect in importin binding and entry to the nucleus) was dramatically decreased in comparison with IFN induction by wt MPyV. Infection of cells with the mutated virus confirmed requirement of replicating MPyV genomes in the nucleus for IFN-β response.
- DNA sensor, p204 (an analogue of human IFI16), is required for IFN-β induction by MPyV. Knockdown of its expression decreased substantially the level of IFN-β mRNA. Confocal microscopy revealed that p204 colocalises with replicating viral DNA (labelled by EdU) and LT antigen in the cell nucleus, suggesting that replicating MPyV genomes are sensed by this DNA sensor.
- Infection of cGAS knockout cells revealed that this DNA sensor is also essential for IFN-β induction by MPyV.
- DNA sensor, cGAS, could be detected in both the nucleus and cytoplasm of infected cells. In the nucleus, cGAS colocalised with the areas of MPyV DNA replication and in the cytosol with DNA leaked from the nucleus and with micronucleus-like bodies. Activation of cGAS was demonstrated by detection of its product, 2'-3'-cGAMP. However, 2'-3'-cGAMP synthesized by cGAS was detected in cytoplasm only.
- Absence of cGAS affected neither the level of p204 sensor, nor its interaction with MPyV genomes in the cell nucleus.
- **Our results indicate that cGAS recognizes MPyV DNA leaked from the nucleus into the cytoplasm and also DNA released from micronucleus-like bodies. The results also point to complex interplay between MPyV and DNA sensors, - p204 activated by MPyV genomes in the cell nucleus and, - cGAS activated by DNA appearing in cytoplasm as a result of genotoxic stress induced by MPyV infection.**

8. Involvement in publication

List of publications enclosed in this doctoral thesis:

This thesis is based upon two first author publications:

1) Soldatova Irina, Prilepskaja Terezie, Abrahamyan Levon, Forstová Jitka, Huérfano Sandra: **Interaction of the Mouse Polyomavirus Capsid Proteins with Importins Is Required for Efficient Import of Viral DNA into the Cell Nucleus.** Viruses. 2018; 10(4):165.
   - First author publication
   - Contribution of the author: 75%
   - I was significantly involved in conceiving the experiments that were predominantly done by myself. I also wrote the first draft of the paper.

2) Ryabchenko Boris, Soldatova Irina, Sroller Vojtech, Forstova Jitka, Huerfano Sandra. **Immune sensing of mouse polyomavirus DNA by p204 and cGAS DNA sensors.** FEBS J. 2021 May 10. https://doi.org/10.1111/febs.15962
   - First author publication (shared)
   - Contribution of the author: 35%
   - I was involved in conceiving the experiments. My contributions are presented for individual experiments throughout the results. I also participated in data analysis and manuscript preparation.

I hereby confirm that the author of this thesis, Irina Soldatova, have substantially contributed to the publications listed above. In case of her first-author unshared publication, she did the majority of experimental work and contributed to the manuscript preparation.

doc. RNDr. Jitka Forstová, CSc.

.....

9. List of References

Abend, J.R., Jiang, M., Imperiale, M.J., 2009. BK virus and human cancer: innocent until proven guilty. Semin. Cancer Biol. 19, 252-260. https://doi.org/10.1016/j.semcancer.2009.02.004

Abend, J.S., Vilchez, R.A., Jorgensen, J.L., Kozinetz, C.A., 2003. Association between SV40 and non-Hodgkin's lymphoma. Leuk. Lymphoma. 44, (Suppl. 3) S33-39. https://doi.org/10.1080/10428190310001623784

Ablasser, A., Goldeck, M., Cavlar, T., Deimling, T., Witte, G., Röhl, I., Hopfner, K.P., Ludwig, J., Hornung, V., 2013. cGAS produces a 2'-5'-linked cyclic dinucleotide second messenger that activates STING. Nature 498, 380–384. https://doi.org/10.1038/nature12306

Ablasser, A., Schmid-Burgk, J.L., Hemmerling, I., Horvath, G.L., Schmidt, T., Latz, E., Hornung, V., 2013. Cell intrinsic immunity spreads to bystander cells via the intercellular transfer of cGAMP. Nature 503, 530–534. https://doi.org/10.1038/nature12640

Adam, S.A., Gerace, L., 1991. Cytosolic proteins that specifically bind nuclear location signals are receptors for nuclear import. Cell 66, 837-847. https://doi.org/10.1016/0092-8674(91)90431-w

Aguirre, S., Luthra, P., Sanchez-Aparicio, M.T., Maestre, A.M., Patel, J., Lamothe, F., Fredericks, A.C., Tripathi, S., Zhu, T., Pintado-Silva, J., Webb, L.G., Bernal-Rubio, D., Solovyov, A., Greenbaum, B., Simon, V., Basler, C.F., Mulder, L.C.F., García-Sastre A., Fernandez-Sesma, A., 2017. Dengue virus NS2B protein targets cGAS for degradation and prevents mitochondrial DNA sensing during infection. Nat. Microbiol. 2, 17037. https://doi.org/10.1038/nmicrobiol.2017.37

Akira, S., Uematsu, S., Takeuchi, O., 2006. Pathogen recognition and innate immunity. Cell 124, 783-801. https://doi.org/10.1016/j.cell.2006.02.015

Alexopoulou, L., Holt, A.C., Medzhitov, R., Flavell, R.A., 2001. Recognition of double-stranded RNA and activation of NF-kappaB by Toll-like receptor 3. Nature 413, 732-738. https://doi.org/10.1038/35099560

Alexopoulou, L., Desnues, B., Demaria, O., 2012. Toll-like receptor 8: the awkward TLR. Med. Sci. 28, 96–102. https://doi.org/10.1051/medsci/2012281023

Allander, T., Andreasson, K., Gupta, S., Bjerkner, A., Bogdanovic, G., Persson M.A.A., Dalianis, T., Ramqvist, T., Andersson, B., 2007. Identification of a Third Human Polyomavirus. J. Virol. 81, 4130–4136. https://doi.org/10.1128/JVI.00028-07

Almine, J.F., O'Hare, C.A., Dunphy, G., Haga, I.R., Naik. R.J., Atrih, A., Connolly, D.J., Taylor, J., Kelsall, I.R., Bowie, A.G., Beard, P.M., 2017. Unterholzner L. IFI16 and cGAS cooperate in the activation of STING during DNA sensing in human keratinocytes. Nat. Commun. 8, 14392. https://doi.org/10.1038/ncomms14392

An, P., Sáenz Robles, M.T., Duray, A.M., Cantalupo, P.G., Pipas, J.M., 2019. Human polyomavirus BKV infection of endothelial cells results in interferon pathway induction and persistence. PLoS Pathog. 15, 1007505. https://doi.org/10.1371/journal.ppat.1007505

Anchisi, S., Guerra, J., Garcin, D., 2015. RIG-I ATPase activity and discrimination of self-RNA versus non-self-RNA. MBio 6, e02349–14. https://doi.org/10.1128/MBIO.02349-14

Andreeva, L., Hiller, B., Kostrewa, D., Lassig, C., de Oliveira Mann, C.C., Jan Drexler, D., Maiser, A., Gaidt, M., Leonhardt, H., Hornung, V., Hopfner, K.P., 2017. cGAS senses long and HMGB/TFAM-bound U-turn DNA by forming protein-DNA ladders. Nature 549, 394–398. https://doi.org/10.1038/nature23890

Anderson, H.A., Chen, Y., Norkin. L.C., 1996. Bound simian virus 40 translocates to caveolin-enriched membrane domains, and its entry is inhibited by drugs that selectively disrupt caveolae. Mol. Biol. Cell 7, 1825-1834. https://doi.org/10.1091/mbc.7.11.1825

Ansari, M.A., Dutta, S., Veettil, M.V., Dutta, D., Iqbal, J., Kumar, B., Roy, A., Chikoti, L.,

Singh, V.V., Chandran, B., 2015. Herpesvirus genome recognition induced acetylation of nuclear IFI16 is essential for its cytoplasmic translocation, inflammasome and IFN-β responses. PLoS Pathog. 11, e1005019. https://doi.org/10.1371/journal.ppat.1005019 PMID: 26134128

Aoshi, T., Koyama, S., Kobiyama, K., Akira, S., Ishii, K. J., 2011. Innate and adaptive immune responses to viral infection and vaccination. Current Opinion in Virology 1, 226–232. https://doi.org/10.1016/j.coviro.2011.07.002

Arthur, R.R., Shah, K.V., 1989. Occurrence and significance of papovaviruses BK and JC in the urine. Prog. Med. Virol. 36, 42-61.

Asselin, C., Gelinas, C., Bastin, M., 1983. Role of the three polyoma virus early proteins in tumorigenesis. Mol. Cell Biol. 3, 1451-1459.

Atkin, S.J.L., Griffin, B.E., Dilworth, S.M., 2009. Polyoma virus and simian virus 40 as cancer models: History and perspectives. Seminars in Cancer Biology 19, 211-217. https://doi.org/10.1016/j.semcancer.2009.03.001

Atwood, W.J., Norkin, L.C., 1989. Class I major histocompatibility proteins as cell surface receptors for simian virus 40.J. Virol. *63*, 4474–4477. https://doi.org/10.1128/JVI.63.10.4474-4477.1989

Au, W.C., Moore, P.A., Lowther, W., Juang, Y.T., Pitha, P.M., 1995. Identification of a member of the interferon regulatory factor family that binds to the interferon-stimulated response element and activates expression of interferon-induced genes. Proc. Natl. Acad. Sci. USA 92, 11657-11661.

Baake, M., Doenecke, D., Albig, W., 2001. Characterisation of nuclear localisation signals of the four human core histones. J. Cell Biochem. 81, 333-346.

Barber, G.N., 2015. STING: infection, inflammation and cancer. Nat. Rev. Immunol. 15, 760-770. https://doi.org/10.1038/nri3921

Barnett, K.C., Coronas-Serna, J.M., Zhou, W., Ernandes, M.J., Cao, A., Kranzusch, P.J., Kagan, J.C., 2019. Phosphoinositide Interactions Position cGAS at the Plasma Membrane to Ensure Efficient Distinction between Self- and Viral DNA. Cell 176, 1432-1446. https://doi.org/10.1016/j.cell.2019.01.049

Barouch, D.H. and Harrison, S.C., 1994. Interactions among the major and minor coat proteins of polyomavirus. J. Virol. 68, 3982-3989. https://doi.org/10.1128/JVI.68.6.3982-3989.1994

Basova, P., Pospisil, V., Savvulidi, F., Burda, P., Vargova, K., Stanek, L., Dluhosova, M., Kuzmova, E., Jonasova, A., Steidl, U., Laslo, P., Stopka, T., 2014. Aggressive acute myeloid leukemia in PU.1/p53 double-mutant mice. Oncogene 33, 4735-4745. https://doi.org/10.1038/onc.2013.414

Beignon, A.S., McKenna, K., Skoberne, M., Manches, O., DaSilva, I., Kavanagh, D.G., Larsson, M., Gorelick, R.J., Lifson, J.D., Bhardwaj, N., 2005. Endocytosis of HIV-1 activates plasmacytoid dendritic cells via Toll-like receptor-viral RNA interactions. J Clin. Invest. 115, 3265-3275. https://doi.org/10.1172/JCI26032

Belgnaoui, S.M., Paz, S., Hiscott, J., 2011. Orchestrating the interferon antiviral response through the mitochondrial antiviral signaling (MAVS) adapter. Curr. Opin. Immunol. 23, 564–572. https://doi.org/10.1016/j.coi.2011.08.001

Benjamin, T.L., 2001. Polyoma Virus: Old Findings and New Challenges. Virology 289, 167–173. https://doi.org/10.1006/viro.2001.1124

Bennett, S.M., 2014. Intracellular trafficking of BK polyomavirus: from the ER to the nucleus. A dissertation submitted in partial fulfillment of the requirements for the degree of Doctor of Philosophy (Cellular and Molecular Biology) in the University of Michigan.

Bennett, S.M., Zhao, L., Bosard, C., Imperiale, M.J., 2015. Role of a nuclear localization signal on the minor capsid proteins VP2 and VP3 in BKPyV nuclear entry. Virology 474, 110–6. https://doi.org/10.1016/j.virol.2014.10.013

Bernard, J.J., Cowing-Zitron, C., Nakatsuji, T., Muehleisen, B., Muto, J., Borkowski, A.W.,

Martinez, L., Greidinger, E.L., Yu, B.D., Gallo, R.L., 2012. Ultraviolet radiation damages self noncoding RNA and is detected by TLR3. Nat. Med. 18, 1286–1290. https://doi.org/10.1038/nm.2861

Boelens, M.C., Wu, T.J., Nabet, B.Y., Xu, B., Qiu, Y., Yoon, T., Azzam, D.J., Twyman-Saint, V.C., Wiemann, B.Z., Ishwaran, H., Ter Brugge, P.J., Jonkers, J., Slingerland, J., Minn, A.J., 2014. Exosome transfer from stromal to breast cancer cells regulates therapy resistance pathways. Cell 159, 499-513. https://doi.org/10.1016/j.cell.2014.09.051

Bonilla, F.A., Oettgen, H.C., 2009. Adaptive immunity. J. Allergy Clin. Immunol. 125 (2 Suppl. 2), S33-40. https://doi.org/10.1016/j.jaci.2009.09.017

Boyer, J.A., Spangler, C.J., Strauss, J.D., Cesmat, A.P., Liu, P., McGinty, R.K., Zhang, Q., 2020. Structural basis of nucleosome-dependent cGAS inhibition. Science 370, 450-454. https://doi.org/10.1126/science.abd0609

Brady, J.N., Winston, V.D., Consigli, R.A., 1977. Dissociation of polyoma virus by the chelation of calcium ions found associated with purified virions. J. Virol. 23, 717-724. https://doi.org/10.1128/JVI.23.3.717-724.1977

Brameier, M., Krings, A., MacCallum, R.M., 2007. NucPred-predicting nuclear localization of proteins. Bioinformatics 23, 1159-1160. https://doi.org/10.1093/bioinformatics/btm066

Briard, B., Place, D.E., Kanneganti, T.D., 2020. DNA Sensing in the Innate Immune Response. Physiology (Bethesda). 35, 112-124. https://doi.org/10.1152/physiol.00022.2019.

Bridgeman, A., Maelfait, J., Davenne, T., Partridge, T., Peng, Y., Mayer, A., Dong, T., Kaever, V., Borrow, P., Rehwinkel, J., 2015. Viruses transfer the antiviral second messenger cGAMP between cells. Science 349, 1228-1232. https://doi.org/10.1126/science.aab3632

Brisse, M., Ly, H., 2019. Comparative Structure and Function Analysis of the RIG-I-Like Receptors: RIG-I and MDA5. Front. Immunol. 10, 1586. https://doi.org/10.3389/fimmu.2019.01586

Brubaker, S.W., Bonham, K.S., Zanoni, I., Kagan, J.C., 2015. Innate immune pattern recognition: a cell biological perspective Annu. Rev. Immunol. 33, 257–290. https://doi.org/10.1146/annurev-immunol-032414-112240

Buck, C.B., Van Doorslaer, K., Peretti, A., Geoghegan, E.M., Tisza, M.J., An, P., Katz, J.P., Pipas, J.M., McBride, A.A., Camus, A.C., McDermott, A.J., Dill, J.A., Delwart, E., Ng, T.F., Farkas, K., Austin, C., Kraberger, S., Davison, W., Pastrana, D.V., 2016. Varsani. A. The Ancient Evolutionary History of Polyomaviruses. PLoS Pathog. 12, e1005574. https://doi.org/10.1371/journal.ppat.1005574

Butin-Israeli, V., Ben-nun-Shaul, O., Kopatz, I., Adam, S.A., Shimi, T., Goldman, R.D., Oppenheim A., 2011. Simian virus 40 induces lamin A/C fluctuations and nuclear envelope deformation during cell entry. Nucleus 2, 320–330. https://doi.org/10.4161/nucl.2.4.16371

Calvignac-Spencer, S., Feltkamp, M.C., Daugherty, M.D., Moens, U., Ramqvist, T., Johne, R., Ehlers, B., 2016. A taxonomy update for the family Polyomaviridae. Arch. Virol. 161, 1739–1750. https://doi.org/10.1007/s00705-016-2794-y

Carbone, M., Ascione, G., Chichiarelli, S., Garcia, M.I., Eufemi, M., Amati, P., 2004. Chromosome-protein interactions in polyomavirus virions. J. Virol. 78, 513-9. https://doi.org/10.1128/jvi.78.1.513-519.2004

Caruso, M., Belloni, L., Sthandier, O., Amati, P., Garcia, M.I., 2003. α4β1 integrin acts as a cell receptor for murine polyomavirus at the postattachment level. J. Virol. 77, 3913-3921. https://doi.org/10.1128/jvi.77.7.3913-3921.2003

Cavlar, T., Ablasser, A., Hornung, V., 2012. Induction of type I IFNs by intracellular DNA-sensing pathways. Immunol Cell Biol. 90, 474-482. https://doi.org/10.1038/icb.2012.11

Chang, D., Haynes, JI.Jr., Brady, J.N., Consigli, R.A., 1993. Identification of amino acid sequences in the polyomavirus capsid proteins that serve as nuclear localization signals. Trans. Kans. Acad. Sci. 96, 35-39.

Chang, D., Haynes, JI. 2nd, Brady, J.N., Consigli, R.A., 1992. The use of additive and subtractive approaches to examine the nuclear localization sequence of the polyomavirus major capsid protein VP1. Virology 189, 821-827. https://doi.org/10.1016/0042-6822(92)90615-v

Chang, D., Haynes, JI. 2nd, Brady, J.N., Consigli, R.A., 1992. Identification of a nuclear localization sequence in the polyomavirus capsid protein VP2. Virology 191, 978-983. https://doi.org/10.1016/0042-6822(92)90276-u

Chang, T.H., Liao, C.L., Lin, Y.L., 2006. Flavivirus induces interferon-beta gene expression through a pathway involving RIG-I-dependent IRF-3 and PI3K-dependent NF-kappaB activation. Microbes Infect. 8, 157–171. https://doi.org/10.1016/j.micinf.2005.06.014

Chen, X.S., Stehle, T., Harrison S.C., 1998. Interaction of Polyomavirus internal protein VP2 with the major capsid protein VP1 and implications for participation of VP2 in viral entry. EMBO J. 17, 3233–3240. https://doi.org/10.1093/emboj/17.12.3233

Chen, L. and Fluck, M., 2001. Kinetic analysis of the steps of the polyomavirus lytic cycle. J. Virol. 75, 8368-8379. https://doi.org/10.1128/jvi.75.18.8368-8379.2001

Chen, Q., Sun, L., Chen, Z.J., 2016. Regulation and function of the cGAS–STING pathway of cytosolic DNA sensing. Nat. Immunol. 17, 1142–1149. https://doi.org/10.1038/ni.3558

Choi, S.J., Lee, H.C., Kim, J.H., Park, S.Y., Kim, T.H., Lee, W.K., Jang, D.J., Yoon, J.E., Choi, Y.I., Kim, S., Ma, J., Kim, C.J., Yao, T.P., Jung, J.U., Lee, J.Y., Lee, J.S., 2016. HDAC6 regulates cellular viral RNA sensing by deacetylation of RIG-I. EMBO J. 35, 429-442. https://doi.org/10.15252/embj.201592586

Choubey, D., Lengyel, P., 1992. Interferon action: nucleolar and nucleoplasmic localization of the interferon-inducible 72-kD protein that is encoded by the Ifi 204 gene from the gene 200 cluster. J. Cell Biol. 116, 1333–1341. https://doi.org/10.1083/jcb.116.6.1333

Civril, F., Deimling, T., de Oliveira Mann, C.C., Ablasser, A., Moldt, M., Witte, G., Hornung, V., Hopfner, K.P., 2013. Structural mechanism of cytosolic DNA sensing by cGAS. Nature 498, 332-337. https://doi.org/10.1038/nature12305

Clever, J., Dean, D.A., Kasamatsu, H., 1993. Identification of a DNA binding domain in simian virus 40 capsid proteins Vp2 and Vp3. J. Biol. Chem. 268, 20877-20883.

Coban, C., Ishii, K.J., Kawai, T., Hemmi, H., Sato, S., Uematsu, S., Yamamoto, M., Takeuchi, O., Itagaki, S., Kumar, N., Horii, T., Akira, S., 2005. Toll-like receptor 9 mediates innate immune activation by the malaria pigment hemozoin. J. Exp. Med. 201, 19-25. https://doi.org/10.1084/jem.20041836.

Cristea, I.M., Moorman, N.J., Terhune, S.S., Cuevas, C.D., O'Keefe, E.S., Rout, M.P., Chait, B.T., Shenk, T., 2010. Human cytomegalovirus pUL83 stimulates activity of the viral immediate-early promoter through its interaction with the cellular IFI16 protein. J. Virol. 84, 7803-7814. https://doi.org/10.1128/JVI.00139-10

Dahl, J., You, J., Benjamin, T.L., 2005. Induction and utilization of an ATM signaling pathway by polyomavirus. J. Virol. 79, 13007–13017. https://doi.org/10.1128/JVI.79.20.13007-13017.2005

Dalianis, T., Hirsch H.H., 2013. Human polyomaviruses in disease and cancer. Virology. 437, 63-72. https://doi.org/10.1016/j.virol.2012.12.015

Damm, E.M., Pelkmans, L., Kartenbeck, J., Mezzacasa, A., Kurzchalia, T., Helenius, A.J., 2005. Clathrin- and caveolin-1-independent endocytosis: entry of simian virus 40 into cells devoid of caveolae. Cell Biol. 168, 477-488. https://doi.org/10.1083/jcb.200407113

Dell'Oste, V., Gatti, D., Gugliesi, F., De Andrea, M., Bawadekar, M., Lo Cigno, I., Biolatti, M., Vallino, M., Marschall, M., Gariglio, M., Landolfo, S., 2014. Innate nuclear sensor IFI16 translocates into the cytoplasm during the early stage of in vitro human cytomegalovirus

infection and is entrapped in the egressing virions during the late stage. J. Virol. 88, 6970-6982. https://doi.org/10.1128/JVI.00384-14

Diner, B.A., Li, T., Greco, T.M., Crow, M.S., Fuesler, J.A., Wang, J., Cristea, I.M., 2015. The functional interactome of PYHIN immune regulators reveals IFIX is a sensor of viral DNA. Mol. Syst. Biol. 11, 787. https://doi.org/10.15252/msb.20145808

Diner, B.A., Lum, K.K., Toettcher, J.E., Cristea, I.M., 2016. Viral DNA Sensors IFI16 and Cyclic GMP-AMP Synthase Possess Distinct Functions in Regulating Viral Gene Expression, Immune Defenses, and Apoptotic Responses during Herpesvirus Infection. mBio 7, e01553-16. https://doi.org/10.1128/mBio.01553-16

Ding, B., Lengyel, P., 2008. p204 protein is a novel modulator of ras activity. J. Biol. Chem. 283, 5831-5848. https://doi.org/10.1074/jbc.M709680200

Dingwall, C. and Laskey, R.A., 1991. Nuclear targeting sequences--a consensus? Trends Biochem. Sci. 16, 478-481. https://doi.org/10.1016/0968-0004(91)90184-w

Dixit, E., Boulant, S., Zhang, Y., Lee, A.S., Odendall, C., Shum, B., Hacohen, N., Chen, Z.J., Whelan, S.P., Fransen, M., Nibert, M.L., Superti-Furga, G., Kagan, J.C., 2010. Peroxisomes are signaling platforms for antiviral innate immunity. Cell 141, 668–681. https://doi.org/10.1016/j.cell.2010.04.018

Drachenberg, C.B., Papadimitriou, J.C., Wali, R., Cubitt, C.L., Ramos, E., 2003. BK polyoma virus allograft nephropathy: ultrastructural features from viral cell entry to lysis. Am. J. Transplant. 3, 1383-1392. https://doi.org/10.1046/j.1600-6135.2003.00237.x

Dugan, A.S., Eash, S., Atwood, W.J., 2005. An N-linked glycoprotein with alpha (2, 3)-linked sialic acid is a receptor for BK virus. J. Virol.79, 14442–14445. https://doi.org/10.1128/JVI.79.22

Dunphy, G., Flannery, S.M., Almine, J.F., Connolly, D.J., Paulus, C., Jønsson, K.L., Jakobsen, M.R., Nevels, M.M., Bowie, A.G., Unterholzner, L., 2018. Non-canonical Activation of the DNA Sensing Adaptor STING by ATM and IFI16 Mediates NF-κB Signaling after Nuclear DNA Damage. Mol. Cell 71,745-760. https://doi.org/10.1016/j.molcel.2018.07.034

Engel, S., Heger, T., Mancini, R., Herzog, F., Kartenbeck, J., Hayer, A., Helenius, A., 2011. Role of endosomes in simian virus 40 entry and infection. J. Virol 85, 4198-4211. https://doi.org/ 10.1128/JVI.02179-10

Erdinest, N., Aviel, G., Moallem, E., Anteby, I., Yahalom, C., Mechoulam, H., Ovadia, H., Solomon, A., 2014. Expression and activation of toll-like receptor 3 and toll-like receptor 4 on human corneal epithelial and conjunctival fibroblasts. J. Inflamm. (Lond) 11, 3. https://doi.org/ 10.1186/1476-9255-11-3

Erickson, K.D., Garcea, R.L., Tsai, B., 2009. Ganglioside GT1b is a putative host cell receptor for the Merkel cell polyomavirus. J. Virol. 83, 10275–10279. https://doi.org/10.1128/JVI.00949-09

Ewers, H., Römer W., Smith, A.E., Bacia, K., Dmitrieff, S., Chai, W., Mancini, R., Kartenbeck, J., Chambon, V., Berland, L., Oppenheim, A., Schwarzmann, G., Feizi, T., Schwille, P., Sens, P., Helenius, A., Johannes, L., 2010. GM1 structure determines SV40-induced membrane invagination and infection. Nat. Cell Biol. 12, 11-8. https://doi.org/10.1038/ncb1999

Fang, R., Jiang, Q., Zhou, X., Wang, C., Guan, Y., Tao, J., Xi, J., Feng, J.M., Jiang, Z., 2017. MAVS activates TBK1 and IKKε through TRAFs in NEMO dependent and independent manner. PLoS Pathog. 13, e1006720. https://doi.org/10.1371/journal.ppat.1006720

Farmerie, W.G. and Folk, W.R., 1984. Regulation of polyomavirus transcription by large tumor antigen. Proc. Natl. Acad. Sci. USA. 81, 6919-6923. https://doi.org/10.1073/pnas.81.22.6919

Fay, N. and Panté, N., 2015. Nuclear entry of DNA viruses. Front. Microbiol. 6, 467. https://doi.org/10.3389/fmicb.2015.00467

Feng, H., Shuda, M., Chang, Y., Moore, P.S., 2008. Clonal integration of a polyomavirus in

human Merkel cell carcinoma. Science 319, 1096-1100. https://doi.org/10.1126/science.1152586
Finberg, R.W., Wang, J.P., Kurt-Jones, E.A., 2007. Toll like receptors and viruses. Rev. Med. Virol. 17, 35-43. https://doi.org/10.1002/rmv.525
Flatt, J.W., Greber, U.F., 2015. Misdelivery at the Nuclear Pore Complex-Stopping a Virus Dead in Its Tracks. Cells 28, 277–296. https://doi.org/10.3390/cells4030277
Fluck, M.M. and Haslam, S.Z., 1996. Mammary tumors induced by polyomavirus. Breast Cancer Res. Treat. 39, 45-56. https://doi.org/10.1007/BF01806077
Fontes, M.R., The, T., Kobe, B., 2000. Structural basis of recognition of monopartite and bipartite nuclear localization sequences by mammalian importin - alpha. J. Mol. Biol. 297, 1183-1194. https://doi.org/10.1006/jmbi.2000.3642
Freitas, N. and Cunha, C., 2009. Mechanisms and signals for the nuclear import of proteins Curr Genomics. 10, 550–557. https://doi.org/10.2174/138920209789503941
Gack, M.U., Nistal-Villan, E., Inn, K.S., Garcia-Sastre, A., Jung, J.U., 2010. Phosphorylation-mediated negative regulation of RIG-I antiviral activity. J. Virol. 84, 3220–3229. https://doi.org/10.1128/JVI.02241-09
Gao, P., Ascano, M., Wu, Y., Barchet, W., Gaffney, B.L., Zillinger, T., Serganov, A.A., Liu, Y., Jones, R.A., Hartmann, G., Tuschl, T., Patel, D.J., 2013. Cyclic [G(2',5')pA(3',5')p] is the metazoan second messenger produced by DNA-activated cyclic GMP-AMP synthase. Cell 153, 1094-1107. https://doi.org/10.1016/j.cell.2013.04.046
Garcea, R.L., Salunke, D.M., Caspar, D.L., 1987. Site-directed mutation affecting polyomavirus capsid self-assembly in vitro. Nature 329, 86-87. https://doi.org/10.1038/329086a0
Garcia-Cattaneo, A., Gobert, F.X., Muller, M., Toscano, F., Flores, M., Lescure, A., Del Nery, E., Benaroch, P., 2012. Cleavage of toll-like receptor 3 by cathepsins B and H is essential for signaling. Proc. Natl. Acad. Sci. USA 109, 9053–9058. https://doi.org/10.1073/pnas.1115091109
Gardner S.D., Field A.M., Coleman D.V., Hulme B., 1971. New human papovavirus (B.K.) isolated from urine after renal transplantation. Lancet 1, 1253-1257. https://doi.org/10.1016/s0140-6736(71)91776-4
Gariano, G.R., Dell'Oste, V., Bronzini, M., Gatti, D., Luganini, A., De Andrea, M., Gribaudo, G., Gariglio, M., Landolfo, S., 2012. The intracellular DNA sensor IFI16 gene acts as restriction factor for human cytomegalovirus replication. PloS Pathog. 8, e1002498. https://doi.org/10.1371/journal.ppat.1002498
Garren, S.B., Kondaveeti, Y., Duff, M.O., Carmichael, G.G., 2015. Global Analysis of Mouse Polyomavirus Infection Reveals Dynamic Regulation of Viral and Host Gene Expression and Promiscuous Viral RNA Editing. PLoS Pathog. 11, e1005166. https://doi.org/10.1371/journal.ppat.1005166
Gaynor, A.M., Nissen, M.D., Whiley, D.M., Mackay, I.M., Lambert, S.B., Wu, G., Brennan, D. C., Storch, G.A., Sloots, T.P., Wang, D., 2007. Identification of a Novel Polyomavirus from Patients with Acute Respiratory Tract Infections. PLoS Pathog. 3, e64. https://doi.org/10.1371/journal.ppat.0030064
Geiger, R., Andritschke, D., Friebe, S., Herzog, F., Luisoni, S., Heger, T., Helenius, A., 2011. BAP31 and BiP are essential for dislocation of SV40 from the endoplasmic reticulum to the cytosol. Nat. Cell Biol. 13, 1305-1314. https://doi.org/10.1038/ncb2339
Gheit T., Dutta S., Oliver J., Robitaille A., Hampras S., Combes J.D., McKay-Chopin S., Le Calvez-Kelm F., Fenske N., Cherpelis B., Giuliano A.R., Franceschi S., McKay J., Rollison D.E., Tommasino M., 2017. Isolation and characterization of a novel putative human polyomavirus. Virology 506, 45-54. https://doi.org/10.1016/j.virol.2017.03.007
Gentili, M., Lahaye, X., Nadalin, F., Nader, G.P.F., Lombardi, E.P., Herve, S., De Silva, N.S.,

Rookhuizen, D.C., Zueva, E., Goudot, C., Maurin, M., Bochnakian, A., Amigorena, S., Piel, M., Fachinetti, D., Londoño-Vallejo, A., Manel, N., 2019. The N-Terminal Domain of cGAS Determines Preferential Association with Centromeric DNA and Innate Immune Activation in the Nucleus. Cell Rep. 26, 3798. https://doi.org/10.1016/j.celrep.2019.03.049

Gentili, M., Kowal, J., Tkach, M., Satoh, T., Lahaye, X., Conrad, C., Boyron, M., Lombard, B., Durand, S., Kroemer, G., Loew, D., Dalod, M., Théry, C., Manel, N., 2015. Transmission of innate immune signaling by packaging of cGAMP in viral particles. Science 349, 1232-1236. https://doi.org/10.1126/science.aab3628

Getz, G.S., 2005. Thematic review series: the immune system and atherogenesis. Bridging the innate and adaptive immune systems. J. Lipid Res. 46, 619-622. https://doi.org/10.1194/jlr.E500002-JLR200

Gilbert, J.M., Benjamin, T.L., 2000. Early steps of polyomavirus entry into cells. J. Virol. 74, 8582-8588. https://doi.org/10.1128/jvi.74.18.8582-8588.2000

Giorda, K.M., Raghava, S., Zhang, M.W., Hebert, D.N., 2013. The viroporin activity of the minor structural proteins VP2 and VP3 is required for SV40 propagation. J. Biol. Chem. 288, 2510-2520. https://doi.org/10.1074/jbc.M112.428425

Glück, S., Guey, B., Gulen, M.F., Wolter, K., Kang, T.W., Schmacke, N.A., Bridgeman, A., Rehwinkel, J., Zender, L., Ablasser, A., 2017. Innate immune sensing of cytosolic chromatin fragments through cGAS promotes senescence. Nat. Cell Biol. 19, 1061– 1070. https://doi.org/10.1038/ncb3586

Goldfarb, D.S., Corbett, A.H., Mason, D.A., Harreman, M.T., Adam, S.A., 2004. Importin alpha: a multipurpose nuclear-transport receptor. Trends Cell Biol. 14, 505-514. https://doi.org/10.1016/j.tcb.2004.07.016

González-Navajas, J.M., Lee, J., David, M., Raz, E., 2012. Immunomodulatory functions of type I interferons. Nat. Rev. Immunol. 12, 125-135. https://doi.org/10.1038/nri3133

Gresser, I., 1990. Biologic effects of interferons. J. Invest. Dermatol. 95,66S–71S. https://doi.org/10.1111/1523-1747.ep12874776

Griffith, G.R. and Consigli, R.A., 1984. Isolation and characterization of monopinocytotic vesicles containing polyomavirus from the cytoplasm of infected mouse kidney cells. J. Virol. 50, 77-85. . https://doi.org/10.1128/JVI.50.1.77-85.1984

Griffith, G.R., Marriott, S.J., Rintoul, D.A., Consigli, R. A., 1988. Early events in polyomavirus infection: fusion of monopinocytotic vesicles containing virions with mouse kidney cell nuclei. Virus Res. 10, 41–51. https://doi.org/10.1016/0168-1702(88)90056-1

Gross, L., 1953. A filterable agent, recovered from Ak leukemic extracts, causing salivary gland carcinomas in C3H mice. Proc. Soc. Exp. Biol. Med. 83, 414–421. https://doi.org/10.3181/00379727-83-20376

Handala, L., Blanchard, E., Raynal, P.I., Roingeard, P., Morel, V., Descamps, V., Castelain, S., Francois, C., Duverlie, G., Brochot, E., Helle, F., 2020. BK Polyomavirus Hijacks Extracellular Vesicles for *En Bloc* Transmission. Jю Virol. 946 e01834-19. https://doi.org/10.1128/JVI.01834-19

Hároníková, L., Coufal, J., Kejnovská, I., Jagelská, E.B., Fojta, M., Dvořáková, P., Muller, P., Vojtesek, B., Brázda, V., 2016. IFI16 Preferentially Binds to DNA with Quadruplex Structure and Enhances DNA Quadruplex Formation. PLoS ONE 11, e0157156. https://doi.org/10.1371/journal.pone.0157156

Hayashi, K., Taura, M., Iwasaki, A., 2018. The interaction between IKKα and LC3 promotes type I interferon production through the TLR9-containing LAPosome. Sci. Signal 11, eaan4144. https://doi.org/10.1126/scisignal.aan4144

Hayden, M.S., Ghosh, S., 2012. NF-kappaB, the first quarter-century: remarkable progress and outstanding questions. Genes Dev. 26, 203–234. https://doi.org/10.1101/gad.183434.111

Helle, F., Brochot, E., Handala, L., Martin, E., Castelain, S., Francois, C., Duverlie, G., 2017.

Biology of the BKPyV: An Update. Viruses 9, 327. https://doi.org/10.3390/v9110327
Hemmi, H., Takeuchi, O., Kawai, T., Kaisho, T., Sato, S., Sanjo, H., Matsumoto, M., Hoshino, K., Wagner, H., Takeda, K., Akira, S., 2000. A Toll-like receptor recognizes bacterial DNA. Nature 408, 740-745. https://doi.org/10.1038/35047123
Herrera, F.J., Triezenberg, S.J., 2004. VP16-dependent association of chromatin-modifying coactivators and underrepresentation of histones at immediate-early gene promoters during herpes simplex virus infection. J. Virol. 78, 9689-9696. https://doi.org/10.1128/JVI.78.18.9689-9696.2004
Hilleman, M.R., 1998. Discovery of simian virus 40 (SV40) and its relationship to poliomyelitis virus vaccines. Dev. Biol. Stand. 94, 183-190.
Hochrein, H., Schlatter, B., O'Keeffe, M., Wagner, C., Schmitz, F., Schiemann, M., Bauer, S., Suter, M., Wagner, H., 2004. Herpes simplex virus type-1 induces IFN-alpha production via Toll-like receptor 9-dependent and -independent pathways. Proc. Natl. Acad. Sci. USA 101, 11416-11421. https://doi.org/10.1073/pnas.0403555101
Hopfner, K.P. and Hornung, V., 2020. Molecular mechanisms and cellular functions of cGAS–STING signalling. Nat. Rev. Mol. Cell Biol. 21, 501–521. https://doi.org/10.1038/s41580-020-0244-x
Horan, K.A., Hansen, K., Jakobsen, M.R., Holm, C.K., Søby, S., Unterholzner, L., Thompson, M., West, J.A., Iversen, M.B., Rasmussen, S.B., Ellermann-Eriksen, S., Kurt-Jones, E., Landolfo, S., Damania, B., Melchjorsen, J., Bowie, A.G., Fitzgerald, K.A., Paludan, S.R., 2013. Proteasomal degradation of herpes simplex virus capsids in macrophages releases DNA to the cytosol for recognition by DNA sensors. J. Immunol. 190, 2311-2319. https://doi.org/10.4049/jimmunol.1202749
Horníková, L., Man, P., Forstová, J., 2011. Blue native protein electrophoresis for studies of mouse polyomavirus morphogenesis and interactions between the major capsid protein VP1 and cellular proteins. J. Virol. Methods 178, 1–2. https://doi.org/10.1016/j.jviromet.2011.08.019
Hornung, V., Rothenfusser, S., Britsch, S., Krug, A., Jahrsdorfer, B., Giese, T., Endres, S., Hartmann, G., 2002. Quantitative expression of toll-like receptor 1–10 mRNA in cellular subsets of human peripheral blood mononuclear cells and sensitivity to CpG oligodeoxynucleotides. J. Immunol. 168, 4531–4537. . https://doi.org/10.4049/jimmunol.168.9.4531
Hornung, V., Ellegast, J., Kim, S., Brzózka, K., Jung, A., Kato, H., Poeck, H., Akira, S., Conzelmann, K.K., Schlee, M., Endres, S., Hartmann, G., 2006. 5′-Triphosphate RNA is the ligand for RIG-I. Science 314, 994–997. https://doi.org/10.1126/science.1132505
Horwin, M., M.A., J.D., 2003. Simian Virus 40 (SV40): A Cancer Causing Monkey Virus from FDA-Approved Vaccines**.** Alb. L.J. Sci. and Tech. 13.
Hotter, D., Bosso, M., Jonsson, K.L., Krapp, C., Sturzel, C.M., Das, A., Littwitz-Salomon, E., Berkhout, B., Russ, A., Wittmann, S., Gramberg, T., Zheng, Y., Martins, L.J., Planelles, V., Jakobsen, M.R., Hahn, B.H., Dittmer, U., Sauter, D., Kirchhoff, F., 2019. IFI16 Targets the Transcription Factor Sp1 to Suppress HIV-1 Transcription and Latency Reactivation. Cell Host Microbe 25, 858–872.e13. https://doi.org/10.1016/j.chom.2019.05.002
Hou, F., Sun L., Zheng, H., Skaug, B., Jiang Q.X., Chen, Z.J., 2011. MAVS forms functional prion-like aggregates to activate and propagate antiviral innate immune response. Cell 146, 448–461. https://doi.org/10.1016/j.cell.2011.06.041
Hou, J., Zhou, Y., Zheng, Y., Fan, J., Zhou, W., Ng, I.O., Sun, H., Qin, L., Qiu, S., Lee, J.M. Lo, C.M., Man, K., Yang, Y., Yang, Y., Yang, Y., Zhang, Q., Zhu, X., Li, N., Wang, Z., Ding, G., Zhuang, S.M., Zheng, L., Luo, X., Xie, Y., Liang, A., Wang, Z., Zhang, M., Xia, Q., Liang, T,, Yu, Y., Cao, X., 2014. Hepatic RIG-I predicts survival and interferon-alpha therapeutic response in hepatocellular carcinoma. Cancer Cell 25, 49–63. https://doi.org/10.1016/j.ccr.2013.11.011

Howes, S.H., Bockus, B.J., Schaffhausen, B.S., 1996. Genetic analysis of polyomavirus large T nuclear localization: nuclear localization is required for productive association with pRb family members. J. Virol. 70, 3581-3588. https://doi.org/10.1128/JVI.70.6.3581-3588.1996

Hu, J., Wang, F., Yuan, Y., Zhu, X., Wang, Y., Zhang, Y., Kou, Z., Wang, S., Gao, S., 2010. Novel importin-alpha family member Kpna7 is required for normal fertility and fecundity in the mouse. J. Biol. Chem. 285, 33113-33122. https://doi.org/10.1074/jbc.M110.117044

Hua, K., Ferland, R.J., 2017. Fixation methods can differentially affect ciliary protein immunolabeling. Cilia 6. https://doi.org/10.1186/s13630-017-0045-9

Huang, Y.L., Wang, M., Ou, W.C., Fung, C.Y., Chen, L.S., Chang, D., 2003. Analysis of DNA-binding activity of the JC virus minor capsid protein VP2. J. Neurovirol 9, 21–24. https://doi.org/10.1080/13550280390195289

Huerfano, S., Zíla, V., Boura, E., Spanielová, H., Stokrová, J., Forstová, J., 2010. Minor capsid proteins of mouse polyomavirus are inducers of apoptosis when produced individually but are only moderate contributors to cell death during the late phase of viral infection. FEBS J. 277, 1270-1283. https://doi.org/10.1111/j.1742-4658.2010.07558.x

Huerfano, S., Ryabchenko, B., Forstová, J., 2013. Nucleofection of expression vectors induces a robust interferon response and inhibition of cell proliferation.DNA Cell Biol. 32, 467–479. https://doi.org/10.1089/dna.2012.1950

Huerfano, S., Ryabchenko, B., Spanielova, H., Forstova, J., 2017. Hydrophobic domains of mouse polyomavirus minor capsid proteins promote membrane association and virus exit from the ER. FEBS J. 284, 883–902. https://doi.org/10.1111/febs.14033

Hummeler, K., Tomassini, N., Sokol, F., 1970. Morphological aspects of the uptake of simian virus 40 by permissive cells. J. Virol. 6, 87–93. https://doi.org/10.1128/JVI.6.1.87-93.1970

Hurdiss, D.L., Morgan, E.L., Thompson, R.F., Prescott, E.L., Panou, M.M., Macdonald, A., Ranson, N.A., 2016. New structural insights into the genome and minor capsid proteins of BK polyomavirus using cryo-electron microscopy. Structure 24, 528–536. https://doi.org/10.1016/j.str.2016.02.008

Hyde-Deruyscher, R. and Carmichael, G.G., 1988. Polyomavirus early-late switch is not regulated at the level of transcription initiation and is associated with changes in RNA processing. Proc. Nati. Acad. Sci. USA 85, 8993-8997. https://doi.org/10.1073/pnas.85.23.8993

Imanishi J., 1994. Interferon-alpha, beta, gamma. Gan To Kagaku Ryoho. 21, 2853-2858.

Inoue, T., Dosey, A., Herbstman, J.F., Ravindran, M.S., Skiniotis, G., Tsai, B. 2015. ERdj5 reductase cooperates with protein disulfide isomerase to promote Simian Virus 40 endoplasmic reticulum membrane translocation. J. Virol. 89, 8897-8908. https://doi.org/10.1128/JVI.00941-15

Inoue, T., Tsai, B., 2013. How viruses use the endoplasmic reticulum for entry, replication, and assembly. Cold Spring Harb. Perspect. Biol. 5, a013250. https://doi.org/10.1101/cshperspect.a013250

Inoue, T., Tsai, B., 2011. A large and intact viral particle penetrates the endoplasmic reticulum membrane to reach the cytosol. PLoS Pathog. 7, e1002037. https://doi.org/10.1371/journal.ppat.1002037

Ishii, N., Nakanishi, A., Yamada, M., Macalalad, M. H., and Kasamatsu, H., 1994. Functional complementation of nuclear targeting-defective mutants of simian virus 40 structural proteins. J. Virol. 68, 8209–8216. https://doi.org/10.1128/JVI.68.12.8209-8216.1994

Ishii, N., Funami, K., Tatematsu, M., Seya, T., Matsumoto, M., 2014. Endosomal localization of TLR8 confers distinctive proteolytic processing on human myeloid cells. J. Immunol. 193, 5118-5128. https://doi.org/10.4049/jimmunol.1401375

Ishikawa, H., Barber, G.N., 2008. STING is an endoplasmic reticulum adaptor that facilitates innate immune signalling. Nature 455, 674–678. https://doi.org/10.1038/nature07317

IARC working group on the evaluation of carcinogenic risks to humans. 2014. Malaria and some polyomaviruses (SV40, BK, JC, and Merkel cell viruses). IARC Monogr. Eval. Carcinog. Risks Hum. 104, 9-350.

Jakobovits, E.B., Bratosin, S., Aloni, Y., 1980. A nucleosome-free region in SV40 minichromosomes. Nature 285, 263-265. https://doi.org/10.1038/285263a0

Jay, G., Nomura, S., Anderson, C.W., Khoury, G., 1981. Identification of the SV40 agnogene product: A DNA binding protein. Nature 291, 346–349. https://doi.org/10.1038/291346a0

Jiang, M., Abend, J.R., Tsai, B., Imperiale, M.J., 2009. Early events during BK virus entry and disassembly. J. Virol. 83, 1350-1358. https://doi.org/10.1128/JVI.02169-08

Jiang, H., Xue, X., Panda, S., Kawale, A., Hooy, R.M., Liang, F., Sohn, J., Sung, P., Gekara, N.O., 2019. Chromatin-bound cGAS is an inhibitor of DNA repair and hence accelerates genome destabilization and cell death. EMBO J. 38, e102718. https://doi.org/10.15252/embj.2019102718

Jønsson, K.L., Laustsen, A., Krapp, C., Skipper, K.A., Thavachelvam, K., Hotter, D., Egedal, J.H., Kjolby, M., Mohammadi, P., Prabakaran, T., Sørensen, L.K., Sun, C., Jensen, S.B., Holm, C.K., Lebbink, R.J., Johannsen, M., Nyegaard, M., Mikkelsen, J.G., Kirchhoff, F., Paludan, S.R., Jakobsen, M.R., 2017. IFI16 is required for DNA sensing in human macrophages by promoting production and function of cGAMP. Nat. Commun. 8, 14391. https://doi.org/10.1038/ncomms14391

Kalderon, D., Roberts, B.L., Richardson, W.D., Smith, A.E., 1984. A short amino acid sequence able to specify nuclear location. Cell 39, 499-509. https://doi.org/10.1016/0092-8674(84)90457-4

Kamei, Y., Yuba, S., Nakayama, T., Yoneda, Y., 1999. Three distinct classes of the alpha-subunit of the nuclear pore-targeting complex (importin-alpha) are differentially expressed in adult mouse tissues. J. Histochem. Cytochem. 47, 363-372. https://doi.org/10.1177/002215549904700310

Kamminga, S., van der Meijden, E., Feltkamp, M.C.W., Zaaijer, H.L., 2018. Seroprevalence of fourteen human polyomaviruses determined in blood donors. PLoS One 13, e0206273. https://doi.org/10.1371/journal.pone.0206273

Karikó, K., Bhuyan, P., Capodici, J., Weissman, D., 2004. Small interfering RNAs mediate sequence-independent gene suppression and induce immune activation by signaling through toll-like receptor 3. J. Immunol. 172, 6545-6549. https://doi.org/10.4049/jimmunol.172.11.6545

Karlsen, T.A., Brinchmann, J.E., 2013. Liposome delivery of microRNA-145 to mesenchymal stem cells leads to immunological off-target effects mediated by RIG-I. Mol. Ther. 21, 1169–1181. https://doi.org/10.1038/mt.2013.55

Kasahara, T., Hooks, J.J., Dougherty, S.F., Oppenheim, J.J., 1983. Interleukin 2-mediated immune interferon (IFN-gamma) production by human T cells and T cell subsets. J. Immunol. 130, 1784–1789.

Kato, H., Sato, S., Yoneyama, M., Yamamoto, M., Uematsu, S., Matsui, K., Tsujimura, T., Takeda, K., Fujita, T., Takeuchi, O., Akira S., 2005. Cell type-specific involvement of RIG-I in antiviral response. Immunity 23, 19–28. https://doi.org/10.1016/j.immuni.2005.04.010

Kato, H., Takeuchi, O., Mikamo-Satoh, E., Hirai, R., Kawai, T., Matsushita, K., Hiiragi, A., Dermody, T.S., Fujita, T., Akira, S., 2008. Length-dependent recognition of double-stranded ribonucleic acids by retinoic acid-inducible gene-I and melanoma differentiation-associated gene 5. J. Exp. Med. 205, 1601–1610. https://doi.org/10.1084/jem.20080091

Kato, H., Takahasi, K., Fujita, T., 2011. RIG-I-like receptors: cytoplasmic sensors for non-self RNA. Immunol. Rev. 243, 91-98. https://doi.org/10.1111/j.1600-065X.2011.01052.x
Kawai, T., Takahashi, K., Sato, S., Coban, C., Kumar, H., Kato, H., Ishii, K.J., Takeuchi, O., Akira, S., 2005. IPS-1, an adaptor triggering RIG-I- and Mda5-mediated type I interferon induction. Nat. Immunol. 6, 981–988. https://doi.org/10.1038/ni1243
Kawai, T., Akira, S., 2010. The role of pattern-recognition receptors in innate immunity: update on Toll-like receptors. Nat. Immunol. 11, 373-384. https://doi.org/10.1038/ni.1863
Kawai, T., Akira, S., 2011. Toll-like receptors and their crosstalk with other innate receptors in infection and immunity. Immunity 34, 637–650. https://doi.org/10.1016/j.immuni.2011.05.006
Kawasaki, T., Kawai, T., 2014. Toll-like receptor signaling pathways. Front. Immunol. 5, 461. https://doi.org/10.3389/fimmu.2014.00461
Kelly, T.J., 1988. SV40 DNA Replication. J. Biol. Chem. 263, 17889-17892.
Khanna, K.K., Lavin, M.F., Jackson, S.P., Mulhern, T.D., 2001. ATM, a central controller of cellular responses to DNA damage. Cell Death Differ. 8, 1052-1065. https://doi.org/10.1038/sj.cdd.4400874
Kishore, N., Huynh, Q.K., Mathialagan, S., Hall, T., Rouw, S., Creely, D., Lange, G., Caroll, J., Reitz, B., Donnelly, A., Boddupalli, H., Combs, R.G., Kretzmer, K., Tripp, C.S., 2002. IKK-i and TBK-1 are enzymatically distinct from the homologous enzyme IKK-2: comparative analysis of recombinant human IKK-i, TBK-1, and IKK-2. J. Biol. Chem. 277, 13840-13847. https://doi.org/10.1074/jbc.M110474200
Ko, H.L., Ren, E.C., 2012. Functional Aspects of PARP1 in DNA Repair and Transcription. Biomolecules 2, 524-548. https://doi.org/10.3390/biom2040524
Kohlway, A., Luo, D., Rawling, D.C., Ding, S.C., Pyle, A.M., 2013. Defining the functional determinants for RNA surveillance by RIG-I. EMBO Rep. 14, 772–779. https://doi.org/10.1038/embor.2013.108
Köhler, M., Speck, C., Christiansen, M., Bischoff, F.R., Prehn, S., Haller, H., Görlich, D., Hartmann, E., 1999. Evidence for distinct substrate specificities of importin alpha family members in nuclear protein import. Mol. Cell Biol. 19, 7782-7791. https://doi.org/10.1128/mcb.19.11.7782
Kolakofsky, D., Kowalinski, E., Cusack, S., 2012. A structure-based model of RIG-I activation. RNA 18, 2118-2127. https://doi.org/10.1261/rna.035949.112
Korup S., Rietscher J., Calvignac-Spencer S., Trusch F., Hofmann J., Moens U., Sauer I., Voigt S., Schmuck R., Ehlers B., 2013. Identification of a novel human polyomavirus in organs of the gastrointestinal tract. PLoS One 8, e58021. https://doi.org/10.1371/journal.pone.0058021
Kowalinski, E., Lunardi, T., McCarthy, A.A., Louber, J., Brunei, J., Grigorov, B., Gerlier, D., Cusack, S., 2011. Structural basis for the activation of innate immune pattern-recognition receptor RIG-I by viral RNA. Cell 147, 423–435. https://doi.org/10.1016/j.cell.2011.09.039
Kranzusch, P.J., Lee, A.S.Y., Berger, J.M., Doudna, J.A., 2013. Structure of human cGAS reveals a conserved family of second-messenger enzymes in innate immunity. Cell Rep. 3, 1362–1368. https://doi.org/10.1016/j.celrep.2013.05.008
Krauzewicz, N., Streuli, C.H., Stuart-Smith, N., Jones, M.D., Wallace, S., Griffin, B.E., 1990. Myristylated polyomavirusVP2: role in the life cycle of the virus. J. Virol. 64, 4414-4420. https://doi.org/10.1128/JVI.64.9.4414-4420.1990
Kumar, M.A., Christensen, K., Woods, B., Dettlaff, A., Perley, D., Scheidegger, A., Balakrishnan, L., Milavetz, B., 2017. Nucleosome positioning in the regulatory region of SV40 chromatin correlates with the activation and repression of early and late transcription during infection. Virology 503, 62–69. https://doi.org/10.1016/j.virol.2016.12.023

Kurtz, J., 2004. Memory in the innate and adaptive immune systems. Microbes Infect. 6, 1410–1417. https://doi.org/10.1016/j.micinf.2004.10.002

Kwak, E.J., Vilchez, R.A., Randhawa, P., Shapiro, R., Butel, J.S. Kusne, S., 2002. Pathogenesis and Management of Polyomavirus Infection in Transplant Recipients. Clin. Inf. Dis. 35,1081–1087. https://doi.org/10.1086/344060

Lahaye, X., Satoh, T., Gentili, M., Cerboni, S., Conrad, C., Hurbain, I., El Marjou, A., Lacabaratz, C., Lelievre, J.D., Manel, N., 2013. The capsids of HIV-1 and HIV-2 determine immune detection of the viral cDNA by the innate sensor cGAS in dendritic cells. Immunity 39, 1132-1142. https://doi.org/10.1016/j.immuni.2013.11.002

Lakin, N.D., Jackson, S.P., 1999. Regulation of p53 in response to DNA damage. Oncogene 18, 7644-7655. 10.1038/sj.onc.1203015

Larabi, A., Devos, J.M., Ng, S.L., Nanao, M.H., Round, A., Maniatis, T., Panne, D., 2013. Crystal Structure and Mechanism of Activation of TANK-Binding Kinase 1. Cell Rep. 3, 734-746. https://doi.org/10.1016/j.celrep.2013.01.034

Lee, B.L., Moon, J.E., Shu. J.H., Yuan, L., Newman, Z.R., Schekman, R., Barton, G.M., UNC93B1 mediates differential trafficking of endosomal TLRs. Elife 2, e00291. https://doi.org/10.7554/eLife.00291

Liddington, R.C., Yan, Y., Moulai, J., Sahli, R., Benjamin, T.L., Harrison S.C., 1991. Structure of simian virus 40 at 3.8-A resolution. Nature 354, 278–284. https://doi.org/10.1038/354278a0

Liao, J.C.C., Lam, R., Brázda, V., Duan, S., Ravichandran, M., Ma, J., Xiao, T., Tempel, W., Zuo, X., Wang, Y.X., 2011. Interferon-inducible protein 16: insight into the interaction with tumor suppressor p53. Structure 19, 418–429. https://doi.org/10.1016/j.str.2010.12.015

Liebl, D., Difato, F., Hornikova, L., Mannova, P., Stokrova, J., 2006. Mouse polyomavirus enters early endosomes, requires their acidic pH for productive infection, and meets transferrin cargo in Rab11-positive endosomes. J. Virol. 80, 4610-4622. https://doi.org/10.1128/JVI.80.9.4610-4622.2006

Li, D., Wu, R., Guo, W., Xie, L., Qiao, Z., Chen, S., Zhu, J., Huang, C., Huang, J., Chen, B., Qin, Y., Xu, F., Ma, F., 2019. STING-Mediated IFI16 Degradation Negatively Controls Type I Interferon Production. Cell Rep. 29, 1249-1260.e4. https://doi.org/10.1016/j.celrep.2019.09.069

Li, X.D., Wu, J., Gao, D., Wang, H., Sun, L., Chen, Z.J., 2013. Pivotal roles of cGAS-cGAMP signaling in antiviral defense and immune adjuvant effects. Science 341, 1390-1394. https://doi.org/10.1126/science.1244040

Li, T., Diner, B.A., Chen, J., Cristea, I.M., 2012. Acetylation modulates cellular distribution and DNA sensing ability of interferon-inducible protein IFI16. Proc. Natl. Acad. Sci. USA 109, 10558–10563. https://doi.org/10.1073/pnas.1203447109

Li, Y., Wu, Y., Zheng, X., Cong, J., Liu, Y., Li, J., Sun, R., Tian, Z.G., Wei, H.M., 2016. Cytoplasm-Translocated Ku70/80 Complex Sensing of HBV DNA Induces Hepatitis-Associated Chemokine Secretion. Front. Immunol. 7, 569. https://doi.org/10.3389/fimmu.2016.00569

Li, A., Yi, M., Qin, S., 2019. Activating cGAS-STING pathway for the optimal effect of cancer immunotherapy. J. Hematol. Oncol. 12, 35. https://doi.org/10.1186/s13045-019-0721-x

Li, X., Lu, C., Stewart, M., Xu, H., Strong, R.K., Igumenova, T., Li, P., 2009. Structural basis of double-stranded RNA recognition by the RIG-I like receptor MDA5. Arch. Biochem. Biophys. 488, 23–33. https://doi.org/10.1016/j.abb.2009.06.008

Li, S.F., Gong, M.J., Zhao, F.R., Shao, J.J., Xie, Y.L., Zhang, Y.G., Chang, H.Y., 2018. Type I Interferons: Distinct Biological Activities and Current Applications for Viral Infection. Cell Physiol. Biochem. 51, 2377-2396. https://doi.org/10.1016/10.1159/000495897

Lim E.S., Reyes A., Antonio M., Saha D., Ikumapayi U.N., Adeyemi M., Stine O.C., Skelton R., Brennan D.C., Mkakosya R.S., Manary M.J., Gordon J.I., Wang D., 2013. Discovery of STL polyomavirus, a polyomavirus of ancestral recombinant origin that encodes a unique T antigen by alternative splicing. Virology 436, 295-303. https://doi.org/10.1016/j.virol.2012.12.005

Lin, J.P., Fan, Y.K., Liu, H.M, 2019. The 14-3-3η chaperone protein promotes antiviral innate immunity via facilitating MDA5 oligomerization and intracellular redistribution. PLoS Pathog. 15, e1007582. https://doi.org/10.1371/journal.ppat.1007582

Liu, H., Zhang, H., Wu, X., Ma, D., Wu, J., Wang, L., Jiang, Y., Fei, Y., Zhu, C., Tan, R., Jungblut, P., Pei, G., Dorhoi, A., Yan, Q., Zhang, F., Zheng, R., Liu, S., Liang, H., Liu, Z., Yang, H., Chen, J., Wang, P., Tang, T., Peng, W., Hu, Z., Xu, Z., Huang, X., Wang, J., Li, H., Zhou, Y., Liu, F., Yan, D., Kaufmann, SHE., Chen, C., Mao, Z., Ge, B., 2018. Nuclear cGAS suppresses DNA repair and promotes tumorigenesis. Nature 563, 131–136. https://doi.org/10.1038/s41586-018-0629-6

Liu, X.Y., Chen, W., Wei, B., Shan, Y.F., Wang, C., 2011. IFN-Induced TPR Protein IFIT3 Potentiates Antiviral Signaling by Bridging MAVS and TBK1. J. Immunol. 187, 2559-2568. . https://doi.org/10.4049/jimmunol.1100963

Lo Cigno, I., De Andrea, M., Borgogna, C., Albertini, S., Landini, M.M., Peretti, A., Johnson, K.E., Chandran, B., Landolfo, S., Gariglio, M., 2015. The Nuclear DNA Sensor IFI16 Acts as a Restriction Factor for Human Papillomavirus Replication through Epigenetic Modifications of the Viral Promoters. J. Virol. 89, 7506–7520. https://doi.org/10.1128/JVI.00013-15

Loo, Y.M., Gale, M.Jr., 2011. Immune signaling by RIG-I-like receptors. Immunity 34, 680–692. https://doi.org/10.1016/j.immuni.2011.05.003

Low, J.A., Magnuson, B., Tsai, B. Imperiale, M.J., 2006. Identification of gangliosides GD1b and GT1b as receptors for BK virus. J. Virol. 80,1361– 1366. https://doi.org/10.1128/JVI.80.3.1361-1366.2006

Lund, J.M., Alexopoulou, L., Sato, A., Karow, M., Adams, N.C., Gale, N.W., Iwasaki, A., Flavell, R.A., 2004. Recognition of single-stranded RNA viruses by Toll-like receptor 7. Proc. Natl. Acad. Sci. USA 101, 5598–5603. https://doi.org/10.1073/pnas.0400937101

Mackay, R.L. and Consigli, R.A., 1976. Early events in polyoma virus infection: attachment, penetration, and nuclear entry. J. Virol. 19, p. 620-636. https://doi.org/10.1128/JVI.19.2.620-636.1976

Mackenzie, K.J., Carroll, P., Martin, C-A., Murina, O., Fluteau, A., Simpson, D., Olova, N., Sutcliffe, H., Rainger, J., Robertson, A., Osborn, R., Wheeler, A., Nowotny, M., Gilbert, N., Chandra, T., Reijns, M.A.M., Jackson, A.P., 2017. cGAS surveillance of micronuclei links genome instability to innate immunity. Nature 548, 461–465. https://doi.org/10.1038/nature23449

Magnuson, B., Rainey, E.K., Benjamin, T., Baryshev, M., Mkrtchian, S., Tsai, B., 2005. ERp29 triggers a conformational change in polyomavirus to stimulate membrane binding. Mol. Cell 20, 289–300. https://doi.org/10.1016/j.molcel.2005.08.034

Maharaj, N.P., Wies, E., Stoll, A., Gack, M.U., 2012. Conventional protein kinase C-α (PKC-α) and PKC-β negatively regulate RIG-I antiviral signal transduction. J. Virol. 86, 1358–1371. https://doi.org/10.1128/JVI.06543-11

Mahy, B.W.J., Türler, H., Beard, P., 1985. Simian virus 40 and polyoma virus: growth, titration, transformation and purification of viral components. Virology: a practical approach 169-192.

Mancuso, G., Gambuzza, M., Midiri, A., Biondo, C., Papasergi, S., Akira, S., Teti, G., Beninati, C., 2009. Bacterial recognition by TLR7 in the lysosomes of conventional dendritic cells. Nat. Immunol. 10, 587–594. https://doi.org/10.1038/ni.1733

Mannová, P., Forstová, J., 2003. Mouse polyomavirus utilizes recycling endosomes for a traffic

pathway independent of COPI vesicle transport. J. Virol. 77, 1672-1681. https://doi.org/10.1128/jvi.77.3.1672-1681.2003
Mason, D.A., Stage, D.E., Goldfarb, D.S., 2009. Evolution of the metazoan-specific importin alpha gene family. J. Mol. Evol. 68, 351-365. https://doi.org/10.1007/s00239-009-9215-8
Matsumoto, M., Kikkawa, S., Kohase, M., Miyake, K. and Seya, T., 2002. Establishment of monoclonal antibody against human Toll-like receptor 3 that blocks double-stranded RNA-mediated signaling. Biochem. Biophys. Res. Commun. 293, 1364–1369. https://doi.org/10.1016/S0006-291X(02)00380-7
Matsumoto, M., Funami, K., Tanabe, M., Oshiumi, H., Shingai, M., Seto, Y., Yamamoto, A., Seya, T., 2003. Subcellular localization of Toll-like receptor 3 in human dendritic cells. J. Immunol. 171, 3154-3162. https://doi.org/10.4049/jimmunol.171.6.3154
Maul, G.G., Rovera, G., Vorbrodt, A., Abramczuk, J., 1978. Membrane fusion as a mechanism of simian virus 40 entry into different cellular compartments. J. Virol. 28, 936–944. https://doi.org/10.1128/JVI.28.3.936-944.1978
McGhee, J.D., Nickol, J.M., Felsenfeld, G., Rau, D.C., 1983. Higher order structure of chromatin: orientation of nucleosomes within the 30 nm chromatin solenoid is independent of species and spacer length. Cell 33, 831-841. https://doi.org/10.1016/0092-8674(83)90025-9
van der Meijden, E., Janssens, R.W., Lauber, C., Bouwes Bavinck, J.N., Gorbalenya, A.E., Feltkamp, M.C., 2010. Discovery of a new human polyomavirus associated with trichodysplasia spinulosa in an immunocompromized patient. PLoS Pathog. 6, e1001024. https://doi.org/10.1371/journal.ppat.1001024
Michalski, S., de Oliveira Mann, C.C., Stafford, C.A., Witte, G., Bartho, J., Lammens, K., Hornung, V., Hopfner, K.P., 2020. Structural basis for sequestration and autoinhibition of cGAS by chromatin. Nature 587, 678–682. https://doi.org/10.1038/s41586-020-2748-0
Mishra N., Pereira M., Rhodes R.H., An P., Pipas J.M., Jain K., Kapoor A., Briese T., Faust P.L., Lipkin W.I., 2014. Identification of a novel polyomavirus in a pancreatic transplant recipient with retinal blindness and vasculitic myopathy. J. Infect. Dis. 210, 1595-1599. https://doi.org/10.1093/infdis/jiu250
Miyamoto, S., 2011. Nuclear initiated NF-κB signaling: NEMO and ATM take center stage. Cell Res. 21, 116-130. https://doi.org/10.1038/cr.2010.179
Moens, U., Calvignac-Spencer, S., Lauber, C., Ramqvist, T., Feltkamp, M.C.W., Daugherty, M.D., Verschoor, E.J., Ehlers, B., ICTV Report Consortium, 2017. ICTV Virus Taxonomy Profile: Polyomaviridae. J. Gen. Virol. 98, 1159–1160. https://doi.org/10.1099/jgv.0.000839
Moreland, R.B., Montross, L., Garcea, R.L., 1991. Characterization of the DNA-binding properties of the polyomavirus capsid protein VP1. J. Virol. 65, 1168-1176. https://doi.org/10.1128/JVI.65.3.1168-1176.1991
Moriyama, T., Marquez, J.P., Wakatsuki, T., Sorokin, A., 2007. Caveolar endocytosis is critical for BK virus infection of human renal proximal tubular epithelial cells. J. Virol. 81, 8552-8562. https://doi.org/10.1128/JVI.00924-07
Morris-Love, J.; Gee, G.V.; O'Hara, B.A.; Assetta, B.; Atkinson, A.L.; Dugan, A.S.; Haley, S.A.; Atwood, W.J., 2019. JC Polyomavirus Uses Extracellular Vesicles To Infect Target Cells. mBio 10, e00379-19. https://doi.org/10.1128/mBio.00379-19
Morrone, S.R, Wang T., Constantoulakis, L.M., Hooy, R.M., Delannoy, M.J., Sohn. J., 2014. Cooperative assembly of IFI16 filaments on dsDNA provides insights into host defense strategy. Proc. Natl. Acad. Sci. USA 111, E62-71. https://doi.org/10.1073/pnas.1313577111
Mosammaparast, N., Jackson, K.R., Guo, Y., Brame, C.J., Shabanowitz, J., Hunt, D.F.,

Pemberton, L.F., 2001. Nuclear Import of Histone H2a and H2b Is Mediated by a Network of Karyopherins. J. Cell Biol. 153, 251–262. https://doi.org/10.1083/jcb.153.2.251
Mosammaparast, N., Guo, Y., Shabanowitz, J., Hunt, D.F., Pemberton, L.F., 2002. Pathways mediating the nuclear import of histones H3 and H4 in yeast. J. Biol. Chem. 277, 862-868. https://doi.org/10.1074/jbc.M106845200
Nabbi, A. and Riabowol, K., 2015. Rapid Isolation of Nuclei from Cells In Vitro. Cold Spring Harb. Protoc. 2015, 769-772. https://doi.org/10.1101/pdb.prot083733
Nakanishi, A., Li, P.P., Qu, Q., Jafri, Q.H., Kasamatsu, H., 2007. Molecular dissection of nuclear entry-competent SV40 during infection. Virus Res. 124, 226-230. https://doi.org/10.1016/j.virusres.2006.10.001
Nakanishi, A., Shum, D., Morioka, H., Otsuka, E., Harumi Kasamatsu, H., 2002. Interaction of the Vp3 Nuclear Localization Signal with the Importin α2/β Heterodimer Directs Nuclear Entry of Infecting Simian Virus 40. J. Virol. 76, 9368–9377. https://doi.org/10.1128/jvi.76.18.9368-9377.2002
Nelson, C.D., Derdowski, A., Maginnis, M.S., O'Hara, B.A., Atwood, W.J., 2012. The VP1 subunit of JC polyomavirus recapitulates early events in viral trafficking and is a novel tool to study polyomavirus entry. Virology 428, 30–40. https://doi.org/10.1016/j.virol.2012.03.014
Nicholson, L.B., 2016. The immune system. Essays Biochem. 60, 275-301. https://doi.org/10.1042/EBC20160017
Nishimura, T., Kawai, N., Ichihara, I., 1991. Interaction of endocytotic vacuoles with the inner nuclear membrane in simian virus 40 entry into CV-1 cell nucleus. Cell Struct. Funct. 16, 441-445. https://doi.org/10.1247/csf.16.441
Nistal-Villan, E., Gack, M.U., Martinez-Delgado, G., Maharaj, N.P., Inn, K.S., Yang, H., Wang, R., Aggarwal, A.K., Jung, J.U., Garcia-Sastre, A., 2010. Negative role of RIG-I serine 8 phosphorylation in the regulation of interferon-beta production. J. Biol. Chem. 285, 20252–20261. https://doi.org/10.1074/jbc.M109.089912
Niu, C., Livingston, C.M., Li, L., Beran, R.K., Daffis, S., Ramakrishnan, D., Burdette, D., Peiser, L., Salas, E., Ramos, H., Yu, M., Cheng, G., Strubin, M., Delaney, W.E.IV, Fletcher, S.P., 2017. The Smc5/6 Complex Restricts HBV when Localized to ND10 without Inducing an Innate Immune Response and Is Counteracted by the HBV X Protein Shortly after Infection. PloS one 12, e0169648. https://doi.org/10.1371/journal.pone.0169648
Norkin, L.C., Anderson, H.A., Wolfrom, S.A., Oppenheim, A., 2002. Caveolar endocytosis of simian virus 40 is followed by Brefeldin A-sensitive transport to the endoplasmic reticulum, where the virus disassembles. J. Virol. 76, 5256–5266. https://doi.org/10.1128/jvi.76.10.5156-5166.2002
Norkin, L.C., 1999. Simian virus 40 infection via MHC class I molecules and caveolae. Immunol. Rev. 168, 13-22. https://doi.org/10.1111/j.1600-065x.1999.tb01279.x
O'Hara, S.D., Stehle, T., Garcea, R.L., 2014. Glycan receptors of the Polyomaviridae: Structure, function, and pathogenesis. Curr. Opin. Virol. 7, 73–78. https://doi.org/10.1016/j.coviro.2014.05.004
Oh, J., Fraser, N.W., 2008. Temporal association of the herpes simplex virus genome with histone proteins during a lytic infection. J. Virol. 82, 3530-3537. https://doi.org/10.1128/JVI.00586-07
Okada, N., Ishigami,Y., Suzuki, T., Kaneko, A., Yasui, K., Fukutomi, R., Isemura, M., 2008. Importins and exportins in cellular differentiation. J. Cell Mol. Med. 12, 1863–1871. https://doi.org/10.1111/j.1582-4934.2008.00437.x
Ondov, B.D., Starrett, G.J., Sappington, A., Kostic, A., Koren, S., Buck, C.B., Phillippy, A.M., 2019. Mash Screen: high-throughput sequence containment estimation for genome discovery. Genome Biol. 20, 232. https://doi.org/10.1186/s13059-019-1841-x

Onomoto, K., Yoneyama, M., Fujita, T., 2007. Regulation of antiviral innate immune responses by RIG-I family of RNA helicases. Curr. Top. Microbiol. Immunol. 316, 193-205. https://doi.org/10.1007/978-3-540-71329-6_10

Orba, Y., Suzuki, T., Makino, Y., Kubota, K., Tanaka, S., Kimura, T., Sawa, H., 2010. Large T antigen promotes JC virus replication in G2-arrested cells by inducing ATM- and ATR-mediated G2 checkpoint signaling. J. Biol. Chem. 285, 1544–1554. https://doi.org/10.1074/jbc.M109.064311

Orlando, S.J., Nabavi, M., Gharakhanian, E., 2000. Rapid small-scale isolation of SV40 virions and SV40 DNA. J. Virol. Methods 90, 109–114. https://doi.org/10.1016/s0166-0934(00)00176-2

Orzalli, M.H., Broekema, N.M., Diner, B.A., Hancks, D.C., Elde, N.C., Cristea, I.M., Knipe, D.M., 2015. cGAS-mediated stabilization of IFI16 promotes innate signaling during herpes simplex virus infection. Proc. Natl. Acad. Sci. USA 112, E1773-81. https://doi.org/10.1073/pnas.1424637112

Padgett, B.L., Walker, D.L., ZuRhein, G.M., Eckroade, R.J, Dessel, B.H., 1971. Cultivation of papova-like virus from human brain with progressive multifocal leucoencephalopathy. Lancet 1, 1257-1260. https://doi.org/10.1016/s0140-6736(71)91777-6

Pathare, G.R., Decout, A., Gluck, S., Cavadini, S., Makasheva, K., Hovius, R., Kempf, G., Weiss, J., Kozicka, Z., Guey, B., Melenec, P., Fierz, B., Thomä, N.H., Ablasser, A., 2020. Structural mechanism of cGAS inhibition by the nucleosome. Nature 587, 668-672. https://doi.org/10.1038/s41586-020-2750-6

Peisley, A., Wu, B., Yao, H., Walz, T., Hur, S., 2013. RIG-I forms signaling-competent filaments in an ATP-dependent, ubiquitin-independent manner. Mol. Cell 51, 573–583. https://doi.org/10.1016/j.molcel.2013.07.024

Pelkmans, L., Kartenbeck, J., Helenius, A., 2001. Caveolar endocytosis of simian virus 40 reveals a new two-step vesicular-transport pathway to the ER. Nat. Cell Biol. 3, 473–483. https://doi.org/10.1038/35074539

Pennock, N.D., White, J.T., Cross, E.W., Cheney, E.E., Tamburini, B.A., Kedl, R.M., 2013. T cell responses: naive to memory and everything in between. Adv. Physiol. Educ. 37, 273-283. https://doi.org/10.1152/advan.00066.2013

Pho, M.T., Ashok, A., Atwood, W.J., 2000. JC virus enters human glial cells by clathrin-dependent receptor-mediated endocytosis. J. Virol. 74, 2288-2292. https://doi.org/10.1128/jvi.74.5.2288-2292.2000

Pichlmair, A., Schulz, O., Tan, C.P., Naslund, T.I., Liljestrom, P., Weber, F., Reis e Sousa C., 2006. RIG-I-mediated antiviral responses to single-stranded RNA bearing 5'-Phosphates. Science 314, 997–1001. https://doi.org/10.1126/science.1132998

Piper, P.W., 1979. Polyoma Virus Transcription Early During Productive Infection of Mouse 3T6 Cells. J. Mol. Biol. 131, 399–407. https://doi.org/10.1016/0022-2836(79)90083-4

Pohar, J., Kužnik Krajnik, A., Jerala, R., Benčina, M., 2015a. Minimal sequence requirements for oligodeoxyribonucleotides activating human TLR9. J. Immunol. 194, 3901-3908. https://doi.org/10.4049/jimmunol.1402755

Pohar, J., Lainšček, D., Fukui, R., Yamamoto, C., Miyake, K., Jerala, R., Benčina, M., 2015. Species-Specific Minimal Sequence Motif for Oligodeoxyribonucleotides Activating Mouse TLR9. J. Immunol. 195, 4396-4405. https://doi.org/10.4049/jimmunol.1500600

Popik, W., Khatua, A.K., Fabre, N.F., Hildreth, J.E.K., Alcendor, D.J., 2019. BK Virus Replication in the Glomerular Vascular Unit: Implications for BK Virus Associated Nephropathy. Viruses 11, 583. https://doi.org/10.3390/v11070583

Pumroy, R.A. and Cingolani, G., 2015. Diversification of importin-α isoforms in cellular trafficking and disease states. Biochem. J. 466, 13-28. https://doi.org/10.1042/BJ20141186

Qian, M., Cai, D., Verhey, K.J., Tsai, B., 2009. A lipid receptor sorts polyomavirus from the

endolysosome to the endoplasmic reticulum to cause infection. PLoS Pathog. 5, e1000465. https://doi.org/10.1371/journal.ppat.1000465
Qian, M., Tsai, B., 2010. Lipids and proteins act in opposing manners to regulate polyomavirus infection. J. Virol. 84, 9840-9852. https://doi.org/10.1128/JVI.01093-10
Qiang, L.J., Zhang, N.N., Ding, F., Li, X.Y., Chen, L., Zhang, H.X., Zhang, W., Chen, S.J., Wang, Z.G., Li, J.M., Chen, Z., Zhu, J., 2011. RA-inducible gene-I induction augments STAT1 activation to inhibit leukemia cell proliferation. Proc. Natl. Acad. Sci. USA 108,1897–1902. https://doi.org/10.1073/pnas.1019059108
Qu, Q., Sawa, H., Suzuki, T., Semba, S., Henmi, C., Okada, Y., Tsuda, M., Tanaka, S., Atwood W.J., Nagashima, K., 2004. Nuclear entry mechanism of the human polyomavirus JC virus-like particle: Role of importins and the nuclear pore complex. J. Biol. Chem. 279, 27735-27742. https://doi.org/10.1074/jbc.M310827200
Rainey-Barger, E.K., Magnuson, B., Tsai, B., 2007. A chaperone-activated nonenveloped virus perforates the physiologically relevant endoplasmic reticulum membrane. J. Virol. 81, 12996-13004. https://doi.org/10.1128/JVI.01037-07
Ranoa, D.R., Parekh, A.D., Pitroda, S.P., Huang, X., Darga, T., Wong, A.C., Huang, L., Andrade, J., Staley, J.P., Satoh, T., Akira, S., Weichselbaum, R.R., Khodarev, N.N., 2016. Cancer therapies activate RIG-I-like receptor pathway through endogenous non-coding RNAs. Oncotarget 7, 26496–26515. https://doi.org/10.18632/oncotarget.8420
Rappold, I., Iwabuchi, K., Date, T., Chen, J., 2001. Tumor suppressor p53 binding protein 1 (53BP1) is involved in DNA damage-signaling pathways. J. Cell Biol. 153, 613-620. 10.1083/jcb.153.3.613
Ravindran, M.S., Spriggs, C.C., Verhey, K.J., Tsai, B., 2018. Dynein Engages and Disassembles Cytosol-Localized Simian Virus 40 To Promote Infection. J. Virol. 92, e00353-18. https://doi.org/10.1128/JVI.00353-18
Rayment, I., Baker, T.S., Caspar, D.L.D., Murakami, W.T., 1982. Polyoma virus capsid structure at 22.5 Å resolution. Nature 295, 110–115. https://doi.org/10.1038/295110a0
Rehwinkel, J., Gack, M.U., 2020. RIG-I-like receptors: their regulation and roles in RNA sensing. Nat. Rev. Immunol. 20, 537-551. https://doi.org/10.1038/s41577-020-0288-3
Richterová, Z., Liebl, D., Horák, M., Palková, Z., Stokrová, J., Hozák, P., Korb, J., Forstová, J., 2001. Caveolae are involved in the trafficking of mouse polyomavirus virions and artificial VP1 pseudocapsids toward cell nuclei. J. Virol. 75, 10880-10891. https://doi.org/10.1128/JVI.75.22.10880-10891.2001
Rodriguez, K.R., Bruns, A.M., Horvath, C.M., 2014. MDA5 and LGP2: accomplices and antagonists of antiviral signal transduction. J. Virol. 88, 8194-8200. https://doi.org/10.1128/JVI.00640-14
Rolle, S., De Andrea, M., Gioia, D., Lembo, D., Hertel, L., Landolfo, S., Gariglio, M., 2001. The interferon-inducible 204 gene is transcriptionally activated by mouse cytomegalovirus and is required for its replication. Virology 286, 249-255. https://doi.org/10.1006/viro.2001.1021
Rowe, W.P., Hartley, J.W., Brodsky, I., Huebner, R.J., Law, L.W., 1958. Observations on the spread of mouse polyoma virus infection. Nature 182, 1617-1619. https://doi.org/10.1038/1821617a0
Sachs, L., Winocour, E., 1959. Formation of different cell-virus relationships in tumour cells induced by polyoma. Nature 184, 1702–1704. https://doi.org/10.1038/1841702a0
Saito, T., Hirai, R., Loo, Y.M., Owen, D., Johnson, C.L., Sinha, S.C., Akira, S., Fujita, T., Gale, M Jr., 2007. Regulation of innate antiviral defenses through a shared repressor domain in RIG-I and LGP2. Proc. Natl. Acad. Sci. USA. 104, 582-587. https://doi.org/10.1073/pnas.0606699104
Saito, T., Owen, D.M., Jiang, F., Marcotrigiano, J., Gale, M.J., 2008. Innate immunity induced by composition-dependent RIG-I recognition of hepatitis C virus RNA. Nature 454, 523–

527. https://doi.org/10.1038/nature07106
Sankhala, R.S., Lokareddy, R.K., Begum, S., Pumroy, R.A., Gillilan, R.E., Cingolani, G., 2017. Three-dimensional context rather than NLS amino acid sequence determines importin α subtype specificity for RCC1. Nat. Commun. 8, 979. https://doi.org/10.1038/s41467-017-01057-7
Saragosti, S., Moyne, G., Yaniv, M., 1980. Absence of nucleosomes in a fraction of SV40 chromatin between the origin of replication and the region coding for the late leader RNA. Cell 20, 65-73. https://doi.org/10.1016/0092-8674(80)90235-4
Schelhaas, M., Malmström, J., Pelkmans, L., Haugstetter, J., Ellgaard, L., Grünewald, K., Helenius, A., 2007. Simian Virus 40 Depends on ER Protein Folding and Quality Control Factors for Entry into Host Cells. Cell 131, 516–529. https://doi.org/10.1016/j.cell.2007.09.038
Schoggins, J.W., MacDuff, D.A., Imanaka, N., Gainey, M.D., Shrestha, B., Eitson, J.L., Mar, K.B., Richardson, R.B., Ratushny, A.V., Litvak, V., Dabelic, R., Manicassamy, B., Aitchison, J.D., Aderem, A., Elliott, R.M., García-Sastre, A., Racaniello, V., Snijder, E.J., Yokoyama, W.M., Diamond, M.S., Virgin, H.W., Rice, C.M., 2014. Pan-viral specificity of IFN-induced genes reveals new roles for cGAS in innate immunity. Nature 505, 691-695. https://doi.org/10.1038/nature12862
Schowalter, R.M. and Buck, C.B., 2013. The Merkel cell polyomavirus minor capsid protein. PLoS Pathog. 9, e1003558. https://doi.org/10.1371/journal.ppat.1003558
Schowalter, R.M., Pastrana, D.V., Buck, C.B., 2011. Glycosaminoglycans and sialylated glycans sequentially facilitate Merkel cell polyomavirus infectious entry. PLoS Pathog. 7, e1002161. https://doi.org/10.1371/journal.ppat.1002161
Schowalter R.M., Pastrana D.V., Pumphrey K.A., Moyer A.L., Buck C.B., 2010. Merkel cell polyomavirus and two previously unknown polyomaviruses are chronically shed from human skin. Cell Host Microbe 7, 509-515. https://doi.org/10.1016/j.chom.2010.05.006
Scuda N., Hofmann J., Calvignac-Spencer S., Ruprecht K., Liman P., Kühn J., Hengel H., Ehlers B., 2011. A novel human polyomavirus closely related to the african green monkey-derived lymphotropic polyomavirus. J. Virol. 85, 4586-4590. https://doi.org/10.1128/JVI.02602-10
Seth, R.B., Sun, L., Ea, C.K., Chen, Z.J., 2005. Identification and characterization of MAVS, a mitochondrial antiviral signaling protein that activates NF-kappa B and IRF 3. Cell 122, 669–682. https://doi.org/10.1016/j.cell.2005.08.012
Shah, K.V., 2004. Simian Virus 40 and Human Disease. J. Infect. Dis. 190, 2061–2064. https://doi.org/10.1086/425999
Shang, G., Zhu, D., Li, N., Zhang, J., Zhu, C., Lu, D., Liu, C., Yu, Q., Zhao, Y., Xu, S., Gu, L., 2012. Crystal structures of STING protein reveal basis for recognition of cyclic di-GMP. Nat. Struct. Mol. Biol. 19, 725–727. https://doi.org/10.1038/nsmb.2332
Sharma, A., Singh, K., Almasan, A., 2012. Histone H2AX phosphorylation: a marker for DNA damage. Methods Mol. Biol. 920, 613-626. https://doi.org/10.1007/978-1-61779-998-3_40
Siebrasse E.A., Reyes. A., Lim E.S., Zhao G., Mkakosya R.S., Manary M.J., Gordon J.I., Wang D., 2012. Identification of MW polyomavirus, a novel polyomavirus in human stool. J. Virol. 86, 10321-10326. https://doi.org/10.1128/JVI.01210-12
Solovei, I., Cremer, M., 2010. 3D-FISH on cultured cells combined with immunostaining. Methods Mol. Biol. 659, 117-126. https://doi.org/10.1007/978-1-60761-789-1_8
Soussi, T., 1986. DNA-binding properties of the major structural protein of simian virus 40. J. Virol. 59, 740-742. https://doi.org/10.1128/JVI.59.3.740-742
Sowd, G.A., Li, N.Y., Fanning, E., 2013. ATM and ATR activities maintain replication fork integrity during SV40 chromatin replication. PLoS Pathog. 9, e1003283. https://doi.org/10.1371/journal.ppat.1003283

Sparrer, K.M J. and Gack, M.U., 2015. Intracellular detection of viral nucleic acids. Curr. Opin. Microbiol. 26, 1–9. https://doi.org/10.1016/j.mib.2015.03.001

Spurgeon, M. E. and Lambert, P.F., 2013. Merkel cell polyomavirus: a newly discovered human virus with oncogenic potential. Virology 435, 118–130. https://doi.org/10.1016/j.virol.2012.09.029

Stehle, T., Gamblin, S.J., Yan, Y., Harrison, S.C., 1996. The structure of simian virus 40 refined at 3.1 A resolution. Structure 4, 165-182. https://doi.org/10.1016/s0969-2126(96)00020-2

Stetson, D.B., Mohrs, M., Reinhardt, R.L., Baron, J.L., Wang, Z.E., Gapin, L., Kronenberg, M., Locksley, R.M., 2003. Constitutive cytokine mRNAs mark natural killer (NK) and NK T cells poised for rapid effector function. J. Exp. Med. 198, 1069-1076. https://doi.org/10.1084/jem.20030630

Stratmann, S.A., Morrone, S.R., van Oijen, A.M., Sohn, J., 2015. The innate immune sensor IFI16 recognizes foreign DNA in the nucleus by scanning along the duplex. Elife. 4, e11721. https://doi.org/10.7554/eLife.11721

Ströh, L.J. and Stehle, T., 2014. Glycan Engagement by Viruses: Receptor Switches and Specificity. Annu. Rev. Virol. 1, 285–306. https://doi.org/10.1146/annurev-virology-031413-085417

Sun, Y.W., 1997. RIG-I, a human homolog gene of RNA helicase, is induced by retinoic acid during the differentiation of acute promyelocytic leukemia cell. Thesis. Shanghai Second Medical University, China.

Sun, Z., Ren, H., Liu, Y., Teeling, J.L., Gu, J., 2011. Phosphorylation of RIG-I by casein kinase II inhibits its antiviral response. J. Virol. 85, 1036–1047. https://doi.org/10.1128/JVI.01734-10

Sun, L., Wu, J., Du, F., Chen, X., Chen, Z.J., 2013. Cyclic GMP-AMP synthase is a cytosolic DNA sensor that activates the type I interferon pathway. Science 339, 786–791. https://doi.org/10.1126/science.1232458

Sun, H., Huang, Y., Mei, S., Xu, F., Liu, X., Zhao, F., Yin, L., Zhang, D., Wei, L., Wu, C., Ma, S., Wang, J., Cen, S., Liang, C., Hu, S., Guo, F., 2021. A Nuclear Export Signal Is Required for cGAS to Sense Cytosolic DNA. Cell Rep. 34, 108586. https://doi.org/10.1016/j.celrep.2020.108586

Takashima, K., Oshiumi, H., Takaki, H., Matsumoto, M., Seya, T., 2015. RIOK3-mediated phosphorylation of MDA5 interferes with its assembly and attenuates the innate immune response.Cell Rep. 11,192–200. https://doi.org/10.1016/j.celrep.2015.03.027

Takahasi, K., Suzuki, N.N., Horiuchi, M., Mori, M., Suhara, W., Okabe, Y., Inagaki, F., 2003. X-ray crystal structure of IRF-3 and its functional implications. Nat. Struct. Biol. 10, 922–927. https://doi.org/10.1038/nsb1001

Takeuchi, O., Akira, S., 2010. Pattern recognition receptors and inflammation. Cell 140, 805-820. https://doi.org/10.1016/j.cell.2010.01.022

Taniguchi, T., Ogasawara, K., Takaoka, A., Tanaka, N., 2001. IRF family of transcription factors as regulators of host defense. Annu. Rev. Immunol. 19, 623–655. https://doi.org/10.1146/annurev.immunol

Tesar, B.M., 2007. Toll-like receptors and their role in transplantation. Frontiers in Bioscience 12, 4221. https://doi.org/10.2741/2382

Thwaites, R., Chamberlain, G., Sacre, S., 2014. Emerging role of endosomal toll-like receptors in rheumatoid arthritis. Front. Immunol. 5, 1. https://doi.org/10.3389/fimmu.2014.00001

Timney, B.L., Raveh, B., Mironska, R., Trivedi, J.M., Kim, S.J., Russel, D., Wente, S.R., Sali, A., Rout, M.P., 2016. Simple rules for passive diffusion through the nuclear pore complex. J. Cell Biol. 215, 57–76. https://doi.org/10.1083/jcb.201601004

Toscano, M.G. and de Haan, P., 2018. How Simian Virus 40 Hijacks the Intracellular Protein Trafficking Pathway to Its Own Benefit and Ours. Front. Immunol. 9, 1160.

https://doi.org/10.3389/fimmu.2018.01160
Triantafilou, K., Vakakis, E., Kar, S., Richer, E., Evans, G.L., Triantafilou, M., 2012. Visualisation of direct interaction of MDA5 and the dsRNA replicative intermediate form of positive strand RNA viruses. J. Cell Sci. 125, 4761-4769. https://doi.org/10.1242/jcs.103887
Tsang, S.H., Wang, X., Li, J., Buck, C.B., You, J., 2014. Host DNA damage response factors localize to Merkel cell polyomavirus DNA replication sites to support efficient viral DNA replication.J. Virol. 88, 3285–3297. https://doi.org/10.1128/JVI.03656-13
Tsai, B., Gilbert, J.M., Stehle, T., Lencer, W., Benjamin, T.L., Rapoport, T.A., 2003. Gangliosides are receptors for murine polyoma virus and SV40. EMBO J. 22, 4346–4355. https://doi.org/10.1093/emboj/cdg439
Tsuji, L., Takumi, T., Imamoto, N., Yoneda, Y., 1997. Identification of novel homologues of mouse importin alpha, the alpha subunit of the nuclear pore-targeting complex, and their tissue-specific expression. FEBS Lett. 416, 30-34. https://doi.org/10.1016/s0014-5793(97)01092-2
Unterholzner, L., Keating, S.E., Baran, M., Horan, K.A., Jensen, S.B., Sharma, S., Sirois, C.M., Jin, T., Latz, E., Xiao, T S., Fitzgerald, K.A., Paludan, S.R., Bowie, A.G., 2010. IFI16 is an innate immune sensor for intracellular DNA. Nat. Immunol. 11, 997–1004. https://doi.org/10.1038/ni.1932
Urbanelli, L., Buratta, S., Tancini, B., Sagini, K., Delo, F., Porcellati, S., Emiliani, C., 2019. The role of extracellular vesicles in viral Infection and transmission. Vaccines 7, 102. https://doi.org/10.3390/vaccines7030102
Varshavsky, A.J., Sundin, O., Bohn, M., 1979. A stretch of "late" SV40 viral DNA about 400 bp long which includes the origin of replication is specifically exposed in SV40 minichromosomes. Cell 16, 453–466. https://doi.org/10.1016/0092-8674(79)90021-7
Veeranki, S., Choubey, D., 2012. Interferon-inducible p200-family protein IFI16, an innate immune sensor for cytosolic and nuclear double-stranded DNA: regulation of subcellular localization. Mol. Immunol. 49, 567–571. https://doi.org/10.1016/j.molimm.2011.11.004
Vilchez, R.A., Butel, J.S., 2004. Emergent human pathogen simian virus 40 and its role in cancer. Clin. Microbiol. Rev. 17, 495–508. https://doi.org/10.1128/CMR.17.3.495-508.2004
Vogt, M., Dulbecco, R., 1960. Virus-cell interaction with a tumor-producing virus. Proc. Natl. Acad. Sci. USA 46, 365–370. https://doi.org/10.1073/pnas.46.3.365
Volkman, H.E., Cambier, S., Gray, E.E., Stetson, D.B., 2019. Tight nuclear tethering of cGAS is essential for preventing autoreactivity. Elife 8, e47491. https://doi.org/10.7554/eLife.47491
Wagstaff, K.M., Glover, D.J., Tremethick, D.J., Jans, D.A., 2007. Histone-mediated Transduction as an Efficient Means for Gene Delivery. Mol. Ther. 15, 721–731. https://doi.org/10.1038/sj.mt.6300093
Wack, A., Terczyńska-Dyla, E., Hartmann, R., 2015. Guarding the frontiers: the biology of type III interferons. Nat. Immunol. 16, 802-809. https://doi.org/10.1038/ni.3212
Walczak, C.P., Tsai, B., 2010. A PDI Family Network Acts Distinctly and Coordinately with ERp29 To Facilitate Polyomavirus Infection. J. Virol. 85, 2386–2396. https://doi.org/10.1128/JVI.01855-10
Wang, E.H. and Prives, C.P., 1991. DNA Helicase and Duplex DNA Fragment Unwinding Activities of Polyoma and Simian Virus 40 Large T Antigen Display Similarities and Differences. J. Biol. Chem. 266, 12668–12675.
Wang, I.H., Suomalainen, M., Andriasyan, V., Kilcher, S., Mercer, J., Neef, A., Luedtke, N.W., Greber, U.F., 2013. Tracking viral genomes in host cells at single-molecule resolution. Cell Host Microbe 14, 468-480. https://doi.org/10.1016/j.chom.2013.09.004
West, A.P., Khoury-Hanold, W., Staron, M., Tal, M.C., Pineda, C.M., Lang, S.M., Bestwick, M.,

Duguay, B.A., Raimundo, N., MacDuff, D.A., Kaech, S.M., Smiley, J.R., Means, R.E., Iwasaki, A., Shadel, G.S., 2015. Mitochondrial DNA stress primes the antiviral innate immune response. Nature 520, 553-557. https://doi.org/10.1038/nature14156

White, M.K., Safak, M., Khalili, K., 2009. Regulation of gene expression in primate polyomaviruses. J. Virol. 83, 10846–10856. https://doi.org/10.1128/JVI.00542-09

Wu, B., Peisley, A., Richards, C., Yao, H., Zeng, X., Lin, C., Chu, F., Walz, T., Hur, S., 2013. Structural basis for dsRNA recognition, filament formation, and antiviral signal activation by MDA5. Cell 152, 276-289. https://doi.org/10.1016/j.cell.2012.11.048

Wu, J., Chen, Z.J., 2014. Innate immune sensing and signaling of cytosolic nucleic acids. Annu. Rev. Immunol. 32, 461–488. https://doi.org/10.1146/annurev-immunol-032713-120156

Wu, J., Sun, L., Chen, X., Du, F., Shi, H., Chen, C., Chen, Z.J., 2013. Cyclic GMP-AMP is an endogenous second messenger in innate immune signaling by cytosolic DNA. Science 339, 826–830. https://doi.org/10.1126/science.1229963

Wu, Y., Li, S., 2020. Role of post-translational modifications of cGAS in innate immunity. Int. J. Mol. Sci. 21, 7842. https://doi.org/10.3390/ijms21217842

Wubben, J.M., Atkinson, S.C., Borg, N.A., 2020. The Role of Protein Disorder in Nuclear Transport and in Its Subversion by Viruses. Cells 9, 2654. https://doi.org/10.3390/cells9122654

Xia, P., Wang, S., Gao, P., Gao, G., Fan, Z., 2016. DNA sensor cGAS-mediated immune recognition. Protein Cell 7, 777-791. https://doi.org/10.1007/s13238-016-0320-3

Xie, W., Lama, L., Adura, C., Tomita, D., Glickman, J. F., Tuschl, T., Patel, D.J., 2019. Human cGAS catalytic domain has an additional DNA-binding interface that enhances enzymatic activity and liquid-phase condensation. Proc. Natl. Acad. Sci. USA 116, 11946-11955. https://doi.org/10.1073/pnas.1905013116

Yamamoto, M., Sato, S., Mori, K., Hoshino, K., Takeuchi, O., Takeda, K., Akira, S., 2002. Cutting edge: a novel Toll/IL-1 receptor domain-containing adapter that preferentially activates the IFN-beta promoter in the Toll-like receptor signaling. J. Immunol. 169, 6668-6672. https://doi.org/10.4049/jimmunol.169.12.6668

Yan, H., Dalal, K., Hon, B.K., Youkharibache, P., Lau, D., Pio, F., 2008. RPA nucleic acid-binding properties of IFI16-HIN200. Biochim. Biophys. Acta. 1784, 1087-1097. https://doi.org/10.1016/j.bbapap.2008.04.004

Yan, N., Chen, Z.J., 2012. Intrinsic antiviral immunity. Nat. Immunol. 13, 214–222. https://doi.org/10.1038/ni.2229

Yang, H.; Wang, H.; Ren, J.; Chen, Q.; Chen, Z.J., 2017. cGAS is essential for cellular senescence. Proc. Natl. Acad. Sci. USA 114, E4612–E4620. https://doi.org/10.1073/pnas.1705499114

Yang, C.H., Murti, A., Pfeffer, S.R., Basu, L., Kim, J.G., Pfeffer, L.M., 2000. IFNalpha/beta promotes cell survival by activating NF-kappa B. Proc. Natl. Acad. Sci. USA 97, 13631-13636. https://doi.org/10.1073/pnas.250477397

Yasuhara, N., Yamagishi, R., Arai, Y., Mehmood, R., Kimoto, C., Fujita, T., Touma, K., Kaneko, A., Kamikawa, Y., Moriyama, T., Yanagida, T., Kaneko, H., Yoneda, Y., 2013. Importin alpha subtypes determine differential transcription factor localization in embryonic stem cells maintenance. Dev. Cell 26, 123-135. https://doi.org/10.1016/j.devcel.2013.06.022

Ye, W., Chew, M., Hou, J., Lai, F., Leopold, S.J., Loo, H.L., Ghose, A., Dutta, A.K., Chen, Q., Ooi, E.E., White, N.J., Dondorp, A. M., Preiser, P., Chen, J., 2018. Microvesicles from malaria-infected red blood cells activate natural killer cells via MDA5 pathway. LoS Pathog. 14, e1007298. https://doi.org/10.1371/journal.ppat.1007298

You, J., O'Hara, S.D., Velupillai, P., Castle, S., Levery, S., Garcea, R.L., Benjamin, T., 2015. Ganglioside and Non-ganglioside Mediated Host Responses to the Mouse Polyomavirus. PLoS Pathog. 11, e1005175. https://doi.org/10.1371/journal.ppat.1005175

Yu, L., Liu, P., 2021. Cytosolic DNA sensing by cGAS: regulation, function, and human diseases. Signal Transduct. Target Ther. 6, 170. https://doi.org/10.1038/s41392-021-00554-y

Zhang, X., Wang, C., Schook, L.B., Hawken, R.J., Rutherford, M.S., 2000. An RNA helicase, RHIV-1, induced by porcine reproductive and respiratory syndrome virus (PRRSV) is mapped on porcine chromosome 10q13. Microb. Pathog. 28, 267–278. https://doi.org/10.1006/mpat.1999.0349

Zhang, X., Shi, H., Wu, J., Zhang, X., Sun, L., Chen, C., Chen, Z.J., 2013. Cyclic GMP-AMP containing mixed phosphodiester linkages is an endogenous high-affinity ligand for STING. Mol. Cell 51, 226-235. https://doi.org/10.1016/j.molcel.2013.05.022

Zhang, X., Flavell, R.A., Li, H.B., 2019. hnRNPA2B1: a nuclear DNA sensor in antiviral immunity. Cell Res. 29, 879-880. https://doi.org/10.1038/s41422-019-0226-8

Zhao, H., Gonzalezgugel, E., Cheng, L., Richbourgh, B., Nie, L., Liu, C., 2015. The roles of interferon-inducible p200 family members IFI16 and p204 in innate immune responses, cell differentiation and proliferation. Genes Dis. 2, 46-56. https://doi.org/10.1016/j.gendis.2014.10.003

Zhao, B., Xu, P., Rowlett, C.M., Jing, T., Shinde, O., Lei, Y., West, A.P., Liu, W.R., Li, P., 2020. The molecular basis of tight nuclear tethering and inactivation of cGAS. Nature 587, 673-677. https://doi.org/10.1038/s41586-020-2749-z

Zhou, R., Xie, X., Li, X., Qin, Z., Wei, C., Liu, J., Luo, Y., 2020. The triggers of the cGAS-STING pathway and the connection with inflammatory and autoimmune diseases. Infect. Genet. Evol. 77, 104094. https://doi.org/10.1016/j.meegid.2019.104094

Zhu, J., Huang, X., Yang, Y., 2007. Innate immune response to adenoviral vectors is mediated by both Toll-like receptor-dependent and -independent pathways. J. Virol. 81, 3170-3180. https://doi.org/10.1128/JVI.02192-06

Zierhut, C., Yamaguchi, N., Paredes, M., Luo, J.-D., Carroll, T., Funabiki, H., 2019. The Cytoplasmic DNA Sensor cGAS Promotes Mitotic Cell Death. Cell 178, 302-315. https://doi.org/10.1016/j.cell.2019.05.035

Zila, V., Difato, F., Klimova, L., Huerfano, S., Forstova, J., 2014. Involvement of microtubular network and its motors in productive endocytic trafficking of mouse polyomavirus. PLoS ONE 9, e96922. https://doi.org/10.1371/journal.pone.0096922

Zou, J., Chang, M., Nie, P., Secombes, C.J., 2009. Origin and evolution of the RIG-I like RNA helicase gene family. BMC Evol. Biol. 9, 85. https://doi.org/10.1186/1471-2148-9-85

Zu Rhein, G.M., 1983. Studies of JC virus-induced nervous system tumors in the Syrian hamster: a review. Prog. Clin. Biol. Res. 105, 205–221.

10. Appendixes

Appendix 1